Coherent Interactions in Rare-Earth-Ion-Doped Crystals for Applications in Quantum Information Science

Nilsson, Mattias

2005

Coherent Interactions in Rare-Earth-Ion-Doped Crystals for Applications in Quantum Information Science

Mattias Nilsson

Department of Physics
Lund Institute of Technology

Additions and errors recognized between the printing of this thesis (Dec. 2004) and the publishing of this electronic version (Feb. 2005) :

ADDENDUM

Since the printing of this thesis, the following papers have been published in their final form:

Paper II	Phys. Rev. B **70**, 214116 (2004)
Paper VII	Phys. Rev. B **70**, 214115 (2004)

ERRATA

Paper I, page 183, Figure 9	The label on the y-axis reads "Absorption / arb. u.", should read "Transmitted light / arb. u."
Paper I, page 184, Equation 1	The first factor on the r.h.s. reads "$\frac{\varepsilon+2^2}{3}$", should read "$\left(\frac{\varepsilon+2}{3}\right)^2$"
Paper II, page 12, Table II, caption line 3	"I≈250 W/cm^2" should be "I≈500 W/cm^2"
Paper II, page 12, second column	Lines 2-10 should be replaced by: "…calculated to be $\mu=2.6\times10^{-32}$ Cm (0.0078 D), corresponding to an oscillator strength of $f=4.7\times10^{-7}$. This can be compared with previously reported values ($f=3\times10^{-7}$ (Ref. 27) and $f=7.7\times10^{-7}$ (Ref. 49)). The relative magnitude of the square of the entries in Table II can be …"

Coherent Interactions in Rare-Earth-Ion-Doped Crystals for Applications in Quantum Information Science

Mattias Nilsson

December 2004

LUND INSTITUTE OF TECHNOLOGY
Lund University

Doctoral Thesis
Atomic Physics Division
Department of Physics
Lund Institute of Technology
P.O. Box 118
SE-221 00 Lund
Sweden

Lund Reports on Atomc Physics
ISSN 0281-2762
LRAP-333

ISBN 91-628-6377-0

Printed by KFS i Lund AB
Lund, December 2004

CONTENTS

PART II

ABSTRACT

This thesis describes investigations of the use of cryogenically cooled rare-earth-ion-doped crystals for quantum information processing and quantum optics. Several aspects of the coherent interaction between light and rare-earth ions in solids are addressed.

Quantum information science has given physicists new views of quantum mechanics. The transmission of quantum states has already found practical use and full scale quantum computers may one day perform computations and simulations that would be impossible on a conventional computer. The work presented in this thesis can be seen as a part of a broad effort to learn how to control and manipulate quantum mechanical systems, which will become necessary as science and technology continue to push ever deeper into the nanoscopic world. Coherent radiation, such as laser light, provides us with an ideal tool for these investigations and, along the way, we may also learn more about the quantum nature of light.

Rare-earth ions in inorganic crystals have several unusual properties that are interesting for applications within quantum information science, including long coherence times and long-lived ground state sublevels that can be used for storage of quantum and classical information. As part of the work presented in this thesis, new materials have been investigated with respect to these properties, and ways to enhance the useful properties of the materials were explored. In one investigation, the lifetime of information stored in the ground state population distribution of Tm^{3+} ions in YAG was shown to increase by several orders of magnitude with the application of a magnetic field.

It is demonstrated how the optical inhomogeneous absorption profile can be prepared, so that the light only interacts with a selected group of ions, absorbing on a specific transition. Narrow absorbing structures, with widths approaching the optical homogeneous linewidth, have been prepared with no absorption in the surrounding spectral interval. This thesis addresses the use of such structures as hardware for quantum bits.

Tailored pulses, capable of inducing controlled changes in the quantum states of the ions (qubits), even in the presence of unknown variations of coupling strengths and frequencies, have been realised experimentally and used for multiple transfer of ions between energy levels.

Ion-ion interactions, which can be used for performing quantum logic operations, have been investigated in some detail. Techniques for selecting strongly interacting ions, by transferring weakly interacting ions to auxiliary states, have been demonstrated.

A scheme for storing the quantum state of light in a solid, using photon-echo-like techniques, is proposed and analysed. In the proposed scheme, an optical wave packet is absorbed and subsequently re-emitted by an inhomogeneous absorption profile, which is tailored and externally controlled by the application of an electric field

Additionally, an accumulated photon echo experiment has been performed using faint optical pulses. The experiment can be viewed as a demonstration of delayed self-interference of a single photon and as a demonstration of how a single photon can act as two of the fields in a photon echo process.

SAMMANFATTNING

Den här avhandlingen handlar om hur kristaller, som innehåller en liten mängd av ämnen tillhörande gruppen sällsynta jordartsmetaller, kan användas för forskning och tillämpningar rörande kvantinformation. Genom att belysa kristallerna med laserljus kan atomernas tillstånd styras och studeras. I avhandlingen diskuteras olika aspekter av hur de sällsynta jordartsatomer som förts in i kristallerna påverkas av laserljus.

En stor del av arbetet som beskrivs har varit inriktat på att undersöka hur materialen kan användas som hårdvara i en kvantdator. Kvantdatorer har fått stor uppmärksamhet eftersom det har visats att de kan lösa problem som i praktiken är olösliga på vanliga datorer och eftersom de kan komma att ändra vår förståelse av informationsbehandling. Kvantdatorer kan till exempel komma att användas för att dechiffrera koder som idag anses olösliga. Relaterade tekniker, som också utnyttjar kvantinformation, kan å andra sidan användas för att överföra eller lagra information på ett sätt som gör det omöjligt att avlyssna eller kopiera informationen utan att det upptäcks.

I en kvantdator utnyttjas kvantmekaniska fenomen, vilka framträder tydligast i mycket små system, t.ex. i atomer, och som kan te sig mycket främmande jämfört med de fenomen vi upplever i vår vardag. I en kvantdator kan till exempel en partikel befinna sig i två olika tillstånd samtidigt, eller snarare i en överlagring av två tillstånd. Därför kan bitarna i en kvantdator, kvantbitarna, vara i både tillståndet 1 och tillståndet 0 samtidigt, till skillnad från bitarna i en vanlig dator som måste vara antingen 1 eller 0. Två bitar ger, i både kvantdatorn och en vanlig dator, fyra kombinationer 00, 01, 10 och 11, men i kvantdatorn kan man välja att ha en blandning av de olika kombinationerna som indata för en beräkning. På så sätt kan kvantdatorn genomföra ett stort antal beräkningsalternativ samtidigt och ge ett resultat som beror på alla dessa.

Byggandet av kvantdatorer befinner sig fortfarande på experimentstadiet och ett antal tekniker för att bygga en kvantdator undersöks idag, var och en med olika fördelar och nackdelar. Teknikutvecklingen för hela tiden kvantmekanikens värld allt närmre vår vardagliga värld och kvantmekaniska effekter får allt större betydelse för t.ex. mikroelektronik och halvledarindustrin. Forskning kring kvantdatorer och kvantinformation kan få betydelse eftersom man inom detta fält på ett strukturerat sätt söker efter metoder för att styra kvantmekaniska system.

De material som använts i denna avhandlig, dvs kristaller i vilka en liten mängd sällsynta jordartsmetaller förts in, har flera egenskaper som gör dem intressanta att använda för att behandla kvantinformation. När kristallen kyls ned till låga temperaturer störs de införda atomerna mycket lite av omgivningen, vilket gör att de kan befinna sig i en kvantmekanisk överlagring av tillstånd under lång tid. Atomerna absorberar ljus vid olika våglängder (olika färger) och genom att skicka in laserljus med rätt våglängd i kristallen kan man välja vilka atomer man vill påverka.

De idéer som undersökts experimentellt i denna avhandling går ut på att använda de atomer som förts in i kristallerna som kvantbitar, där olika energitillstånd får representera talen 1 och 0 och där atomerna kan kontrolleras genom att ljus skickas genom kristallen. Eftersom atomerna absorberar ljus vid ett stort antal olika våglängder kan man ha många

kvantbitar, som adresseras med hjälp av laserljus med motsvarande våglängder. Kvantbitarna (atomerna) kan även påverka varandra, genom en lättkontrollerad mekanism, vilket är en förutsättning för kvantdatorer. De tekniker som utvecklats går ut på att preparera materialen för att få att en uppsättning kvantbitar, på vilka enkla kvantdator-operationer kan testas.

Inom ramen för denna avhandling har mekanismen för påverkan mellan kvantbitarna studerats och metoder för att välja ut vilka atomer som skall utgöra en kvantbit har utvecklats. I avhandlingen visas hur elementära kvantdatoroperationer kan genomföras även när det finns systematiska fel, t.ex. om laserljusets intensitet varierar eller om ljusets våglängd inte stämmer exakt med den våglängd som atomerna i en kvantbit absorberar.

I avhandlingen presenteras också ett experiment där enskilda fotoner (ljuspartiklar) skickats in i en kristall där de absorberats. Ljuset delades upp så att varje foton kunde gå två olika vägar till kristallen. Efter att många enskilda fotoner skickats in i materialet var det möjligt att få information om tidsskillnaden mellan de två möjliga vägarna, trots att en direkt mätning skulle visat att fotonerna antingen gått den ena vägen eller den andra, men aldrig båda. Experimentet kan tolkas som att varje foton interfererar med en tidsfördröjd del av sig själv.

I avhandlingsarbetet har också ingått sökande efter nya material av samma typ, med egenskaper som är ännu bättre lämpade för den typ av försök som gjorts. Undersökningar av egenskaperna hos ett nytt material presenteras, samt även försök där ett material av denna typ placerats i ett starkt magnetfält. Magnetfältet gav upphov till en mekansim för långtidslagring av information i kristallen, vilket kan vara användbart för optisk datalagring och databehandling.

Slutligen presenteras i avhandlingen också ett förslag på hur kristaller innehållande små mängder sällsynta jordartsatomer kan användas för att tillfälligt lagra tillståndet hos en svag ljuspuls. Den föreslagna metoden kan användas för att lagra tillståndet hos ljus även i andra material där det går att påverka atomerna så att olika atomer absorberar ljus på olika våglängder.

Avhandlingen består av två delar. I den första delen (kapitel 1-8) ges en bakgrund till den forskning som presenterats i artiklarna i den andra delen. Den första delen innehåller också en del diskussioner och material som inte inkluderats i artiklarna. Den andra delen av avhandlingen (*Paper I-VII*) innehåller de vetenskapliga publikationer som ligger till grund för avhandlingen.

LIST OF PAPERS

This thesis is based on the following papers:

I. M. Nilsson, L. Rippe, N. Ohlsson, T. Christiansson and S. Kröll, "*Initial experiments concerning quantum information processing in rare-earth-ion-doped crystals*" , http:// nobel.se/ physics/ symposia/ ncs-2001-1/ kroll.pdf, Physica Scripta **T102**,178-185 (2002)

II. M. Nilsson, L. Rippe, R. Klieber, D. Suter and S. Kröll, *"Hole-burning techniques for isolation and study of individual hyperfine transitions in inhomogeneously broadened solids, demonstrated in* $Pr^{3+}:Y_2SiO_5$", cond-mat/0408515, accepted for publication in Phys. Rev. B (Nov. 2004)

III. L. Rippe, M. Nilsson, R. Klieber, D. Suter and S. Kröll, "*Experimental demonstration of efficient and selective population transfer and qubit distillation in a rare-earth-ion-doped crystal*", submitted to Phys. Rev. A (Dec. 2004)

IV. N. Ohlsson, M. Nilsson and S. Kröll*, "Experimental investigation of delayed self-interference for single photons*", Phys. Rev. A **68**, 063812 (2003)

V. M. Nilsson and S. Kröll, "*Solid state quantum memory using tailored and externally controlled inhomogeneous absorption profiles and photon-echo-like techniques*", accepted for publication in Opt. Comm. (Nov. 2004)

VI. N. Ohlsson, M. Nilsson, R.K. Mohan and S. Kröll*, "Long-time storage mechanism for Tm:YAG in a magnetic field*", Opt. Lett. **28**, 450 (2003)

VII. H.L. Xu, M. Nilsson, S. Ohser, N. Rauhut and S. Kröll, *"Hyperfine structure and homogeneous broadening in* $Pr^{3+}:KY(WO_4)_2$", accepted for publication in Phys. Rev. B (Nov. 2004)

PART I

CHAPTER 1

INTRODUCTION

The main motivation for the present work was a search for ways to use rare-earth-ion-doped crystals as hardware for quantum information processing. Quantum information science is a new and exciting field, which gained momentum when it was realised that a computing device utilising the full potential of quantum mechanics could solve problems with fewer computational steps than intuitively believed to be possible [1-3]. Another exciting discovery was the realisation that a quantum system can be used to store or transmit information in such a way that it is not possible to copy or intercept the information without being detected [4-6]. *Quantum cryptography* and rudimentary *quantum computing* were realised experimentally in the late 1990s [7-10]. Today, researchers around the would are working hard to improve these results and to find physical systems in which quantum information technology can be further developed [11-14]. The push to control the world on the level of quantum systems can also be seen in light of the emergence of nanotechnology and the ever-decreasing feature size of semiconductor devices. Eventually, these devices will be so small that their operation will be governed by quantum mechanics, and knowledge of how to design and control quantum systems will then be essential.

Rare-earth ions, sited in a single crystal which is cooled to cryogenic temperatures, have several unusual properties that make them interesting for applications in the field of quantum information science. One such property is long coherence times, which means that the ions can be placed in quantum superposition states that evolve undisturbed by the environment for a long time. Another interesting property is the large difference between the homogeneous and inhomogeneous linewidths of optical transitions in the ions, which means that individual ions are only affected by light with a very specific frequency and that different ions will absorb light at different frequencies. This has inspired the proposal of many techniques for using these materials to store or process optical signals in the time and frequency domains.

Although the focus of the work presented here has not been materials science or spectroscopy, an important part has been the investigation of the properties of the materials used and the search for new materials that would be even more suited for use in quantum information processing. Another major part of the practical work has been to investigate and develop equipment and techniques that will allow control of the quantum state of the ions in the material. The primary tool for manipulating the state of the ions has been laser radiation [15-17]. Apart from the coherent interactions between rare-earth ions and light, the interactions with applied static electric or magnetic fields and interactions with other ions in the material have also been recurring topics of investigation. Deterministic interactions between quantum systems, in this case between rare-earth ions, are a prerequisite for quantum logic operations and quantum information processing.

During this research, an experiment was performed where an accumulated photon echo was generated from the interaction of many pulse pairs, each containing on the average less than one photon, with a rare-earth-ion-doped crystal. The experiment demonstrated an effect that has been called *delayed single-photon self-interference* – a kind of time analogue to Young's double-slit experiment. The experiment can also be seen as a demonstration that non-linear and non-classical optical processes can be performed using fields on the few-photon level, in a material with a macroscopic number of absorbers with long-lived coherences.

The work described in this thesis has also included the study of possible ways to implement a proposed scheme for storage of quantum states of light. A new way to implement the scheme, using artificially induced inhomogeneous broadening of optical absorption lines, has been proposed. Such schemes for quantum state storage are important because they enable transformation between stationary and moving quantum bits of information (*stationary/flying qubits*).

This thesis consists of two parts: The first part (Chapters 1-8) is intended to provide an introduction to this field of research and a background to the papers in the second part. It also contains some discussions and considerations not included in the papers. Part II contains the scientific papers on which the thesis is based (Papers I-VII). The brief surveys of various topics in Part I are in no way intended to be complete reviews, but should rather be seen as a collection of material that the author has found interesting or useful in the study of how materials doped with rare-earth ions can be used in quantum optics and quantum information processing.

In Chapter 2, the relevant optical properties of rare-earth-ion-doped crystals are described, for example, coherence properties and the properties of ground state sublevels that can be used for storing quantum information.

Chapter 3 presents a discussion of persistent spectral hole-burning and optical pumping between hyperfine levels, which can been used for spectrally isolating groups of ions and for placing the ions in specific energy eigenstates. These techniques have been used to prepare the ions in the material for quantum information processing.

The coherent interaction between two-level atoms and light is treated in Chapter 4, using a description based on the Bloch equations and the Bloch vector. The chapter also contains a discussion of certain coherent transient phenomena, in particular photon echoes. The photon echo process is an important tool for studying coherence in these materials and it is also the basis for many techniques for storage and processing of information. This chapter also describes how coherent radiation can be used to manipulate the quantum state of a two-level system in a controlled manner, e.g. the state of an ion used to store a bit of quantum information.

Chapter 5 provides a brief review of how storage and processing of classical information can be performed in rare-earth-ion-doped crystals using coherent transients. Although this has not been the subject of investigation in this work, it has provided important background knowledge and much inspiration and insight have been gained from this field.

In Chapter 6, various types of equipment used in the experiments are discussed. Some comments are given on technical issues that were found to be particularly important when using rare-earth ions for quantum information science.

Chapter 7 discusses some quantum optical experiments that can be performed in rare-earth-ion-doped crystals, in particular an experiment related to delayed single-photon self-interference and experiments where the quantum state of light is stored in an absorbing medium, using coherent interactions between light and rare-earth ions.

Finally, in Chapter 8, quantum computing is discussed. The features of a scheme for performing quantum computing in rare-earth-ion-doped materials are described, in particular techniques for selecting ions that are suited for quantum computing, which has been one of the main topics of the experimental investigations described in the papers. Some comments are given on how to perform quantum gate operations in the presence of inhomogeneities, for example, variations in resonance frequency, and on the possible performance of a quantum information processor based on rare-earth-ion-doped materials.

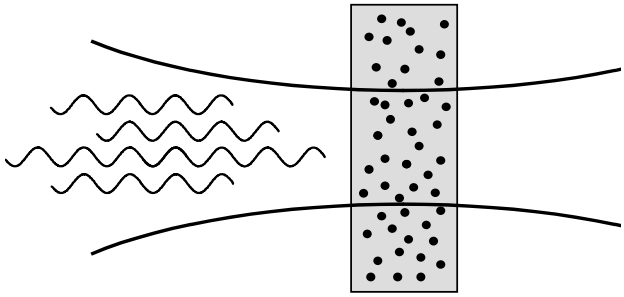

Figure 1.1. *Rare-earth ions, trapped inside a transparent crystal, interacting with a focused beam of coherent laser light.*

CHAPTER 2

RARE-EARTH-ION-DOPED INORGANIC CRYSTALS

The work presented in this thesis was concerned with the interaction between laser light and *rare-earth ions* doped into insulating and optically transparent solids. When the host material is cooled down to around 4 K, these ions have optical properties, such as long dephasing times and slow relaxation rates, which make them suitable for studying the coherent interaction between light and atoms. Through such studies, the physics and possible applications of their quantum world become accessible.

In many ways the optical properties of these ions resemble those of free atoms or ions, with the important difference that the embedded ions have fixed positions in space. Thus, rare-earth ions in a transparent solid can be thought of as a "frozen gas" or as naturally occuring "trapped ions". The analogy should be used with some caution, however, since the optical properties of the impurity ions are strongly affected by their interaction with the surrounding atoms and by the fact that the ions are not in an isotropic surrounding.

The rare-earth elements, also known as rare-earth metals or the *Lanthanides*, have atomic numbers ranging from 57 (lanthanum) to 70 (ytterbium). See Fig. 2.1. When doped into the inorganic crystals considered here, they occur as triply charged ions (RE^{3+}). Optical transitions involve electrons in the 4f shell, which is only partially filled, going from 1 electron in cerium to 14 in lutetium. It is often stated that the long coherence times of these transitions are due to the fact that the 4f electrons are shielded by the outer-lying electrons in the filled 5s and 5p shells.

Historically, there is a strong connection between these elements and Ytterby, outside Stockholm, which has given name to several of the rare earths (ytterbium, terbium and erbium). The names gadolinium, holmium and thulium are also connected to the circumstances of their discovery in minerals from the mine at Ytterby [18,19].

In this chapter the relevant optical properties of rare-earth-ion-doped inorganic crystals (*RE materials*) will be briefly reviewed. Many of the details are taken from Refs. [20-23] where, in particular, the work of R.M. Macfarlane and R.M. Shelby provides excellent reviews of the spectroscopy of solids containing rare-earth ions. Although the focus of this thesis was not spectroscopy of RE materials, an important part was the search for materials with suitable properties for proposed experiments within quantum optics and quantum computing. Rare-earth-ion spectroscopy is a rich field of study and many interesting spectroscopic techniques are used, including hole-burning spectroscopy (described in Chapter 3) and the study of coherent transient phenomena, such as photon echoes (described in Chapter 4). These techniques were used in one of the studies (Paper VII), where a new material, $Pr:KY(WO_4)_2$, was studied in some detail.

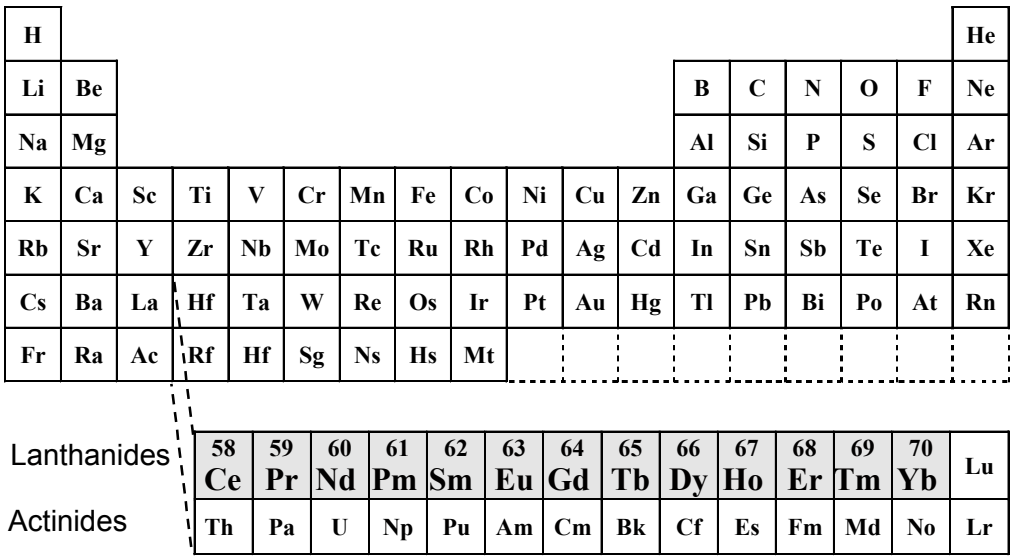

Figure 2.1. *Periodic table of the elements, with the rare earths in boldface.*

Apart from the uses discussed in this thesis, rare-earth-doped materials are of great interest because of their use as laser materials [24], such as the widely used Nd:YAG lasers and erbium-doped amplifiers.

The experimental work reported in this thesis has mainly involved europium (Eu), praseodymium (Pr) and thulium (Tm) ions, and the host materials Y_2SiO_5 (YSO), $Y_3Al_5O_{12}$ (YAG) and $YAlO_3$ (YAP). All investigations were performed at cryogenic temperatures between 2 and 4 K.

2.1 Level structure

The energy levels of a rare-earth ion in a crystal host can often be approximated by starting from the free-ion levels and then taking the crystal field into account and treating the remaining interactions as small perturbations. A manifold of energy levels having the same electronic structure, i.e. the same values of L, S and J, will be split into at most 2J+1 *Stark levels* by the electrostatic crystal field. The Stark level separations are typically 0.1-1 THz (10-100 cm^{-1}). The crystal field will also cause mixing of the electronic states, which can cause transitions that would be forbidden in a free ion to become weakly allowed [25]. The conventional labelling of states using the labels of free ion states ($^3H_4$, $^7F_0$ etc.) is therefore slightly misleading, since quantities such as J are in general only approximately good quantum numbers. The higher lying levels of a Stark manifold usually relax very rapidly through phonon emission and in this work only transitions from the lowest Stark level of the ground state to the lowest level of an optically excited state have been used. The transitions of interest do not involve the absorption or emission of phonons and are therefore known as z*ero-phonon lines*. The transitions that have been used here are in the visible or near-infrared regime, notably the $^3H_4 \leftrightarrow {}^1D_2$ transition of Pr^{3+} ions (λ=606 nm) [26,27], the $^7F_0 \leftrightarrow {}^5D_0$ transition of Eu^{3+} (λ=580 nm) [28-30] and $^3H_6 \leftrightarrow {}^3H_4$ in Tm^{3+} (λ=793 nm) [31-33]. The $^4I_{15/2} \leftrightarrow {}^4I_{13/2}$ transition of Er^{3+} (λ=1.5 μm) [34,35] is of special interest for applications, because it occurs in the telecommunications band.

Ions with an odd number of 4f electrons, after forming RE^{3+}, have electronic doublet levels, so-called *Kramers' doublets*, with magnetic moments of the order of a Bohr

magneton. For non-Kramers' ions, with an even number of electrons, the levels are electronic singlets and the electronic angular momentum is quenched by the crystal field, except if the ions are located in a site with axial or higher symmetry, in which case so-called *non-Kramers' doublets* occur [20]. Ions with a non-quenched electronic angular momentum experience large first-order Zeeman and hyperfine interactions. These ions tend to have short dephasing times, unless magnetic interactions are frozen by the application of a strong magnetic field (see below). For the most part of the following, only materials without first-order Zeeman or hyperfine interactions are considered.

For rare-earth ions with a nuclear spin greater than 1/2, the levels are split into *hyperfine levels* by second-order hyperfine and quadrupole interactions. Typical hyperfine level separations range from a few MHz (e.g. in Pr^{3+}:Y_2SiO_5 [36]) to several hundred MHz (e.g. in Eu^{3+}:Y_2SiO_5 [28]). In some cases it can be useful also to consider a *superhyperfine splitting*, due to the additional energy of the interaction between the nuclear magnetic moment of the ion and the nuclei of the surrounding atoms in the host material.

The energy and structure of the quantum states depend strongly on the host material and the symmetry properties of the *site* in which the rare-earth ion has substituted a host material atom, i.e. its position within a unit cell. Calculations of Stark and hyperfine level properties from crystal field parameters can be quite involved and in the following we will take a phenomenological approach, taking many of the material parameters as given.

2.2 Homogeneous linewidths

The *homogeneous linewidth*, Γ_h, is the width of the spectral region within which a particular ion will absorb or emit radiation. Homogeneous broadening of the resonance frequency is due to dynamic processes and relaxation, and is the same for all ions. The linewidth is connected – through the time-frequency Fourier transform – to the *phase memory* or *coherence time*, T_2, of an ion, according to

$$\Gamma_h = \frac{1}{\pi T_2}. \tag{2.1}$$

The minimum homogeneous linewidth is determined by the spontaneous relaxation of the states involved, since the phase memory (the lifetime of a coherence between the levels) can at most be equal to twice the population lifetime, T_1. Linewidths approaching this limit can be seen in materials where all other dephasing processes have been minimised, such as in Eu-doped Y_2SiO_5, with a linewidth of 122 Hz, corresponding to a T_2 of 2.6 ms [28,38], and in Er-doped Y_2SiO_5, where an optical linewidth of 50 Hz has been reported [39]. To the authors knowledge, these are the narrowest linewidths observed for any optical resonance in solids.

The long phase memory of the rare-earth ions opens the possibility for interesting physics and applications, because the ions may be put in quantum superposition states which can evolve undisturbed for a relatively long time. In a more immediate application, the narrow absorption lines have been used as frequency references for highly stabilised laser sources [40,41]. As we shall see, the small homogeneous broadening is also interesting because it makes it possible to address groups of ions by tuning to a particular frequency, since individual ions only respond to light within a very narrow frequency interval.

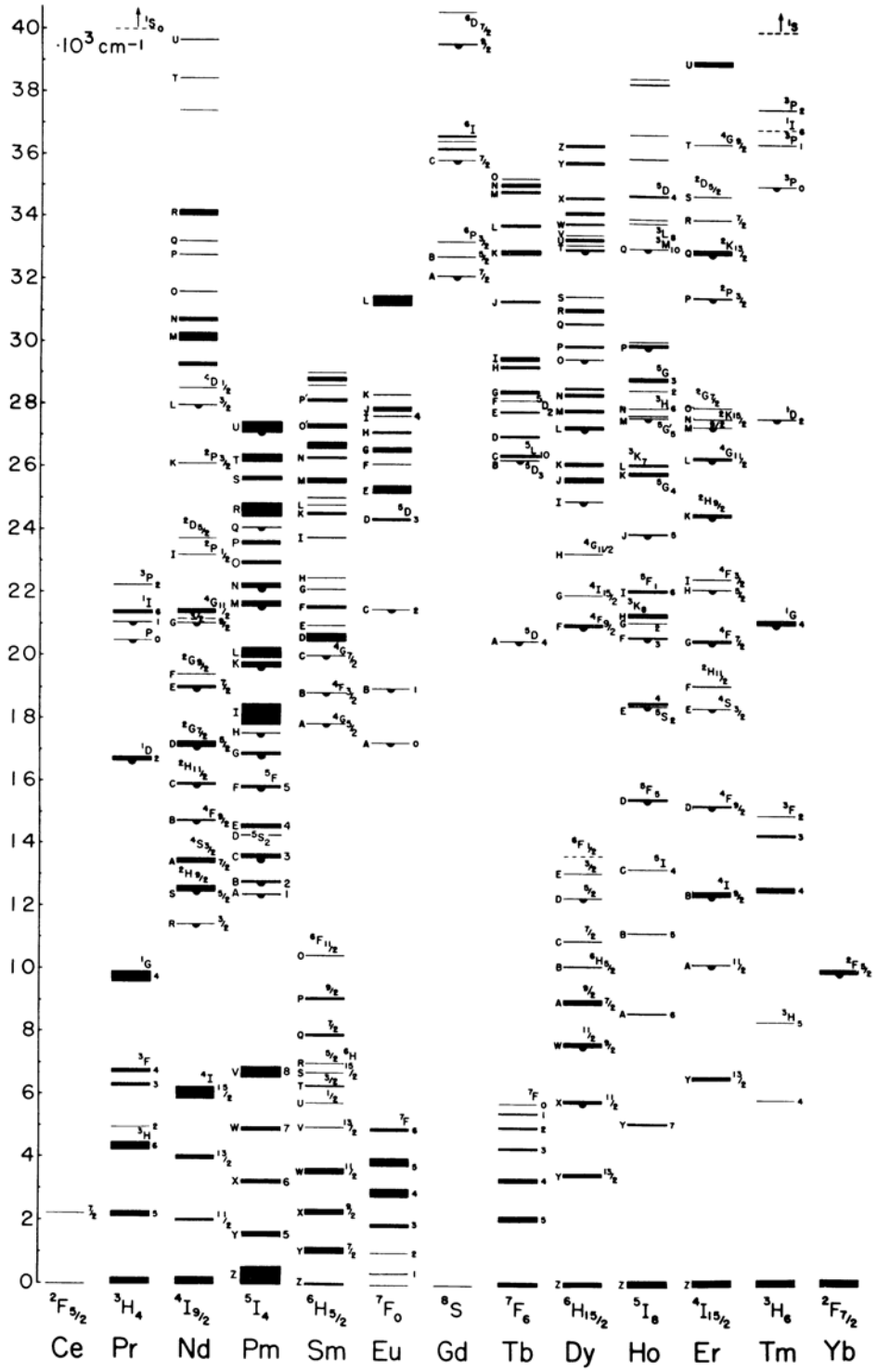

Figure 2.2. *The energy levels of triply ionised rare earths in $LaCl_3$, as reported by Dieke et al. [37]. The energy levels are similar for other hosts, since they are mainly determined by the spin-orbit interaction, rather than the crystal field interaction. Figure reproduced from Ref. [23].*

One process that contributes to decoherence in a rare-earth ion in a crystal is fluctuating fields due to spin flips in neighbouring atoms. This effect can be minimised by choosing host materials where all host atoms have small or zero nuclear magnetic moments, e.g. silicates such as Y_2SiO_5. Spin flipping can also be inhibited by applying a static magnetic field, which will thus increase the coherence time of the optical transition [42,43]. This is particularly useful for ions with an odd number of *4f* electrons (e.g. Er^{3+}) [44], with electronic Kramers' doublet levels, which have an unquenched electronic spin of the order of a Bohr magneton and thus have strong magnetic interactions. Rare-earth ions with an even number of electrons, doped into crystalline sites of less than axial symmetry, have non-magnetic electronic levels, which is an important reason for their relatively long optical coherence times [45,46].

Another process leading to homogeneous broadening is the coupling of levels by emission, absorption or scattering of lattice phonons [47]. The importance of these processes is determined by the density of phonon states, as a function of energy, and by the separations between energy levels. In order to obtain narrow lines it is in general favourable to have a large separation between the levels connected by the optical transition and their nearest Stark levels. At low temperatures the number of available phonons is small, but if the temperature is increased above a few K, the density of lattice phonons increases and the phonon contribution to the homogeneous linewidth will dominate, limiting coherence times to ns or ps timescales.

Finally, there will be a contribution to the line broadening from the interaction between the rare-earth ion and other impurities in the material. As will be discussed below, this interaction can be put to use for quantum information processing, but for most applications it will be an unwanted effect. The easiest way to minimise it is to decrease the dopant concentration in order to increase the average distance between the ions. Ion-ion interaction is particularly noticeable when some ions in the material change state through optical excitation or decay. This will change the interaction with neighbouring atoms, leading to an instantaneous shift of their resonance frequencies. The resulting dynamical broadening of an absorption line is known as *instantaneous spectral diffusion* [48-50].

Processes that contribute to the homogeneous linewidth of rare earths in solids have been discussed, for example in Refs. [45,51-53].

2.3 Inhomogeneous linewidths

Since the environment in which the ions are embedded is not an ideal crystal lattice of infinite extent, the ions will have slightly different surroundings in the crystal. This causes the energy levels and transition frequencies to differ slightly from ion to ion. This variation in resonance frequency leads to what is called *inhomogeneous broadening* of an absorption line and the width of the spectral interval within which the ensemble of ions absorbs is known as the *inhomogeneous linewidth*, Γ_{ih}. Inhomogeneous broadening is due to static interactions which are different for different absorbers [30,54,55]. The resultant absorption profile for the ensemble can be seen as the sum of the homogeneously broadened lines of the individual ions.

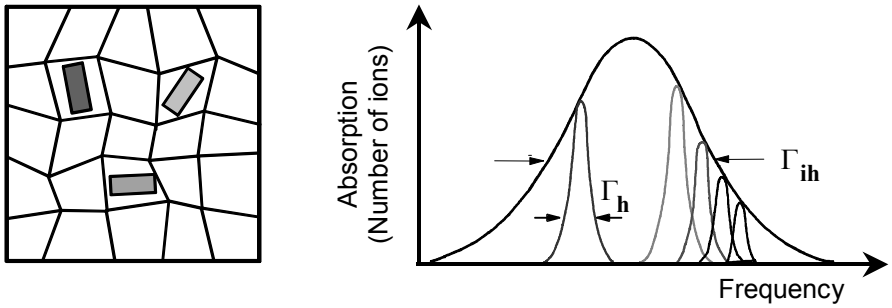

Figure 2.3. *Ions in different surroundings (left) have slightly different resonance frequencies. The inhomogeneous optical absorption line (right) is the sum of the homogeneously broadened absorption lines of the individual ions. Figure adopted from Ref. [59].*

A similar kind of broadening occurs for free atoms in a gas, where the resonance frequency of an atom is *Doppler shifted*, depending on whether the atom is moving towards or away from the light source. In a low-density gas the homogeneous linewidth of the atoms, Γ_h, will be narrow, and is determined by the excited state relaxation rate or the rate of dephasing collisions, but the total absorption of the gas will be a *Doppler broadened line*, with a width determined by the velocity of the atoms ($\Gamma_{ih}\approx 1$ GHz).

In RE materials with a low dopant concentration, the inhomogeneous widths of absorption lines are typically a few GHz, but range from less than 1 GHz up to hundreds of GHz. The linewidth generally increases with increasing dopant concentration [52,56] as more impurity ions lead to more interactions and to crystal strain. The narrowest homogeneous and inhomogeneous linewidths are achieved with dopant concentrations of 0.01% or less. Inhomogeneous lines as narrow as $\Gamma_{ih}=40$ MHz have been measured in low-strain and isotopically pure crystals [57]. In the present work samples with concentrations between 0.05% and 0.5% ($\sim 10^{23}$ m^{-3}) have been used. The inhomogeneous linewidth can also vary with the quality and method of producing the crystal sample. The inhomogeneous linewidth is generally much greater in unstructured materials, such as glasses, than in crystalline materials.

At low temperatures the inhomogeneous broadening dominates the homogeneous broadening. This means that an individual ion only interacts with light within a narrow part of the inhomogeneous absorption line and that different groups of ions can be addressed by tuning the light source to a particular frequency (Fig. 2.3). The ratio Γ_{ih}/Γ_h gives the number of addressable frequency channels, which determines the capability for processing or storing information in the frequency domain. Much work has been devoted to increasing this figure of merit, and materials with $\Gamma_{ih}/\Gamma_h\approx 10^8$ have been found [21,39,58].

2.4 Hyperfine levels

Many of the RE material applications discussed in this thesis, for example, the quantum computing scheme discussed in Chapter 8, rely on the fact that there are states of a rare-earth ion with lifetimes considerably longer than the lifetime of the optically excited state. This gives a semi-permanent memory mechanism and allows the ions to store quantum or

classical information. The mechanism may be population trapping in a metastable excited electronic state, such as the $^3H_4$ state of Tm^{3+}, or population redistribution among the hyperfine levels of the ground state, which is the case in materials doped with Eu^{3+} or Pr^{3+}. In this section the relevant properties of these hyperfine levels will be discussed.

In the RE materials that this work has focused on, hyperfine splitting is caused by second-order hyperfine interaction and electric quadrupole interaction. As the electronic magnetic moment is quenched by the crystal field, there is no first-order hyperfine interaction (I-J coupling). As the second-order hyperfine interaction has the form of a pseudo-quadrupole interaction [60,61] it can be combined with the electric quadrupole interaction into an effective quadrupole Hamiltonian, describing the interaction:

$$H_Q = D \cdot \left(I_z^2 - I(I+1)/3 \right) + E \cdot \left(I_x^2 - I_y^2 \right) \tag{2.2}$$

where D and E are coupling constants. From this, the separation between the hyperfine levels can be calculated. In the absence of a magnetic field, the levels are doubly degenerate and for ions with nuclear spin I<1, e.g. Tm^{3+}, there will be no zero-field hyperfine splitting. The levels are conventionally labelled using the quantum number I_z (e.g. $|\pm 1/2\rangle$, $|\pm 3/2\rangle$ and $|\pm 5/2\rangle$ for Eu^{3+} with I=5/2), although the wavefunctions are mixed and may be far from angular momentum eigenstates. The hyperfine level separations will differ for different isotopes (e.g. ^{151}Eu and ^{153}Eu) and for ions in non-equivalent crystal sites.

Ions can be transferred between hyperfine levels by optical pumping, as will be described in Chapter 3, or by applying radio-frequency (RF) pulses, resonant with the hyperfine transition. The ion population will return to the equilibrium distribution through spin exchange with the surrounding nuclei, or through phonon-assisted processes such as the direct phonon process, the two-step Orbach process or inelastic Raman scattering of phonons [47]. As the phonon density of states is low at the typical hyperfine splitting frequencies, this relaxation will be slow at cryogenic temperatures. In $Eu:Y_2SiO_5$ the hyperfine level lifetime, $T_1^{(hfs)}$, is several days and in $Pr:Y_2SiO_5$ it is around 100 s. Relaxation of the ion population between hyperfine levels can be inhibited by applying an external magnetic field, which inhibits spin flips in the host and splits the degenerate levels into Zeeman levels. This was used to extend the storage time for spectral features in the materials $Pr:Y_2SiO_5$ and Tm:YAG, respectively (Papers IV and VI).

If the hyperfine levels are used to encode quantum (coherent) information, the dephasing time for coherent superpositions of the states, $T_2^{(hfs)}$, is of interest. The decoherence time of the hyperfine levels is typically longer than that of the optically excited states, e.g. at least 500 μs in $Pr:Y_2SiO_5$ [62]. Thus, in many suggested applications the optical transitions are used for high-speed processing and the hyperfine levels are used for long-term storage. The phase memory of the hyperfine transitions is limited by the same processes that cause decoherence on the optical transitions and by the processes that cause relaxation between the hyperfine levels, most notably the magnetic interaction with spins in the host material. As was mentioned above, dephasing due to the interaction with flipping spins in the crystal host nuclei can be inhibited to some extent by applying a static magnetic field to the crystal, which will freeze the spin directions. Remarkable improvements can be achieved by applying a magnetic field with a critical strength and at

a critical angle, which Zeeman shifts the levels such that they become insensitive to magnetic field fluctuations. In Pr^{3+}:Y_2SiO_5 this has been used to make the hyperfine levels of the Pr ions insensitive to the spin flipping of the surrounding Y nuclei, which increases the duration of the hyperfine level phase memory to $T_2^{(hfs)}$=82 ms [63]. Recently, hyperfine coherence times exceeding 10 s have been observed [64].

Analogous to the optical transitions, hyperfine transitions can exhibit an inhomogeneous broadening, $\Gamma_{ih}^{(hfs)}$, if the hyperfine splittings are slightly different for different ions, due to differences in their surroundings. The inhomogeneous width of the hyperfine transitions in RE materials is typically a few tens of kHz, e.g. 30-80 kHz for the 10 and 17 MHz splittings of the ground state in Pr:Y_2SiO_5 [26] and 20-30 kHz in Eu:$YAlO_3$ [30,65]. In some cases the inhomogeneous shift of the hyperfine transition frequency is correlated to some extent, to the optical inhomogeneous shift (see e.g. Ref. [30]), which means that a subset of ions absorbing at a particular optical frequency may have a smaller $\Gamma_{ih}^{(hfs)}$ than the set of all ions in the crystal.

2.5 Transition strengths

The optical transitions used in RE materials, for example in optical information processing, are usually weak compared with allowed electric-dipole atomic transitions. Typical oscillator strengths range from $f=10^{-8}$ to $f=10^{-6}$, corresponding to transition dipole moments of the order of $\mu_{ge}=10^{-31}$ - 10^{-32} Cm (0.001-0.01 D). A higher transition strength means that it is easier to drive the optical transition using laser light (i.e. that less optical power is required), but also implies a higher rate of spontaneous emission and faster relaxation. The lifetime of the excited state can be obtained by summing the rates of relaxation from the state to all lower levels, and is of the order of 200 μs-2 ms, for the transitions used in the present work.

When the ground and excited states are split into several hyperfine levels, there will be a number of possible optical transitions, corresponding to transitions between different hyperfine levels. A direct measurement of the strength of the transitions between specific hyperfine levels is usually difficult, as the transitions are generally hidden by the inhomogeneous broadening. However, Paper II, describes how hole-burning techniques can be used to isolate individual hyperfine transitions and how absolute values of the transition strengths can be obtained.

The optical absorption ($\alpha(\omega_0)$) in the materials used in the present work is typically of the order of 0.1-10 cm^{-1} at the centre of the inhomogeneously broadened absorption line, for dopant concentrations of 0.01-0.1 at.%. Interestingly enough, the peak absorption is only proportional to the density of absorbing impurities within certain limits, because the inhomogeneous width of the transition also increases if the dopant concentration is increased (cf. Section 2.3). This demonstrates the important difference between the absorption coefficient and cross-section for a particular frequency, $\alpha(\omega)=n\cdot\sigma(\omega)$, and the frequency-integrated quantities α_0 and σ_0. Ref. [66] is very useful in clarifying the relationships and for converting between parameters describing the strength of optical transitions, such as Einstein coefficients, cross-sections, f values and dipole moments.

2.6 Interaction with static external fields

If a static electric or magnetic field is applied across a rare-earth-ion-doped crystal, it will cause a shift of the energy levels of the rare-earth ions, due to their *electric* and *magnetic dipole moments*. This can be used to split degenerate levels and to shift spectral features in a controlled way.

The Zeeman shift of an energy level, caused by the interaction with a magnetic field B, can be of the order of 10 GHz/T if there is an electronic magnetic moment. However, in many materials, including the ones used in this work, the electronic magnetic moment is quenched by the crystal field. Thus, the shift is due only to the interaction with the nuclear magnetic moment, possibly enhanced by the surrounding electrons [20,65,67]. Typical effective nuclear gyromagnetic ratios are of the order of γ=10-100 MHz/T. In the absence of an external field, the nucleus is still subjected to a small magnetic field, due to the nuclear spins of the surrounding atoms. The resulting energy shift is known as superhyperfine splitting. The magnetic field at the site of the ion fluctuates due to spin flips and, over time, this leads to dephasing.

Paper VI describes how the degenerate ground state of Tm:YAG, with nuclear spin I=1/2, can be split by the application of an external magnetic field. Since relaxation between Zeeman levels is relatively slow, this gives a memory mechanism which is more persistent than population storage in the metastable $^3F_4$ state, which has previously been used. Since the publication of Paper VI, the effect of a magnetic field on Tm:YAG has been analysed in detail by researchers at CNRS-ENSCP [68] (cf. Ref. [69]).

Ions in an isotropic environment, e.g. free space, have electronic wavefunctions of definite parity and hence can have no permanent electric dipole moments. However, in a low symmetry site in a crystal, the ions acquire a dipole moment, μ, with a magnitude and direction dependent on the electronic state. The electric dipole moment is due to a mixing between electronic states of different parity and can be calculated as [70]

$$\boldsymbol{\mu} = \frac{\langle \psi | V_u | \varphi \rangle \langle \psi | e\mathbf{r} | \varphi \rangle}{\Delta}. \tag{2.3}$$

Here, V_u is an odd crystal field potential, Δ is the energy separation between the electronic states and $\mathbf{r}$ is the position vector. The direction of μ depends only on the symmetry of the impurity centre. For example, in centres with a single rotation symmetry axis the dipole moment is directed along this axis [70].

If an external electric field, E_{ext}, is applied, the energy of the electronic eigenstates will shift, and if two states have different dipole moments the energy difference between them will change. Typical values of the Stark shift of optical transitions, $\Delta\nu$, are around 100 kHz/Vcm^{-1}, from which the difference between the dipole moments of the two levels involved, $|\Delta\mu|$, can be calculated [51]

$$|\Delta\mu| = \frac{3}{\varepsilon(0)+2} \cdot \left| \frac{\Delta\nu}{E_{ext}} \right|. \tag{2.4}$$

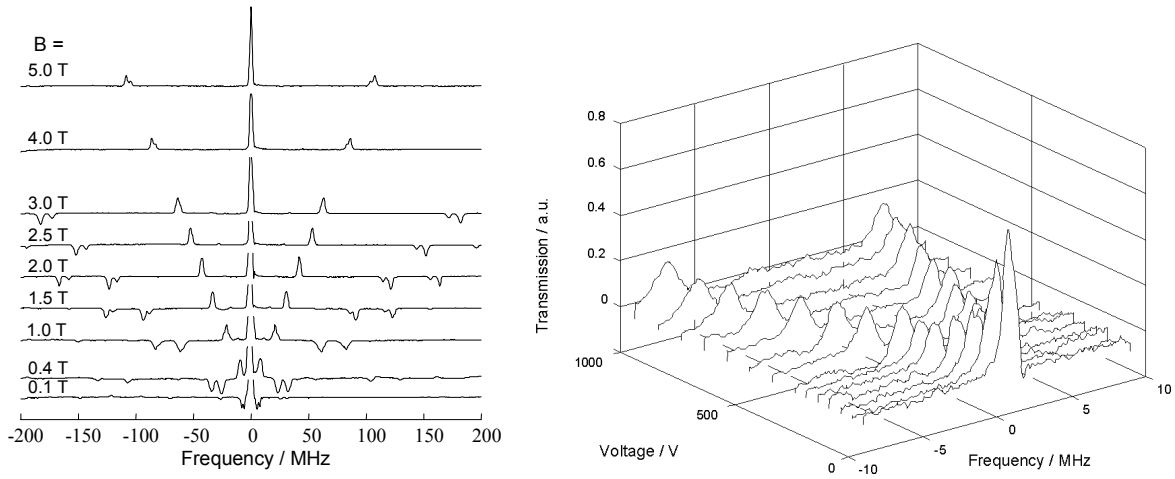

Figure 2.4. *Left: The doubly degenerate nuclear spin states in Tm:YAG (I=1/2) split into Zeeman levels as a magnetic field is applied. The splitting can be seen in a spectral hole transmission spectrum. Right: Pseudo-Stark splitting in Eu:$YAlO_3$. Depending on the orientation of the ions, their optical resonance frequency is shifted to higher or lower energies when an electric field is applied across the sample, which is seen here as a splitting of a spectral hole.*

The first factor on the right-hand side of the equality corrects for the dielectric properties of the crystal, as μ is the dipole moment in vacuum, and $\varepsilon(0)$ is the dielectric constant for DC fields (zero frequency).

Ions doped into a crystal are distributed among suitable sites in the host material, e.g. in Y_2SiO_5, YAG and $YAlO_3$, where the rare-earth ions replace yttrium. Ions in *non-equivalent sites* have slightly different properties, e.g. Eu ions in "site I" in Y_2SiO_5 absorb at 579.88 nm, whereas Eu ions in "site II" absorb at 580.05 nm [28,71]. Within a unit cell, there may also be several *equivalent sites*, with the same symmetry and the same type of neighbouring atoms, but with different orientations. This is of relevance when external fields are applied, as ions with different orientations with respect to the field sites will couple differently to the fields. In a Stark shift experiment this means that some ions will have their optical transitions shifted to higher frequencies and some to lower frequencies, depending on whether their electric dipole moments are oriented parallel to or anti-parallel to the applied electric field. This will be seen as a *pseudo-Stark splitting* of the transition [24,72-74]. See Fig. 2.4.

The transition dipole moments for optical transitions will also have definite directions, which means that ions in sites with different orientations will couple with varying strength to light with a specific polarisation, depending on the projection of the electric field of the light onto the transition dipole moment. However, it has been shown that by choosing the light polarisation and the direction of propagation with care, it is always possible to make all ions couple to the light with equal strength [75].

2.7 Ion-ion interaction

A dopant ion will affect its surroundings, e.g. through a slight distortion of the crystal lattice and through its permanent electric or magnetic dipole moment. This means that closely situated ions will interact. In most applications, this is an unwanted effect, since it leads to line broadening or dephasing, but it is a key element in the quantum computing

experiments described in this thesis. In a computing application where bits of information are stored in the state of different ions it is necessary to have a mechanism for interaction between ions, in order to perform logic operations.

The main interaction considered here is ion-ion interaction through the *permanent electric dipole moments* discussed in the previous section. If an ion has different dipole moments in the ground and the excited states, with a difference $\Delta\boldsymbol{\mu} = \boldsymbol{\mu}_g - \boldsymbol{\mu}_e$, then the field in the surrounding medium will change if the ion is excited. Nearby ions couple to the field and their optical resonance frequencies will change as the field changes. The energy change associated with the interaction between two dipoles with a separation **r**, is

$$\Delta E = \frac{(\varepsilon(0)+2)^2}{9\varepsilon(0)} \frac{|\Delta\boldsymbol{\mu}|^2}{4\pi\varepsilon_0 |\mathbf{r}|^3} \left(\delta\hat{\boldsymbol{\mu}}_1 \cdot \delta\hat{\boldsymbol{\mu}}_2 - 3(\delta\hat{\boldsymbol{\mu}}_1 \cdot \hat{\mathbf{r}})(\hat{\mathbf{r}} \cdot \delta\hat{\boldsymbol{\mu}}_2)\right) \tag{2.5}$$

where the first factor is a local field correction [76], of the order of 1, and the last factor is a geometrical factor which varies between -2 and 1, depending on the relative orientations of the dipole moments of the two atoms, $\Delta\hat{\boldsymbol{\mu}}_1$ and $\Delta\hat{\boldsymbol{\mu}}_2$. For typical values of the dipole moments and assuming $\varepsilon(0) \approx 7$, the energy shift is approximately 1 GHz for two ions at a distance of 1 nm, 1 MHz for a separation of 10 nm and 1 kHz for a separation of 100 nm.

The *excitation-induced frequency shifts* described above lead to an effect known as *optical instantaneous spectral diffusion* [48,49], when a large number of ions change state through excitation or relaxation. A group of ions originally absorbing at the same frequency and oscillating in phase will experience pseudo-random frequency shifts according to how the local electric field in their surrounding changes, as neighbouring ions decay to the ground state, and will spread out in frequency and in phase. This type of line-broadening mechanism was first studied in the form of broadening of magnetic resonance lines, due to random flipping of nuclear spins, with a magnetic dipole-dipole interaction [77,78]. The effect has been studied in some detail [50,51,79-83], because it limits the efficiency of many applications relying on the narrow homogeneous linewidths of RE-doped materials.

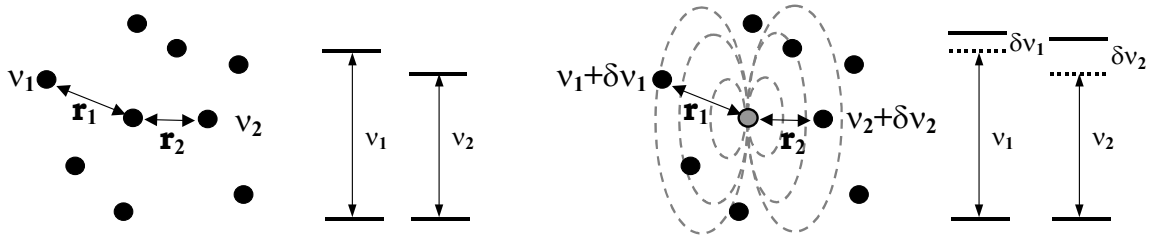

Figure 2.5. *Dipole-dipole interaction between ions in a solid. The interaction strength scales as $1/r^3$, where r is the distance between the ions. If an ion changes electronic state, e.g. through optical excitation or relaxation, its static electric dipole moment is changed, which changes the interaction with nearby ions. The figure illustrates how the optical resonance frequencies of two ions, with original resonance frequencies, ν_1 and ν_2, are shifted as a nearby ion is excited. The same figure could also be used to illustrate spectral diffusion due to magnetic dipole-dipole interaction, e.g. how the flip of a nuclear spin in the host material changes the energy of nearby rare-earth ions.*

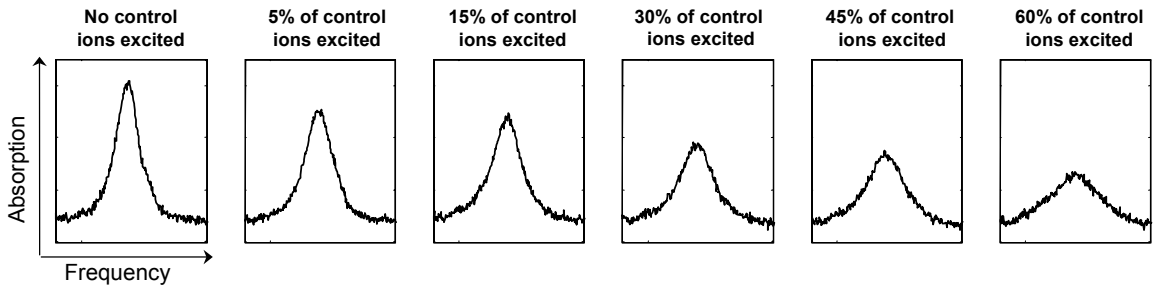

Figure 2.6. *Instantaneous spectral diffusion due to ion-ion interaction, studied in Pr:Y_2SiO_5. The resonance frequencies of a group of ions, originally absorbing within a 100 kHz wide interval, are shifted as an increasing number of neighbouring ions are excited. The ions that are excited (the control ions) absorb within a wide spectral region, elsewhere in the inhomogeneous absorption profile, i.e. outside the frequency region shown in the figures.*

Most investigations of excitation-induced frequency shifts have been performed in the time domain, using photon echoes to study the dephasing due to instantaneous spectral diffusion. However, the mechanism could be studied directly in the frequency domain by recording the broadening of a spectral feature as the density of excited ions in the material was increased (Papers I and III) (Fig. 2.6).

The shift of the resonance frequency of an ion, caused by a random distribution of nearby ions changing state and hence dipole moment, can be described by a displacement function $D(\Delta\nu)$. This function describes the probability that the resonance frequency of an ion is shifted by an amount $\Delta\nu$, and it also describes the shape of an originally sharp spectral feature (e.g. the absorption due to a group of ions with exactly the same optical resonance frequency) after instantaneous spectral diffusion has occurred. It has been shown analytically [77,78,84] and numerically (Paper I and Ref. [56]) that, in the case of a low density of excited ions, $D(\Delta\nu)$ will have a Lorentzian shape with a width proportional to the density of excited ions, ρ_e. Although the most likely shift is $\Delta\nu=0$, since the effects of many randomly distributed and oriented dipoles tend to cancel, the average shift is proportional to ρ_e, and, for some ions, which happen to be very close to an excited ion, the shift can be much larger than the average shift. For many applications, the magnitude of spectral diffusion in a particular material is well described by noting the average shift, $\Delta\nu_{ave}$, caused by the excitation of all ions within a certain spectral interval, $\Delta\nu_{exc}$, within the inhomogeneous absorption profile, and by assuming that the number of excited ions is proportional to the width of this interval. For example, $\Delta\nu_{ave}/\Delta\nu_{exc}\approx 5$ kHz/MHz=0.005 in Tm:YAG (Paper I) and ~0.01 in Pr:YSO (Longdell et al. reports 1 kHz/300kHz in Ref. [85], whereas our group has measured average shifts larger than 20 kHz/MHz (cf. Paper III). It has been shown that if only dipoles with a certain orientation are excited, the shift will closely resemble a Lorentzian, but with a small displacement of the most likely shift [84]. This situation can be realised experimentally, by using spectral hole-burning to select ions with a certain orientation [86].

It is possible that the dipole-dipole interaction between dopant ions is the main cause of the inhomogeneous line broadening of optical transitions in some rare-earth-ion-doped materials [56]. For a given ion, the sum of all interactions with the dipole moments of all other ions in the material causes a permanent energy shift of the order of a few GHz, i.e. the same order of magnitude as the typical inhomogeneous linewidths. This is consistent

with the fact that the inhomogeneous linewidth is seen to scale linearly with dopant concentration [52]. This scaling implies that it is difficult to increase the spectral density of ions, which would be desirable in quantum computing applications, by increasing the dopant concentration.

Ion-ion interactions can also cause *satellite lines* in the inhomogeneous line structure. These weakly absorbing structures lie outside the main inhomogeneous absorption line and can be attributed to pairs or clusters of ions that are located so close to each other that their interaction causes a large shift in the optical resonance frequency [30,56]. Such lines can be of importance for quantum computing in RE materials, since they correspond to ions with a known strong interaction, which is useful for performing quantum logic operations.

SUMMARY

- The experiments discussed in this thesis have been performed using inorganic dielectric crystals (Y_2SiO_5, $YAlO_3$, YAG, $KY(WO_4)_2$, …) doped with a low concentration of rare-earth elements (Pr, Eu, Tm, Ho, …).
- The crystal samples are kept at low temperatures (2-4 K) where the dopant ions are relatively undisturbed by phonons and behave much as a "frozen gas".
- The rare-earth ions are manipulated with laser light, on (zero-phonon) optical transitions from the lowest Stark level of the ground state J-multiplet to the lowest Stark level of an electronically excited state.
- The optical transitions have long coherence times, T_2, and hence narrow homogeneous linewidths, Γ_h.
- The transitions have an inhomogeneous width, Γ_{ih}, which is many orders of magnitude greater than the homogeneous linewidth.
- Subsets of ions can be addressed by tuning the laser light to a particular frequency position (frequency channel) within the inhomogeneous absorption line.
- Some materials have long-lived hyperfine levels in the ground state, which provides a mechanism for storage of information.
- Application of a static magnetic field causes Zeeman splitting of the degenerate hyperfine levels and may increase lifetimes and coherence times by inhibiting spin flips in the host.
- Application of a static electric field causes a Stark shift of the optical absorption frequency, due to different static electric dipole moments in the ground and excited states.
- The ions can be distributed among sites with different orientations and will then be differently affected by externally applied fields and by light of definite polarisation.
- Ions that are situated close to each other will interact, e.g. through dipole-dipole interactions.

CHAPTER 3

SPECTRAL HOLE-BURNING

The homogeneous absorption linewidth in rare-earth-ion-doped crystals, i.e. the resonance linewidth of individual absorbers, is significantly narrower than the inhomogeneous linewidth, i.e. the total spectral width over which the absorbers are distributed. This makes it possible to selectively excite ions absorbing at a particular frequency, using a narrowband light source. Such an excitation causes a decrease in absorption at that frequency, seen as a *spectral hole* in the inhomogeneous absorption profile. Spectral hole-burning is a powerful spectroscopic tool, making it possible to overcome the resolution limit imposed by inhomogeneous broadening due to strains and imperfections. It can also be the basis for applications such as frequency domain optical memories and spatial-spectral filters. In the work presented in this thesis, optical hole-burning has been used to characterise the state and dynamics of rare-earth ions, but also as a tool for preparing groups of ions in specific states and for tailoring the absorption within part of the inhomogeneous absorption profile. In Paper II, some recently developed hole-burning techniques are described and a brief discussion of conventional hole-burning is included. Reviews of the science and applications of persistent spectral hole-burning can be found in Ref. [59] and an overview of hole-burning spectroscopy work done in rare-earth-ion-doped (RE) materials can be found, e.g. in Refs. [20] and [21].

3.1 Persistent spectral hole-burning

In a typical hole-burning experiment, a laser selectively excites a narrow portion of an inhomogeneous absorption line, and the absorption is bleached as absorbers are removed from the ground state. This can be seen by scanning the laser frequency through the originally excited frequency while monitoring transmission, fluorescence or the light diffracted off the spectral hole [59,87]. Assuming a Lorentzian line profile, the observed frequency width of the hole, Γ_{hole}, will be twice the homogeneous linewidth of the absorbers, provided that the laser linewidth is considerably narrower than Γ_h, or otherwise twice the laser linewidth. This can be intuitively understood by noting that the laser interacts twice with the absorption line – once during burning and once during read-out. The spectral hole will remain as long as the population difference between the ground and the excited state (n_g- n_e) differs from thermal equilibrium, e.g. until all absorbers have returned to the original ground state. The width, shape and relaxation dynamics of the hole can reveal much information about the absorbers which would otherwise be hidden by the inhomogeneous broadening of the optical transition. Both transient [88] and persistent [89,90] spectral hole-burning in solids were first demonstrated in 1974 and have been used extensively since then.

3.1.1 Long-lived spectral holes

Permanent or semi-permanent holes will occur if some absorbers are transferred to a long-lived reservoir state and can no longer absorb at their original frequency. Such *persistent hole-burning* may be due to photo-ionisation [91] or photochemical reactions [89,92], or

due to absorbers being trapped in a metastable electronic energy level. If the process only occurs when a second laser field is present it is known as *photon-gated hole-burning* [93].

In a material where the ground state is split into sublevels, with an energy separation larger than the homogeneous linewidth, persistent hole-burning may occur due to population redistribution among the sublevels. This type of hole-burning is common in RE materials with zero-field hyperfine splitting or where the ground state is split into Zeeman levels by an applied magnetic field. It is a form of optical pumping [94,95], as the holes appear when ions are excited from one hyperfine level and relax to another level. If there are several sublevels in the excited state, *side-holes* will appear at frequencies corresponding to each of the transitions from the ground state level with depleted population, in addition to the hole at the burning frequency. *Anti-holes*, i.e. increased absorption, will occur at frequencies corresponding to transitions from the ground state hyperfine levels with increased population, i.e. levels to which ions have been optically pumped. Due to inhomogeneous broadening of the optical transitions, different subsets of ions will have different transition frequencies between ground and excited state levels. Since inhomogeneous broadening is usually large compared with hyperfine splitting, any laser frequency inside the inhomogeneous line will be resonant with all possible optical transitions, but for different subsets of absorbers. Burning at a single frequency therefore creates a complex pattern of side-holes and anti-holes, see Fig. 3.1.

3.1.2 Hole-burning spectroscopy

Such a *hole-burning spectrum* contains much information about the absorbers that are being studied. The frequency separations between side-holes and between anti-holes give direct information about the hyperfine splittings of the excited and the ground state, respectively. If a rare-earth-ion-doped material contains different isotopes of the same RE element, the different isotopes usually have different hyperfine splittings, which can be studied directly. The hole width gives information about the homogeneous linewidth, as was stated earlier. The relative sizes of the side-holes are related to the relative strengths of the transitions between different hyperfine levels in the ground and excited states. The decay of holes and anti-holes over time gives information about the relaxation between hyperfine levels in the ground state. However, in general it is difficult to extract information about transitions between specific hyperfine levels from a conventional hole-burning spectrum, and for many materials branching ratios and relative transition strengths are unknown. The techniques for tailoring inhomogeneous absorption profiles to reveal ions absorbing on specific transitions, described in Paper II and below, can be very useful for obtaining such information.

If a hole is monitored while an external field is being applied to the material, small Zeeman and Stark interactions can be studied (Fig. 2.4). The hole will be displaced as the transition frequencies are shifted by the field and it will split if ions in different states, or with different orientations, are affected differently by the field. This was used to monitor the splitting of the doubly degenerate spin states in Tm:YAG, as a magnetic field of up to 5 T was applied (Paper VI).

If a large number of ions are excited in the material, interaction between ions may cause their transition frequencies to change, as was described in Chapter 2. This will cause a spectral hole to broaden in frequency and decrease in amplitude, as ions have their resonance frequencies shifted into the hole. The effect was used to characterise dipole-dipole interactions in Tm:YAG (Paper I) and it provides the basic mechanism for selecting

strongly interacting ions from the random distribution of ions in the material, which is necessary for quantum information processing [96] (Cf. Papers I and III).

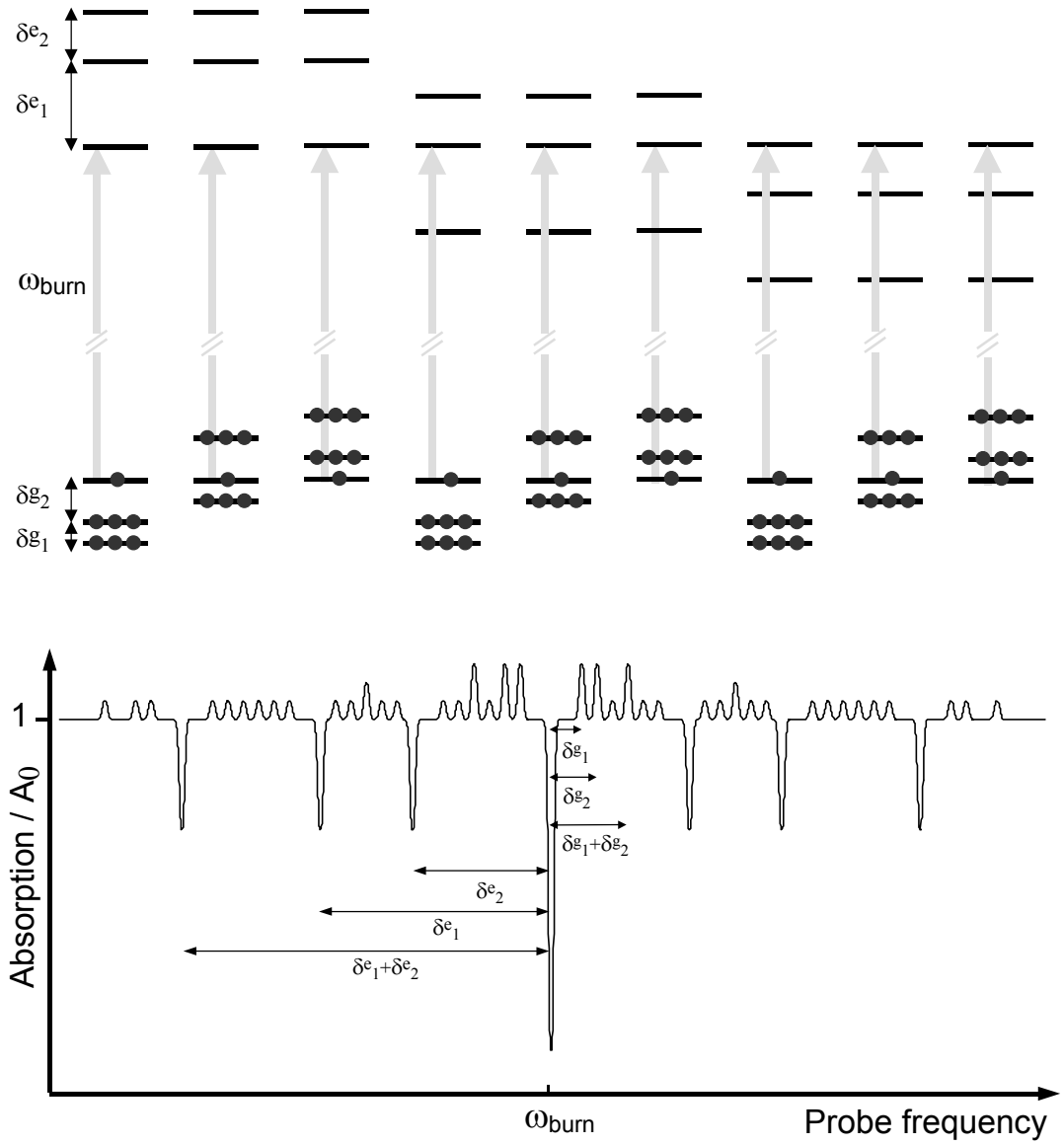

Figure 3.1. *Spectral hole-burning through redistribution of population in the ground state sublevels (optical pumping), for the case of absorbers with three hyperfine levels in the ground state and three hyperfine levels in the excited state. Top: Due to the inhomogeneous distribution of optical resonance frequencies, different absorbers will have different transitions resonant with the burning field. Bottom: The absorption will decrease at the burn frequency, ω_{burn}, and at frequencies corresponding to transitions from ground state hyperfine levels with depleted population, creating a main hole and side-holes. The absorption will increase at frequencies corresponding to transitions from levels with increased population to each of the excited state hyperfine levels, creating anti-holes.*

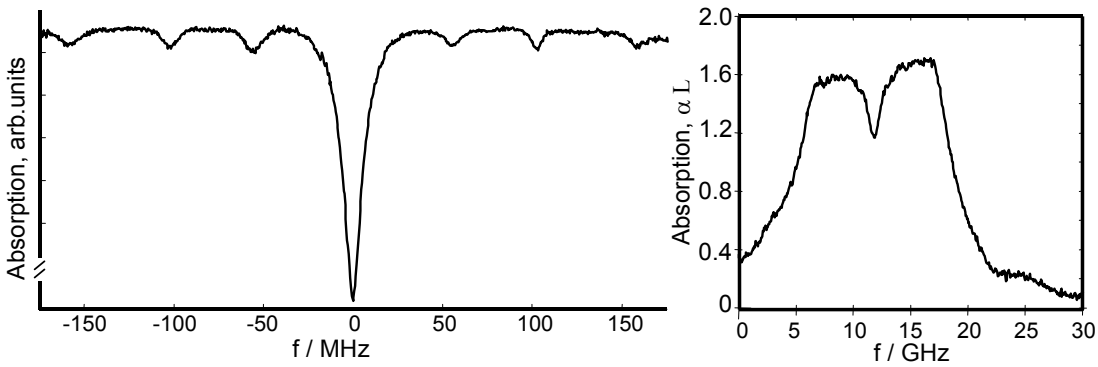

Figure 3.2. *Left: Partial hole-burning spectrum in Ho:YVO_4. The width of the spectral hole is determined by the homogeneous linewidth ($\Gamma_h \approx 15$ MHz). The hole lifetime was of the order of 1 ms. The side-holes at $\delta = \pm 55$ MHz, ± 103 MHz and ± 159 MHz reveal that the hyperfine level separations in the excited state are of the order of 50-100 MHz ($I = {}^7/_2$). Right: The inhomogeneous absorption profile of Ho:YVO_4, before any hole-burning has occurred. The reason for the unusual line profile is not known, but it could be due to the superposition of inhomogeneously broadened transitions from different ground state hyperfine levels, separated by several GHz.*

3.1.3 Applications of persistent spectral hole-burning

In addition to being a spectroscopic technique, spectral hole-burning is also the basis for numerous proposed applications [59], where persistent spectral holes provide a memory mechanism that can be used in processing or storage of information. The basic application is frequency domain data storage [97,98], where the occurrence or absence of a hole is used to signify a logical 0 or 1. In this way one bit of data can be stored in each addressable frequency channel within the inhomogeneous absorption profile, which means that up to Γ_{ih}/Γ_h bits can be stored at a single spatial location in the storage medium. Another application is the use of spectral holes as programmable frequency references [99]. This has been used to frequency stabilise lasers to linewidths of less than 200 Hz [41]. Other applications involving spectral hole-burning mechanisms include time-domain data storage [100-102], spectral-spatial correlation and temporal pattern recognition [103-105], radio-frequency spectrum analysis [106] and optical signal processing [107]. These applications rely on the fact that the material stores interference patterns and temporal Fourier transforms of an incoming field, as spatial-spectral holes. A modulated pulse, sent into the material, will have a specific frequency content and, since the ions are frequency selective, a hole pattern corresponding to the spectral content of the pulse will be engraved in the inhomogeneous absorption profile.

3.2 Tailoring the inhomogeneous absorption profile

In the quantum optics and quantum computing experiments described later in this thesis, rare-earth ions were manipulated by driving optical transitions using coherent light. In many cases it is necessary to first prepare the optical inhomogeneous absorption profile, so that the light only interacts with a selected group of ions, absorbing on a specific transition. This can be done through spectral hole-burning, using optical pumping to move ions between hyperfine levels (nuclear spin states). Some of the long-lived hyperfine levels are used as auxiliary storage states, in which non-participating ions can be deposited, and other designated hyperfine levels are used for storing quantum information.

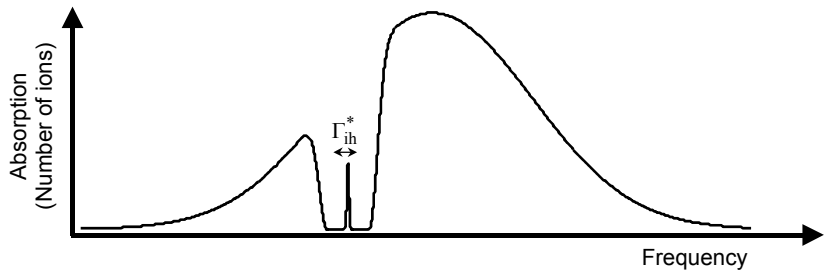

Figure 3.3. *A wide pit, containing almost no absorbing ions, can been cleared within the inhomogeneous absorption line using spectral hole-burning. Inside the pit, a group of ions, absorbing within a narrow frequency interval, is prepared. The width, Γ_{ih}^{*}, of the absorbing peak corresponding to the selected ions can, in principle, be close to the homogeneous linewidth Γ_h. The spectral interval surrounding the structure will be significantly affected by the sequence of burning pulses used in the preparation, but the resulting modulation of the absorption line has been omitted here, for clarity. The figure is not drawn to scale, as the typical spectral widths can be 10 GHz inhomogeneous linewidth, a 10 MHz wide pit and a 50 kHz wide peak.*

For a discussion of hole-burning techniques we assume ions with long-lived ground state hyperfine levels with energy separations δ_1^g, δ_2^g etc. (starting from the splitting between the two lowest states) and an optically excited state with hyperfine splittings δ_1^e, δ_2^e etc. In the Pr^{3+}- and Eu^{3+}-doped materials that we will focus on, there are three doubly degenerate hyperfine levels in the ground and the excited states. The lifetime of the ground state hyperfine levels is several minutes or hours in certain host materials, whereas the lifetime of the optically excited states is of the order of 0.1-1 ms. This means that the optical transition can be cycled – i.e. the ions can be excited and allowed to relax – thousands of times before population relaxation between hyperfine levels becomes significant.

3.2.1 Creating peaks and pits

The basic spectral structure that we wish to create is a narrow peak of absorption, due to an ensemble of selected ions, with a specific optical resonance frequency, on a background of zero absorption. This *spectral peak* can be viewed as the equivalent of a narrow resonance line in a free atom or an atom caught in a trap – systems that are frequently considered for use in quantum optical studies – and it is the basis of the applications suggested in Papers I, II, III and V.

A straightforward method for creating such a structure is by simply burning away the ions in the surrounding spectral interval, i.e. by repeatedly exciting them until they relax to a new hyperfine state. This can be done using phase-modulated pulses [108,109] or chirped pulses [110] that excite a broad spectral interval but leave ions at a central frequency in the ground state.

A more convenient way to create an isolated absorbing peak is to first empty a wide spectral interval of absorbing ions, in the process pumping the ions to an auxiliary hyperfine state, and then shift the laser frequency to pump ions absorbing within a narrow spectral interval back into the emptied region. This method was introduced in Paper I and has subsequently been used in Papers II and III and in Refs. [85] and [111]. In its simplest version, this method prepares a group of ions in a specific hyperfine level in the ground

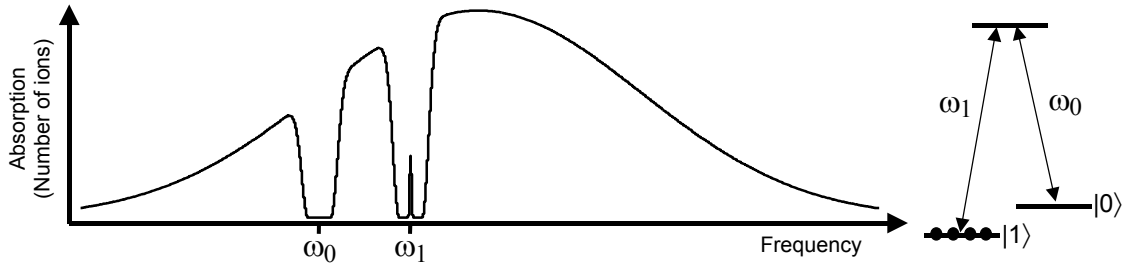

Figure 3.4. *A group of ions is prepared in a specific ground state sublevel, |1⟩, and the surrounding spectral interval is emptied of other ions, using spectral hole-burning. Another pit in the inhomogeneous absorption profile is created in the around the frequency where the ions will absorb if they are in ground state sublevel |0⟩. The selected ions can now be manipulated using light with frequencies* ω_0 *and* ω_1.

state, but this includes several subsets of ions, absorbing to different hyperfine levels in the excited state. Using more elaborate schemes it is possible to select only a subset of ions absorbing on a transition between specific hyperfine levels in the ground and excited states. This involves hole-burning/optical pumping at several frequencies, separated by suitable combinations of the hyperfine splittings (δ_1^g, δ_2^g, δ_1^e, δ_2^e, etc). See Paper II.

One bit of quantum or classical information can be stored by putting ions, absorbing at a particular frequency within the inhomogeneous absorption profile, in a specific hyperfine state or superposition of hyperfine states. The state of the ions is manipulated by optical coupling to an excited state. In order to address the same ions on several different transitions, going from different ground state hyperfine levels, it is necessary to create several pits in the absorption profile, at frequency distances corresponding to the separations between the hyperfine levels, δ_1^g, δ_2^g etc. In total, in order to prepare and manipulate a group of ions it is necessary to access a frequency range of the order of $\delta_{tot}^g + \delta_{tot}^e$, where δ_{tot}^g and δ_{tot}^e are the total hyperfine splitting of the ground and excited state, respectively. This can be done by using external optical frequency modulators or direct modulation of the laser source. The spectral structure can be prepared at any position within the inhomogeneous absorption profile and several such structures, corresponding to several bits of information, can be prepared at different frequencies.

The reason for isolating ions absorbing on a zero background, i.e. with no absorption on nearby frequencies or on other transitions, is partly that there may be very few ions participating in the process under study, so any signal from non-participating ions, in the following called *spectator ions*, may drown the signal of interest. Also, any excitation of spectator ions may lead to unwanted ion-ion interactions, as described in Section 2.7. Therefore, the possibility of creating *spectral pits*, i.e. wide spectral regions completely empty of resonant ions, has been examined in some detail as part of the work presented in this thesis.

3.2.2 Burning "all the way down"

Experiments were performed in Eu-doped $YAlO_3$, to see to what extent a spectral interval can be emptied of ions by repeated hole-burning, i.e. how deep a hole can be burned. The number of ions still resonant with the burning frequency was detected by monitoring the decrease in fluorescence as ions were burned away. When analysing repeated hole-burning, it can be assumed that all transitions between different hyperfine levels in the

ground and the excited states can be saturated with a pulse shorter than the excited state lifetime, so that close to 50% of the ions resonant with the laser are excited. It is often further assumed that the ions have equal probability of relaxing to each of the hyperfine levels in the ground state, since they relax through a complex route of transitions. Then the fraction of ions still absorbing at the laser frequency, n/n_0, after N hole-burning pulses can be calculated as

$$\frac{n}{n_0} = \left(1 - p\left(\frac{d-1}{d}\right)\right)^N \tag{3.1}$$

where p is the probability that an ion will be excited and d is the number of frequency separated hyperfine levels in the ground state. Thus for Eu:$YAlO_3$, with d=3 and assuming p≈0.5, less than 0.1% of the ions should be left after applying only N=20 burning pulses. However, the experiments indicated that approximately 0.5% of the ions remained, even after many seconds of burning, corresponding to thousands of excitation-relaxation cycles. Various explanations of the remaining resonant absorbers have been suggested, e.g. mechanisms that make some ions relax between hyperfine levels faster than average. An important contributing factor is probably that the exciting field has a small broadband component or contains weak spurious frequencies. This would excite ions absorbing outside the hole and might also re-pump some ions back into the hole. This is one reason why a narrowband and spectrally pure laser source is necessary if these materials and methods are to be used for applications in quantum information science.

Laser light inside a spectral pit emptied of all absorbing ions will also cause *off-resonant excitation* of ions outside the pit. The ions have a finite linewidth, Γ_h, and a Lorentzian resonance line-shape with wings stretching far out in frequency. Since the spectral hole/pit occurs within a wide inhomogeneous absorption line, the integrated absorption from ions outside the hole places a fundamental limit on how far the absorption can be reduced, in the case where the laser source has a narrower bandwidth than the ions. The off-resonance single-atom absorption cross-section, as a function of frequency detuning, $\Delta\nu$, can be written as

$$\sigma(\Delta\nu) \propto \frac{1}{\pi T_2} \frac{1}{(2\pi\Delta\nu)^2 + (1/T_2)^2} \propto \frac{1}{1 + (2\Delta\nu/\Gamma_h)^2} \tag{3.2}$$

showing the familiar Lorentz shape with a full-width at half maximum (FWHM) of Γ_h. The remaining absorption in the centre of a pit, with a spectral width $\delta << \Gamma_{ih}$, compared with the full absorption in an undisturbed line, can be calculated as

$$\frac{A(\delta)}{A(0)} = \frac{\int_{-\infty}^{-\delta/2} \frac{1}{1+(2\nu/\Gamma_h)^2} d\nu + \int_{\delta/2}^{\infty} \frac{1}{1+(2\nu/\Gamma_h)^2} d\nu}{\int_{-\infty}^{\infty} \frac{1}{1+(2\nu/\Gamma_h)^2} d\nu} = 1 - \frac{2}{\pi}\arctan\frac{\delta}{\Gamma_h} \approx \frac{2}{\pi}\frac{\Gamma_h}{\delta} \tag{3.3}$$

where the last equality holds for large values of (δ / Γ_h). According to this, if we burn a pit with a width of $\delta = 1000 \cdot \Gamma_h$ in the inhomogeneous absorption profile, the remaining

absorption (probability of exciting ions) for laser frequencies within the pit will be approximately 0.1% of the original absorption, assuming a perfectly monochromatic source.

3.2.3 Erasing spectral structures

Apart from tailoring the inhomogeneous absorption profile, optical pumping can also be used to erase structures that have been burnt into the absorption profile. By applying radiation within a wide spectral interval ($>>\delta^{g}_{tot}+\delta^{e}_{tot}$) for some time, the ions will be excited from all of the ground state hyperfine levels and cycled through the excited state many times. The population distribution will eventually reach an equilibrium-like state, possibly with some amount of order given by the spectral distribution of the light and by the branching ratios of the spontaneous relaxation. Since population relaxation between hyperfine levels may otherwise take hours or days, this is a good way of creating a standard initial state for experiments. Another way to erase spectral holes is to raise the temperature temporarily, which increases the rate of relaxation.

3.3 Designing hole-burning sequences

The hole-burning schemes used to prepare the inhomogeneous absorption lines in rare-earth-ion-doped solids all involve burning at several different frequencies, using up to 1000 laser pulses. The design of appropriate pulse sequences must take into account the fact that the same ions can absorb at several different frequencies and it can be complicated by coincidences between absorption frequencies for ions in different states and by the linewidths of laser and atoms. This will restrict the width of the pits that can be created and the transitions that can be isolated from absorption on other transitions.

To see where the complexity stems from, one can consider a material where the ions have three hyperfine levels in the ground and excited states. These ions can emit or absorb light at nine different frequencies, depending on what state they are in. Expressed differently, because of the inhomogeneous broadening of the optical transition, there are nine different classes of ions at each frequency, with transitions between different hyperfine states resonant with that frequency. Although the total inhomogeneous absorption line may be viewed as the sum of nine different inhomogeneously broadened transitions (between different hyperfine states), it is important to note that the lines are not independent, as the same ions will contribute to absorption at three different frequencies, corresponding to excitation to each of the three excited state hyperfine levels. If the ions are pumped to another ground state hyperfine level, the absorption at these three frequencies will decrease and the absorption at three other frequencies will increase.

3.3.1 Computer simulations

During the course of this work, a computer program for simulating the effect of optical hole-burning in RE materials with metastable sublevels in the ground state was developed. This made it possible to reproduce and analyse experimental results and to predict the effect of applying a hole-burning sequence to a sample, i.e. what the resulting absorption profile would look like, and what transitions the ions at a particular frequency would be absorbing on. The main ideas behind the program follow below.

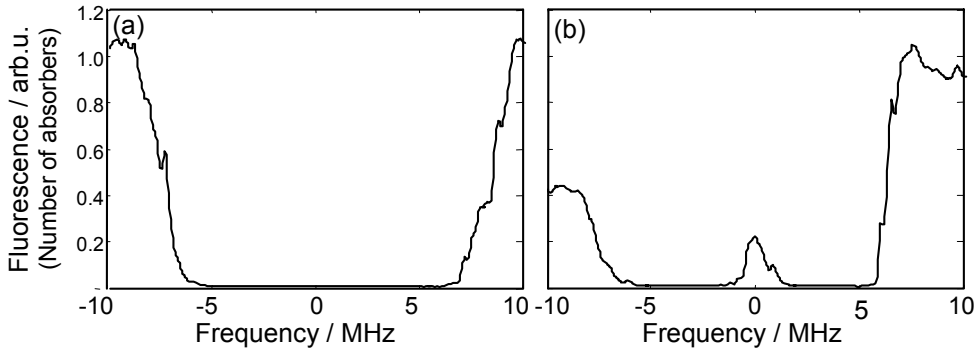

Figure 3.5. *Preparation of a spectrally narrow packet of ions within the inhomogeneously broadened $^7F_0$ - $^5D_0$ transition in Eu^{3+}:$YAlO_3$. The amount of Eu ions absorbing at a particular frequency has been measured by recording laser induced fluorescence. (a) A 12 MHz wide interval has been completely emptied of absorbing ions through spectral hole-burning. (b) A group of ions has been pumped back into the pit, by shifting the laser frequency by 69 MHz to excite ions from an auxiliary ground state hyperfine level and let them relax into a new hyperfine level.*

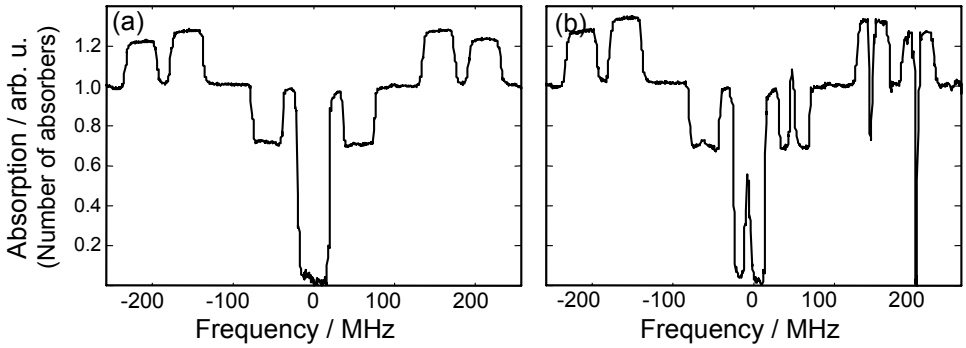

Figure 3.6. *Preparation of a spectrally narrow packet of Tm ions in YAG, using persistent spectral hole-burning in the $^3H_6$ - $^3H_4$ transition in Tm^{3+}:YAG in a strong magnetic field. (a) A wide spectral pit is created in the absorption profile. The data has been normalised and some absorption may remain in the pit. (b) The laser frequency is shifted, to burn at a single frequency approximately 200 MHz from the pit (corresponding to the Zeeman splitting of the ground state). This pumps a peak of ions back from the Zeeman level to where they were pumped by the previous step. The structure outside the central pit can be viewed as holes and anti-holes, created by the hole-burning.*

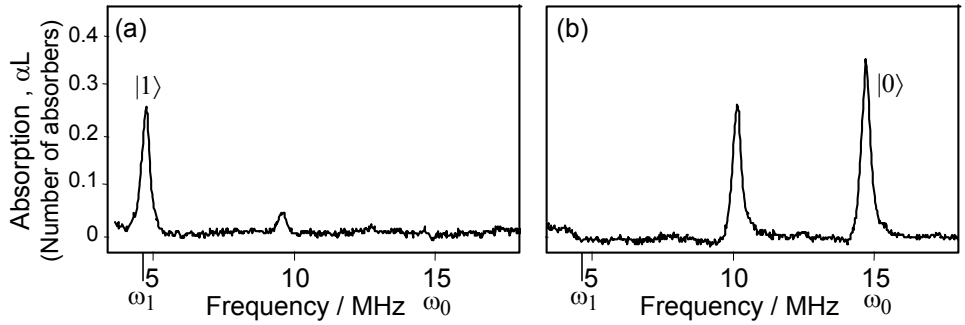

Figure 3.7. *Ions absorbing within a spectral pit in the inhomogeneously broadened $^1D_2$ - $^3H_4$ transition in Pr^{3+}:Y_2SiO_5. (a) Ions prepared in ground state hyperfine level $|1\rangle$ and absorbing to a specific sublevel in the excited state. (b) The same ions, transferred to level $|0\rangle$ in the ground state. The additional (unmarked) peaks of absorption are due to the same ions absorbing on transitions going to other sublevels of the excited state. In this material, the resonance frequencies, ω_0 and ω_1, of the transitions from states $|0\rangle$ and $|1\rangle$ to the excited state can occur within a single pit. The separation between states $|0\rangle$ and $|1\rangle$ (ω_1-ω_0) is 10.2 MHz.*

- The ions are divided into a large number of classes, or frequency channels, according to the resonance frequency of the transition from the lowest hyperfine level in the ground state to the lowest hyperfine level in the excited state, for example considering ions within a 100 MHz spectral interval, divided into 0.05 MHz wide frequency channels.
- For each class, a record is kept of the number of ions in each of the ground state hyperfine levels. If several isotopes, or otherwise non-equivalent ions, are present, they are kept track of independently.
- At any point during the simulation, the total absorption, or the absorption on a specific transition, or from a specific sub-set of ions, can be plotted. For each frequency the current population of each of the classes and states causing absorption at that frequency is added, to obtain the total absorption.
- The effect of burning pulses is simulated by removing a fraction, p, of the ions from each of the resonant states and classes. In an experiment p would correspond to the excitation efficiency of the burning pulse. The ions are distributed among the ground state hyperfine levels according to the assumed branching ratios.
- The effect of spectrally broad or frequency-chirped pulses is simulated by repeating the procedure for a range of frequency channels.

As can be seen, some simplifications have been made in the model. The effects of hyperfine relaxation are neglected, since the relaxation is very slow in the materials that were used in experiments, but they could easily be incorporated. All ions are assumed to relax between burning pulses, i.e. stimulated emission or coherent driving of the transitions is not included in the model. The probability of excitation, p, is introduced rather casually and in most cases the same value was used for all transitions, even when the transition probabilities were known to be different. This is because in most cases it is the presence or absence of resonant ions, after a large number of burn pulses, which is of interest, rather than the absolute number. In practice, the hole-burning efficiency can usually be fine-tuned by varying the length or number of burning pulses.

Among other things, the computer simulations successfully explained why a simple hole-burning sequence applied to Eu^{3+}:Y_2SiO_5 did not quite produce the intended qubit structure (Paper I). The program was also used extensively in the planning and analysis of the experiments presented in Papers II and III.

SUMMARY

- Spectral hole-burning occurs when ions absorbing at a specific frequency within the inhomogeneous absorption profile are removed from the ground state through optical excitation, which bleaches the absorption at that frequency.
- In many rare-earth-ion-doped materials, persistent spectral holes occur due to optical pumping, which redistributes ion population between the metastable hyperfine levels. That is, ions are excited from one hyperfine level and relax to another level, from where they no longer absorb at the original frequency.
- Since the inhomogeneous broadening is usually large compared with the hyperfine splitting, different subsets of ions will have different optical transition frequencies between ground and excited state levels. Any laser frequency inside the

inhomogeneous line will initially be resonant with all possible optical transitions, but for different subsets of absorbers.

- Using hole-burning it is possible to create spectral pits, i.e. wide frequency intervals within the inhomogeneous absorption profile that are completely empty of all absorption. The maximum width of the pits is determined by the hyperfine level separations.
- It is possible to prepare narrow absorbing peaks on a non-absorbing background, i.e. isolated spectral features corresponding to a group of ions absorbing at a specific frequency. The peaks can have a width of the order of the homogeneous linewidth if a laser with a sufficiently narrow linewidth is used for the preparation.
- Using a sequence of hole-burning pulses, it is possible to prepare the inhomogeneous absorption profile such that selected groups of ions can be manipulated on specific optical transitions without the light interacting with other ions and other transitions.

CHAPTER 4

COHERENT LIGHT-MATTER INTERACTION

The discussion in the preceding chapter concerned experiments where light is used to transfer atoms between states with a specific energy, i.e. *energy eigenstates*. The basic requirement for this is that the energy of the light matches the energy difference between the two states. However, for many of the experiments described later in this thesis, it is also necessary that the light is coherent, i.e. that there is a well-defined phase relation between two points in the light wave. We also need a description of the state of an atom where an atom can not only be in specific energy states (with a certain probability), but also in a *coherent superposition* of such states, with an associated phase. In this chapter, the interaction between coherent light and absorbers with long-lived coherences will be described and some comments will be given on how the quantum state of an atom can be manipulated using light.

This chapter also contains a brief description of coherent transient phenomena, such as *photon echoes* [112] and *free induction decay* [113], which occur when an ensemble of atoms emit coherent light after interacting with an applied electromagnetic field. These phenomena are the basis for many of the experiments and techniques described in this thesis and are also the basis for many related techniques for optical processing of classical information. A study of coherent transients can give insight into the coherent behaviour of atoms on the quantum level. Many RE materials are good *photon-echo materials*, i.e. they are well suited for study or applications of coherent transients and this is a main reason why they are now considered for use in quantum optics and quantum information science.

In this chapter the atoms will mainly be approximated by *two-level systems*, i.e. systems with only two stationary states (energy eigenstates). Two-level systems play an important role in the theory of quantum mechanics, partly because they are relatively simple to analyse. Many of the basic building blocks of the world around us are two-level systems and they appear in physics in a multitude of varieties. A nice consequence of quantum mechanics is that all kinds of two-level systems are in a sense equivalent, so that when the behaviour of one type of system has been analysed, the results can often be directly transferred to all other two-level systems. In general, atoms have a large, or infinite, number of eigenstates, but in many cases it is sufficient to consider only two or three levels in order to understand the physics of a situation. This is the case when an atom interacts with electromagnetic radiation with an energy that is equal to, or nearly equal to, the energy difference between two specific states.

Much of the theory of coherently driven two-level systems was originally developed for nuclear spins driven by a radio-frequency (RF) field, and many of the terms and ideas outlined below originate from the field of *nuclear magnetic resonance* (NMR). As coherent radiation at optical frequencies (laser light) has become available, the optical

equivalents of many NMR techniques and experiments have been demonstrated. Interestingly enough, there is now a flow of information in both directions, as some techniques involving coherent interactions between radiation and matter are first developed in the optical regime and later applied in NMR. However, it is still a technological challenge to achieve the same control of the electromagnetic field at optical frequencies (~500 THz) and timescales (down to fs), as can be achieved in NMR.

Coherent optical interactions are treated in many textbooks. The book by Allen and Eberly [114] provides a comprehensive treatment of the basic principles behind optical resonance phenomena and two-level atoms. Similar descriptions can be found in Refs. [115-117]. The work by Shoemaker [118] is useful because it contains detailed analyses of coherent optical interactions between light and an inhomogeneously broadened ensemble of absorbers, and of various types of coherent transient spectroscopy. In most cases, the authors deal mainly with the interaction between monochromatic light and atoms with a single resonance frequency. However, if the light interacts with an inhomogeneously broadened resonance line, atoms with different resonance frequencies will respond differently to the field. The response of the material to the light will be the sum of the responses of all the different frequency channels.

4.1 Coherently driven two-level systems

4.1.1 A two-level atom interacting with electromagnetic radiation

The state of an atom with two energy levels, a ground state |g> and an excited state |e>, can be written as

$$\left|\psi(t)\right\rangle = c_g(t)\left|g\right\rangle + c_e(t)e^{-i\omega_{ge}t}\left|e\right\rangle, \tag{4.1}$$

where ω_{ge} is the (angular) resonance frequency of the atomic transition, $\omega_{ge} = \left(E_g - E_e\right)/\hbar$. The coefficients $c_g(t)$ and $c_e(t)$ are the *probability amplitudes* of states $|g\rangle$ and $|e\rangle$, and $|c_g(t)|^2$ and $|c_e(t)|^2$ are the probabilities of finding the atom in the ground or the excited state, respectively. Thus, we require

$$\left|c_g(t)\right|^2 + \left|c_e(t)\right|^2 = 1. \tag{4.2}$$

In the *dipole approximation*, the interaction of the atom with a time-varying electric field **E**(t) can be described by the perturbation

$$V(t) = -\boldsymbol{\mu}_{ge} \cdot \mathbf{E}(t) \tag{4.3}$$

where μ_{ge} is the transition dipole moment,

$$\boldsymbol{\mu}_{ge} = -e\left\langle g\left|\mathbf{r}\right|e\right\rangle. \tag{4.4}$$

Introducing the Hamiltonian of the unperturbed atom, H_0, the time evolution of the atom coupled to a field will be governed by the following Hamiltonian

$$H = H_0 + V(t) \tag{4.5}$$

and by the Schrödinger equation. All other interactions apart from that between the atom and the field are disregarded, or included in the model in the form of decoherence or relaxation towards an equilibrium state. If such interactions with an environment are present, the state can no longer be described as a *pure state* as in Eq. 4.1, but must instead be described as a *mixture* of such states.

In the semi-classical model outlined in this chapter, the electromagnetic field is described as a classical continuous field, rather than as a stream of photons. When effects arising from the quantisation of the electromagnetic field are studied, as in Chapter 7 it will be necessary to refine the model. Here we assume the field to be monochromatic, possibly with a slowly varying amplitude, $E_0(t)$, and linearly polarised:

$$\mathbf{E}(t) = E_0(t)\hat{\mathbf{e}}\cos(\omega_L t)\,. \tag{4.6}$$

Using the equations above, solutions are obtained where the atomic state changes at a rate which depends on the strength of the interaction, i.e. the transition dipole moment and the amplitude of the field, and on the detuning between the laser frequency and the resonance frequency of the atomic transition. In obtaining these solutions, the so-called *rotating wave approximation* is usually made, where a reference frame (reference phase), rotating with the frequency of the atomic transition or with the laser frequency, is introduced. The amplitude of the laser field is assumed to change slowly compared with the oscillations on the carrier frequency, ω_L, and terms oscillating with frequency $2\omega_L$ are assumed to average to zero and are excluded.

4.1.2 The Bloch vector picture

A convenient way of describing the state of a two-level atom and its evolution is by using the *Bloch vector* and the *Bloch equations*. This formalism was introduced in the 1940s, to describe nuclear spins coupled to static and oscillating magnetic fields [119,120], but it is useful for describing any two-level system.

A new coordinate system is introduced, where the new (real valued) coordinates *u, v* and *w* can be expressed in terms of the probability amplitudes $c_g(t)$ and $c_e(t)$, as

$$\begin{aligned} u(t) - iv(t) &= 2 \cdot c_g(t) \cdot c_e^*(t) \\ w(t) &= |c_e(t)|^2 - |c_g(t)|^2 \end{aligned} \tag{4.7}$$

The coordinate w expresses the level of *inversion*, i.e. the probability of finding atoms in the excited state compared with the probability of finding them in the ground state. u and v express the part of the atomic state that oscillates coherently at frequency ω_{ge}, with u being the component that oscillates in phase with the applied electromagnetic field, and v being the component in quadrature (90° out of phase) with the field. For an atomic wavefunction describing the electron distribution, u and v will correspond to an oscillating electric dipole moment (polarisation), which can absorb or emit radiation. Different labelling of the coordinates is often used by different authors depending on the two-level system being described. X, Y and Z or r_1, r_2 and r_3 are also widely used, instead of u, v and w.

The atomic state is visualised as a vector, the *Bloch vector* (also known as the *state vector*, *pseudo-spin* or *electric dipole vector*), going from the origin to the point (u, v, w). For an atom in a pure quantum state, the vector will be normalised according to $u^2 + v^2 + w^2 = 1$ and will thus point somewhere on the unit sphere – the *Bloch sphere*. If the Bloch vector is used to represent an ensemble average, and relaxation and dephasing are included in the model, the vector can point at any position inside the sphere. For example, the ground state of an atom is represented by a vector pointing in the negative w direction, with w=-1 and u=v=0, since there is no coherent superposition between the ground and excited states. A vector with u=1, v=0 and w=0 represents a 50/50 superposition state, oscillating in phase with the applied field, and a vector with u=v=w=0 represents a completely mixed state, with equal probability of finding the atom in any state.

For convenience, some additional variables are introduced: the (angular) *Rabi frequency*, Ω, which is a measure of the strength of the interaction between an atom and a resonant laser field;

$$\Omega = \frac{\mathbf{E} \cdot \boldsymbol{\mu}_{ge}}{\hbar} \ , \tag{4.8}$$

the *detuning*, Δ, which is the difference between the laser frequency and the resonance frequency of the atomic transition;

$$\Delta = \omega_{ge} - \omega_L \tag{4.9}$$

and the *generalised Rabi frequency*, which can be said to describe the rate of change of the phase of the atomic state relative to the phase of the laser field

$$\Omega_G = \sqrt{\Omega^2 + \Delta^2} \ . \tag{4.10}$$

The dynamics of the Bloch vector, i.e. of the atomic state, in the rotating reference frame, can now be expressed in the form of the optical *Bloch equations*:

$$\begin{aligned} \frac{\partial u}{\partial t} &= -\Delta v - \frac{u}{T_2}, \\ \frac{\partial v}{\partial t} &= \Delta u + \Omega w - \frac{v}{T_2} \\ \frac{\partial w}{\partial t} &= -\Omega v - \frac{w - w_{eq}}{T_1} \end{aligned} \tag{4.11}$$

where we have introduced the phenomenological decay constants T_1 and T_2. $1/T_1$ is the rate at which the atoms relax towards equilibrium, and $1/T_2$ is the rate at which collisions or other random dephasing interactions occur. The presence of dephasing (finite T_2) will cause the Bloch vector to shrink towards the w-axis and the presence of relaxation (finite lifetime, T_1) will cause it to sink towards the equilibrium state, usually w_{eq}=-1. An upper bound on the coherence time is given by $T_2 \leq 2T_1$, with equality if the coherence is only limited by natural decay.

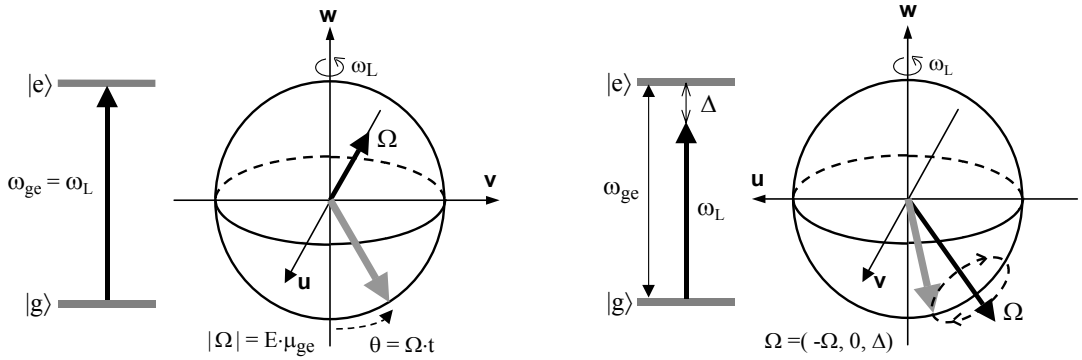

Figure 4.1. *The state of a two-level system can be represented by a state vector inside a unit sphere, the Bloch sphere, where the north and the south poles (w=±1) represent the energy eigenstates |e⟩ and |g⟩ . Left: If the transition between the two states is driven by a resonant electromagnetic field, the Bloch vector will rotate around a pseudo-vector, Ω, pointing along the u axis. Right: If the field is not resonant, i.e. has some detuning, Δ, the pseudo-vector will have an angle to the u axis and the Bloch vector will rotate around this vector at a rate proportional to |Ω|.*

The interaction with the laser field causes the Bloch vector to precess in the (u,v,w) system, around a *pseudo-vector* Ω=(-Ω , 0, Δ), at a rate proportional to the length of the pseudo-vector. If the laser field is perfectly resonant (Δ=0), the pseudo-vector will point in the -u direction and a Bloch vector starting in the ground state (0,0,-1) will rotate through the v-axis, up to the excited state (0,0,1) and then back to the ground state. If the interaction continues, the atom will continue to move up and down between the ground and the excited states – a phenomenon known as *Rabi flopping* or *optical nutation* [121].

The quantity

$$\theta = \Omega \cdot t = \frac{\mu E_0}{\hbar} t \tag{4.13}$$

is known as the *pulse area* and corresponds to the angle through which the Bloch vector of a resonant atom is rotated by the interaction with the laser field. Thus, a *π-pulse*, i.e. a pulse with θ=π, will rotate the state vector 180°, e.g. from the ground state to the excited state, or vice versa. A *π/2-pulse* can, for example, take the Bloch vector from one of the poles (w=-1 or w=1) into the u-v plane or vice versa.

If the laser field is somewhat detuned from resonance (Δ≠0), the pseudo-vector will point slightly up or down from the u-v plane, depending on whether the detuning is to higher or lower frequencies. The inversion, i.e. the w-component of the Bloch vector, will also in this case oscillate between a maximum and a minimum value, but it will never reach full inversion, i.e. w=1. The inversion of an atom starting in the ground state, i.e. w(t=0)=-1, can be explicitly expressed as

$$w(t) = -\frac{\Delta^2 + \Omega^2 \cos \Omega_G t}{\Omega_G^2}. \tag{4.12}$$

For small pulse areas (low optical intensity or short pulse duration), the amount of excitation, on resonance, can be approximated by $\sin^2|\theta/2| \approx \theta^2/4$ (cf. Fig 4.1), which implies a linear dependence on the optical intensity, as would be expected. In the case of temporally complex pulses (e.g. a data sequence), applied to a material with an inhomogeneously broadened absorption line, the effective pulse area experienced by an atom absorbing at frequency ν_a can be calculated [100,122] in the frequency domain as

$$\theta(\nu_a) = \frac{2\mu}{\hbar}\left|E(\nu_a)\right|, \tag{4.14}$$

where $E(\nu_a)$ is the Fourier transform of the electric field amplitude of the pulse, E(t). This means that the state of the atomic ensemble will contain all the information on the Fourier transform of the applied field.

In the Bloch equations above, we have taken the phase of the laser as the reference phase. An atomic state oscillating at a frequency different from ω_L, i.e. with $\Delta \neq 0$, will acquire a phase difference relative to the laser over time, which corresponds to a rotation in the u-v plane. Alternatively, this can be seen by noting that if the field amplitude is zero, the pseudo-vector will be $\Omega=(0,0,\Delta)$, which means that the free evolution of an atom is described by rotation around a vector pointing along the w-axis, at a rate proportional to Δ.

In order to complete the description of the interaction between the atoms and the radiation field, the Bloch equations should be complemented to include the action of the atoms on the field. An atom in a superposition state can be seen as a small electric dipole, oscillating at the transition frequency ω_{ge}. An ensemble of atoms can give rise to a macroscopic polarisation which will affect the field according to Maxwell's equations. In this context, u and v are sometimes called the electric dipole dispersion and absorption components, respectively. Atoms 90° out of phase with the incoming laser field, with a negative v component, will emit radiation 180° out of phase with the field. They thus cancel some of the incoming radiation, which is interpreted as absorption. Atoms oscillating with the opposite phase, with a Bloch vector pointing in the positive v direction, will emit radiation in phase with the applied field, which is seen as stimulated emission.

The polarisation density caused by an ensemble of atoms with a distribution of resonance frequencies can be written

$$P(t) = N\mu_{ge}\int_{-\infty}^{\infty} v(t,\Delta)g(\Delta)d\Delta \tag{4.15}$$

where N is the density of atoms, μ_{ge} is the transition dipole moment and $g(\Delta)$ is a normalised function describing the shape of the inhomogeneous absorption line. For an electromagnetic wave travelling in the positive z direction through a medium with (nearly) resonant two-level atoms, Maxwell's wave equation, coupling to the Bloch equations (Eq. 4.11), can be written in the form [114,123]

$$\frac{\partial\Omega(z,t)}{\partial z} + \frac{n}{c}\frac{\partial\Omega(z,t)}{\partial t} = \frac{\alpha_0}{2\pi}\int_{-\infty}^{\infty} v(z,t,\Delta)g(\Delta)d\Delta \ . \tag{4.16}$$

Here n is the refractive index of the medium, c is the velocity of light in vacuum and α_0 is the frequency-integrated absorption, which may be calculated using $\alpha_0=\alpha(\omega_0)/g(\omega_0)$. We see that if the polarisation, integrated over all atoms at a specific spatial location, is non-zero, Ω will be increased or decreased, i.e. light will be emitted or absorbed by the atoms. In an optically thick medium, i.e. when $\alpha L>>1$, this coupling can give rise to interesting propagation phenomena, such as the formation of solitons and self-induced transparency [124]. The second term on the left-hand side of Eq. 4.16 can be neglected if the envelop of the field varies slowly compared with L/c, where L is the length of the medium through which the wave propagates. This exclusion makes direct integration of the equation possible and the combination of Eq. 4.11 and Eq. 4.16 can be conveniently used in numerical simulations of pulse propagation through a medium with resonant atoms. The equations above are valid for a quasi-monochromatic field with a fixed phase and must be augmented to include the possibility of polarisation in both quadratures, if the interaction with a field with a time-varying phase or frequency is to be analysed. Numerical modelling of the Maxwell-Bloch equations has been described, for example, by C.S. Cornish [125] and G.W. Burr et al. [126].

4.2 Coherent transients

We now turn to two coherent transient effects that are conveniently described using the Bloch formalism, namely *free induction decay* and *photon echoes*. These phenomena are of great interest because of their usefulness in spectroscopy [20,118] and in numerous applications (see Chapter 5). The effects arise due to the fact that an ensemble of atoms oscillating in phase will emit strong coherent radiation, in contrast to the radiation emitted by atoms with a random distribution of phases. When atoms emit incoherently, as is the case for spontaneous emission, the intensity is proportional to the number of emitters, N, as might be expected. However, if the phases of the emitted light fields are such that the field amplitudes interfere constructively, it is the electric field amplitude which is proportional to N, and the emitted intensity will be proportional to N^2.

In this respect photon echoes and free induction are closely related to the phenomenon of *superradiance* [127], but many authors prefer to reserve that term for correlated spontaneous emission processes and other effects that need to be described using quantum electrodynamics. Using that definition, superradiance occurs when a group of atoms in a correlated state spontaneously emit radiation at a rate proportional to N^2, which decreases the lifetime of the individual atoms to T_1/N. On the other hand, free induction emission and photon echoes similarly decrease the lifetime of the atoms, as energy is extracted during the period of coherent emission [125].

If the emitting atoms are distributed in space, their emission can only add coherently in specific directions, given by phase matching, in close analogy to the emission from phased array antenna. If the number of atoms is large, the angular distribution of the coherent emission follows the standard laws of diffraction and the angle of emission can be approximated by

$$\sin\theta \approx \frac{\lambda}{d} \tag{4.17}$$

where d is the size of the emitting volume. If d is much less that the wavelength of the emitted light, the emission can interfere constructively in all directions.

The coherent emission will be transient in a medium where the atoms emit at a distribution of frequencies, such as a Doppler-broadened gas or for rare-earth ions in a crystal. The atoms can only radiate in phase for a limited time, before they dephase due to the difference in frequency. On the other hand, by preparing atoms at specific frequencies and with specific phases, the medium can be programmed to emit coherently at a particular time or even to emit a complicated sequence of pulses.

The magnitude of coherent transient emission is decreased by spontaneous decay to the ground state and by decoherence. If atoms oscillating at the same frequency are disturbed by collisions or other energy-conserving interactions, their phases will spread out, which means that their dipole moments will not add constructively. This means that the expectation value of their oscillating dipole moment will decrease, i.e. the u-v component of the corresponding Bloch vector will shrink at a rate determined by the coherence time T_2. Rare-earth-ion-doped materials at cryogenic temperatures are particularly well suited for studies of coherent transient phenomena, because of their long optical coherence times.

4.2.1 Free induction decay

If a strong, brief pulse excites an inhomogeneously broadened ensemble of atoms from their ground state, it will excite atoms within a frequency interval $\Delta\nu$, approximately given by

$$\Delta\nu \propto \frac{1}{\tau_p} \tag{4.18}$$

where τ_p is the duration of the pulse and where we have assumed that the pulse is monochromatic and has a duration shorter than T_2. Unless the pulse area θ is an even multiple of π, the state of the atoms will acquire a component in the u-v plane of the Bloch sphere, corresponding to an oscillating dipole moment, and the atoms will radiate. Maximum dipole emission will come from atoms that experience a pulse area equal to $\pi/2$, placing them exactly in the u-v plane. Just after the exciting pulse, all atoms will oscillate with the same phase, causing strong coherent emission in the propagation direction of the incoming pulse. However, since the atoms oscillate at different frequencies, they will start to dephase, which decreases the rate of emission – a phenomenon known as *free induction decay* (FID) [113]. The dephasing will be faster if the atoms have a large frequency spread, whereas atoms oscillating with almost the same frequency can remain in phase for a long time. Thus, the duration and shape of the FID can give information about the width and shape of the excited atomic line [21,113]. The decay time of the FID, τ_{FID}, is given by

$$\tau_{FID} \propto \frac{1}{\Delta\nu} \tag{4.20}$$

where $\Delta\nu$ is the spectral width of the emitting ensemble of atoms. If the inhomogeneous width of the absorption line is much wider than the Fourier width of the exciting pulse, the duration of the FID will be roughly equal to the duration of the pulse.

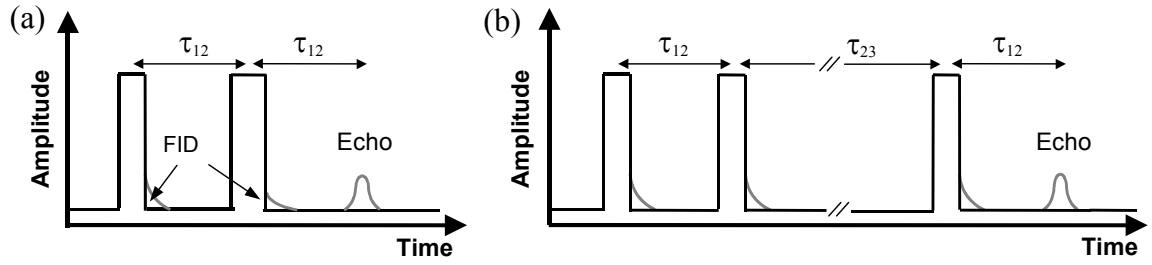

Figure 4.2. *(a) Two-pulse photon echo sequence: the interaction with two laser pulses causes free induction decay (FID) emission from the atoms and, after a time equal to the time between the pulses, an echo. (b) Three-pulse photon echo: a pair of pulses, separated by time τ_{12}, is followed by a third pulse, after a longer delay τ_{23}. The atoms will emit a stimulated echo at a time τ_{12} after the third pulse. Emission from the atoms drawn as the grey curves.*

4.2.2 Photon echoes

An *echo* is a temporary rephasing of quantum oscillations, which causes the emission of a burst of coherent radiation if the oscillators are radiating atoms. This was first studied in the form of *spin echoes*, in bulk NMR [128]. Inspired by this, an optical analogue, *photon echoes*, was demonstrated in ruby crystals in 1964 [112]. Below, the photon echo process is described using the Bloch sphere formalism, assuming that we are dealing with an inhomogeneously broadened ensemble of atoms, excited by laser pulses with a fixed frequency. Alternative or more general descriptions of the photon echo process are given in Refs. [122,129-132].

A typical pulse sequence for generating a *two-pulse photon echo (2PPE)* is shown in Fig. 4.2a. Two laser pulses are sent through an optically absorbing material and the atoms emit an echo after a time equal to the time, τ_{12}, between the pulses. The first laser pulse sets up coherence between the ground and the excited state. Ideally, this should be a $\pi/2$-pulse, placing the Bloch vector in the u-v plane. Initially, all atoms will have the same phase, determined by the phase of the laser pulse, and their Bloch vectors will point in the v direction. However, if the atoms oscillate at slightly different frequencies, i.e. if the absorption line is inhomogeneously broadened, the atoms will start to acquire a phase difference relative to the laser, at a rate proportional to their detuning. For atoms with negative detuning, the Bloch vector will rotate clockwise in the u-v-plane, and atoms with positive detuning will correspondingly rotate counterclockwise. The effect of the second pulse should be to flip the phase of the atomic state, i.e. it should ideally be a π-pulse, which rotates the Bloch sphere 180° around the u-axis. Atoms which have acquired a negative phase difference relative to the laser will now effectively have a positive phase, which will now start to decrease. After a period of free evolution, all atoms will again oscillate with the same phase, which gives rise to a large dipole moment and the emission of light.

In the description above it was assumed that the pulses had pulse areas of $\pi/2$ and π, and that the atoms start in the ground state. However, the only requirement is that there is an initial population difference between the ground and the excited state, i.e. that the Bloch vector does not start at w=0. In a more general situation, for example if the inhomogeneous width of the atoms is much larger than the Fourier width of the pulses, the probability of finding an atom in the excited state will vary depending on the detuning. Thus, the pulse areas will in general not be optimal for all frequencies.

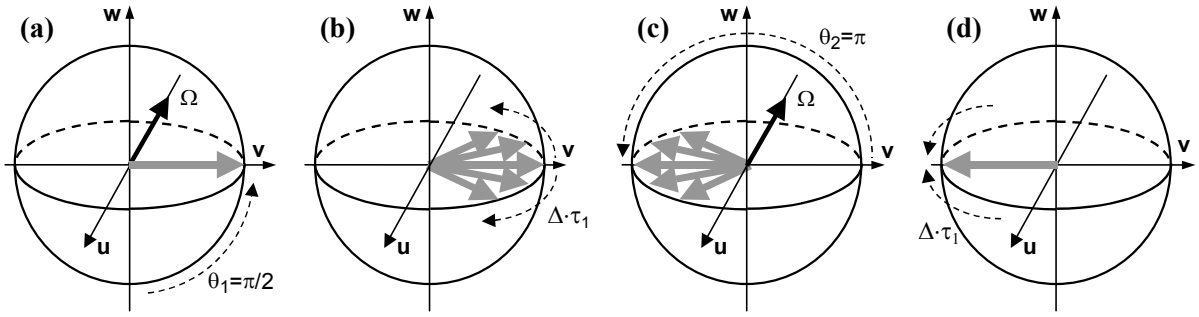

Figure 4.3. *Bloch vector description of the two-pulse photon echo process. (a) The first pulse creates a coherent superposition of two states. (b) The state evolves freely during the time τ_{12} and different atoms accumulate different phases relative to the laser, at a rate determined by their individual detuning, Δ. (c) The second pulse rotates the state by an angle π, which inverts the relative phases of the states (changes the sign of the v component of the Bloch vector). The atoms then evolve freely again. (d) After an additional time equal to τ_{12}, the atomic superposition states rephase, which causes the emission of coherent light – a photon echo.*

4.2.3 The three-pulse photon echo

Another type of photon echo is the *three-pulse photon echo (3PPE)*, shown in Fig. 4.2b. This can be intuitively described as a 2PPE where the second pulse is split into two halves, separated by a delay τ_{23}. The three-pulse echo, or *stimulated echo*, appears a time τ_{12} after the third pulse, where τ_{12} is the delay between the first two pulses. As in the 2PPE, the first pulse should create coherence between the ground and the excited states, ideally placing the Bloch vectors of the atoms in the u-v plane. The second pulse should also be a $\pi/2$-pulse, which rotates the Bloch vectors 90° around the u axis. Atoms that have a positive v component when the second pulse strikes them will move towards the ground state, whereas atoms with a negative v component will move towards the excited state. Since the phase of the atoms depends on their frequency relative to the laser frequency, $\Delta=(\omega_{ge}-\omega_L)$, and on the time, τ_{12}, they have had accumulate phase, we the following condition is obtained for atoms that are moved towards the excited state

$$-\frac{\pi}{2} < \Delta \cdot \tau_{12} + 2\pi n < \frac{\pi}{2} \ . \tag{4.21}$$

Thus, the effect of the two pulses is to create a frequency-dependent periodic modulation of the population in the ground and excited states, as atoms which differ in phase by an even multiple of 2π will be affected equally by the second pulse. This *population grating* contains full information about the relative phase and time separation between the two pulses.

The effect of the third pulse is to "stimulate" the atoms to emit an echo, based on the population grating set up by the first two pulses. This pulse, which should also have an area of $\pi/2$ for optimal signal strength, rotates the Bloch vectors of atoms in the ground state to point in the negative v direction and causes atoms from the excited state to point in the positive v direction. According to the discussion above, these two groups of atoms oscillate at frequencies such that after a time τ_{12} they have $v<0$ and $v>0$, respectively. Starting on different sides of the Bloch sphere, they will thus rephase at a time τ_{12} after the third pulse and an echo will be emitted. If the atomic ensemble has a mechanism for

persistent storage of spectral features, e.g. in a spectral hole-burning material, the third pulse can stimulate an echo even after the population in the excited state has decayed. As was discussed in Chapter 3, the upper state population can be trapped, e.g. in a third metastable electronic state or in different hyperfine levels of the ground state, which means that the population grating (frequency-dependent periodic modulation) in the ground state will remain.

If all atoms contributing to the echo are assumed to experience the same pulse area, the intensity of a 3PPE, I_e, can be calculated as

$$I_e \propto \sin^2\theta_1 \cdot \sin^2\theta_2 \cdot \sin^2\theta_3 \tag{4.22}$$

where θ_1, θ_2 and θ_3 are the pulse areas of the first, second and third pulses, respectively. For small pulse areas we see that the echo intensity is proportional to the product of the intensities of the three pulses, since $\sin\theta \approx \theta \propto E \propto \sqrt{I}$.

Another way of writing the output amplitude in a three-pulse echo process, assuming that the pulses are far from saturating the transitions ($\theta << \pi/2$), is

$$E_{echo}(t) \propto E_1(t) \otimes \left(E_2(t) * E_3(t)\right) \tag{4.23}$$

where $\otimes$ denotes a correlation and * a convolution operator. In the frequency domain, this can be expressed [100,133]

$$E_{echo}(t) \propto \int_{-\infty}^{\infty} E_1(\omega)^* E_2(\omega) E_3(\omega) e^{-i\omega t} d\omega . \tag{4.24}$$

Using this relation either in the time or in the frequency domain, various types of optical signal processing can be implemented. We see that if two of the pulses are brief enough to be nearly constant over the spectral interval of interest, the equation essentially expresses a Fourier transform. We can also note that if the product of pulses one and three has a flat spectrum, the echo will replicate the second pulse, which is the basis for photon-echo-based data storage [100,134].

Many observations can be made concerning the connection between the time and frequency domains in a photon echo experiment. For example, as we saw earlier, the two first pulses in a 3PPE set up a periodic grating of excited atoms in the frequency domain. The period of the grating, $\Delta\nu$, is proportional to the inverse of the time interval between the pulses $1/\tau_{12}$. This becomes obvious if we note that the spectral energy distribution (Fourier transform) of two pulses, separated by a time τ_{12}, has exactly this shape. A beautiful demonstration of the relation between the time and the frequency domain is given in Ref. [135], where the first two pulses in the three-pulse photon echo process are replaced by direct periodic hole-burning, in the frequency domain. The connection between time and frequency domains has also been directly applied for performing Fourier transformations [136] and the intermediate domain has been explored with respect to its connections to Fresnel diffraction by a straight edge [137].

The direction of the emission of the photon echo is basically given by the same phase-matching conditions as in other four-wave mixing processes, even though the fields are separated in time. Writing the wave-vectors for the incoming laser fields and the echo as $\mathbf{k}_1$, $\mathbf{k}_2$, $\mathbf{k}_3$ and $\mathbf{k}_e$, we have

$$\mathbf{k}_e = \mathbf{k}_2 + \mathbf{k}_3 - \mathbf{k}_1 . \tag{4.25}$$

In an experiment it is often useful to let the input pulses come from different directions, in order to spatially separate a weak echo signal from the strong laser fields. The directionality of the echo also gives additional possibilities for optical signal processing, such as spatial-spectral filtering and correlation [105,138,139].

4.2.4 Accumulated echoes

The emission of photon echoes is a coherent effect and thus depends on the phase memory (T_2) of the atoms. For a two-pulse photon echo to occur, the atomic coherence (the u and v components of the Bloch vector) must survive from the first pulse until the emission of the echo. However, for a three-pulse photon echo to occur, it is only necessary that the population difference between the ground and excited states remain during the time τ_{23} between the second and third pulses, since the echo can be stimulated from the spectral population grating created by the first two pulses [140,141]. If the atoms that are excited by the first two pulses can relax to a metastable state, the frequency-dependent modulation of population in the ground state can remain even after times much longer than the excited state lifetime, T_1. In a material with a mechanism for persistent spectral hole-burning (see Chapter 3), we can therefore think of the first pulses as *write pulses*, which prepare a spectral modulation of the inhomogeneous absorption profile, and of the third pulse as a *read-out* pulse, which stimulates the atoms to emit light according to the spectrally programmed information.

If the write pulses are weak, i.e. if they create only a small modulation of the population in the ground state, they may be repeated many times in order to obtain a coherent build-up of the population grating. In an *accumulated photon echo* experiment [142,143], many pairs of pulses with equal pulse separation, τ_{12}, are sent into the sample. Finally, a single laser pulse is applied and a stimulated echo will be emitted, after a time τ_{12}. If N pulse pairs are sent into the medium, and each pulse pair prepares the same number of atoms in the population grating, the echo signal will scale as

$$I_e \propto N^2 \tag{4.26}$$

since the echo intensity is proportional to the square of the number of contributing atoms. The photon echo experiment described in Paper IV was performed by accumulating more than 10^9 pulses with (on average) less than one photon per pulse pair.

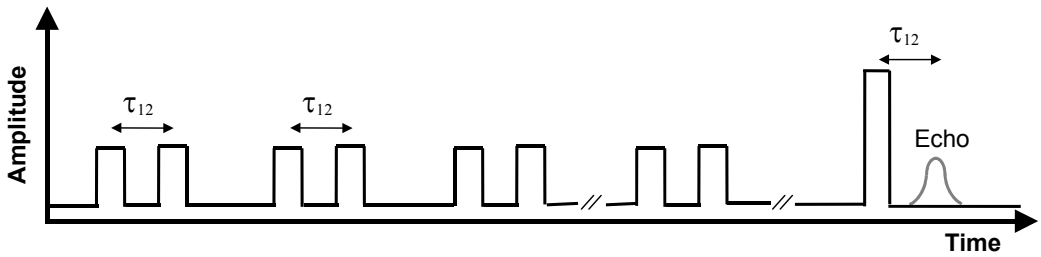

Figure 4.4. *Accumulated photon echo. Several pulse pairs, with a separation τ_{12} between the pulses within a pair, are sent into a photon echo material. Each pair of excitation pulses contribute to the build-up of a spectral grating in the material, provided that there is a mechanism for storage of spectral features, e.g. a metastable state. Finally, a single read-out pulse can stimulate the emission of an echo, which will be emitted after a delay equal to τ_{12}.*

4.3 Manipulating the state of a two-level system

From the theory presented above, we see that it is possible to perform any rotation of the Bloch sphere, by applying pulses or a sequence of pulses with a suitable phase, frequency and duration. For example, an atom in a known state, e.g. the ground state, can in principle be brought into any other state by applying the right laser pulse. This is important within quantum information science, where a two-level system may be used to represent one bit of quantum information and where controlled rotations of the state vector correspond to quantum logic operations. It is also useful in situations where the state of a two-level system is to be determined, but where the measurement is limited to a particular property of the state. For example, in optical spectroscopy it is usually easy to measure the inversion of a group of optically excited atoms (the w component of the Bloch vector), for example by measuring the fluorescence, but in NMR it is easier to measure the oscillating spin components (u and v) than to measure the static magnetisation (w). In this case, the state can be rotated by applying a $\pi/2$-pulse before the measurement, turning a population difference into a polarisation (turning the w component of the Bloch vector into a v component) and vice versa.

A special case of quantum state manipulation is the transfer of atoms between two energy eigenstates, e.g. from a ground state into an excited state. If this can be achieved on several transitions, atoms can be transferred efficiently even between states that are not connected by an optical transition, by using the excited state as an intermediate state. As part of the work presented in this thesis, a method for efficient transfer of rare-earth ions between hyperfine levels, via the excited state, was developed and demonstrated (Paper III).

Within the field of NMR, radio pulses have long been used to manipulate nuclear spins, and sometimes very complex pulse sequences are used in order to extract information about the nuclei and their surroundings. Very advanced techniques have been developed for dealing with the fundamental and technical problems regarding the generation of *hard pulses*, i.e. pulses that interact with all absorbers in an ensemble with a well-defined phase and pulse area. Because it has been difficult to create optical pulses with comparable phase and amplitude stability, it is only recently that similar experiments have been performed using laser light to drive optical transitions. Now, however, there is a significant exchange of ideas between the fields and many of the techniques discussed below were first used within NMR. Using ultra-stable lasers it is possible to apply hard pulses and complicated pulse sequences, resembling those used in NMR, to optical transitions in dopant ions in solids [108,144].

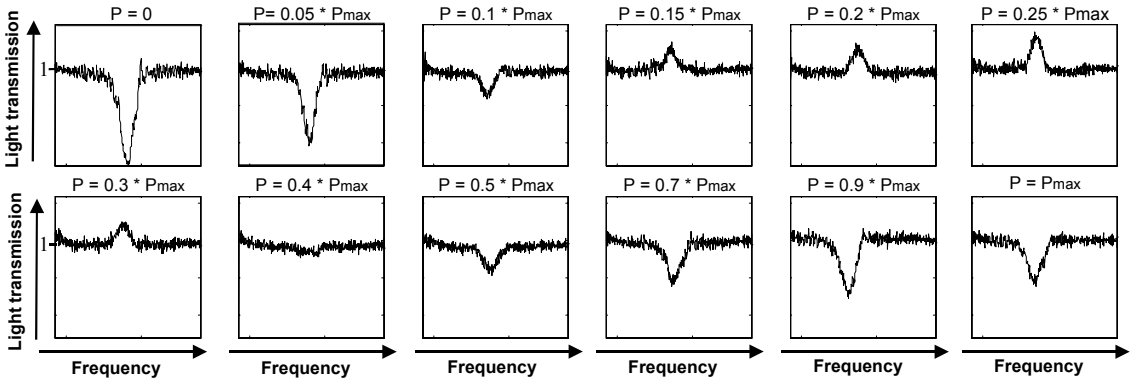

Figure 4.5. *Manipulation of the state of an ensemble of Pr ions in Y_2SiO_5. The ions are prepared in the ground state and are then subjected to a laser pulse with a fixed frequency, which rotates their state on the optical transition. The pulse duration is kept constant and brief pulses with increasing intensity, corresponding to increasing pulse areas (from top left to lower right), are applied. The level of inversion (the w component of the state vector) is monitored by measuring the transmission/absorption of a weak, frequency-chirped, probe pulse. Maximum transmission (top right) occurs when the state has been rotated into the excited state (w=1, i.e. complete population inversion). The most intense pulses applied (lower right) rotates the state by slightly more than 2π, i.e. one full Rabi period.*

The difficulties that need to be dealt with, when the state of a two-level system is manipulated using coherent radiation, are mainly inhomogeneities of various types, i.e. the fact that different atoms are affected differently by the applied pulses. For example, the intensity of a laser beam usually varies spatially, which means that atoms in different parts of the beam are driven with different Rabi frequencies, Ω. Variations in the detuning between the atomic resonance line and the laser frequency will also cause the atoms to evolve differently during pulses and delays. The experiments may also require the pulses to be spectrally selective, so that only atoms absorbing within a specific frequency interval are affected by them. This is usually the case for the experiments using rare-earth-ion-doped materials described in this thesis.

4.3.1 Composite pulses

One way of tackling systematic errors in quantum state rotations is to use *composite pulses* [145,146]. Instead of a single pulse to achieve the desired state change, several pulses are applied, which together perform the same rotation, even if there are small variations in detuning and pulse areas. Thus, by using suitable composite pulses it is possible to compensate for off-resonance and errors in pulse length or Rabi frequency.

One example is the "$90_{90}180_{0}90_{90}$" pulse, designed to efficiently invert the population on the driven transition, i.e. to be equivalent to a π-pulse for atoms in the ground or the excited states. Here we use the notation θ_ϕ to denote a pulse with a pulse area $\theta=\Omega\cdot t$ and with a phase ϕ. Thus, the $90_{90}180_{0}90_{90}$ composite pulse consists of a π/2-pulse (90° rotation), followed by a π-pulse (180° rotation) which is 90° out of phase with the first pulse, and finally another π/2-pulse, with the same phase as the first pulse. The first pulse rotates the Bloch vector from the ground state up to a position close to the u axis in the equatorial plane of the Bloch sphere. If the pulse area is too small or too large ($\theta=\theta_0+\delta\theta$), the Bloch vector will end up below or above the u axis. If there is a small detuning

($\omega_L=\omega_{ge}+\delta\omega$), the Bloch vector will end up to the side of the u axis. The π-pulse compensates for this by performing a rotation around the u axis, which (almost) inverts the sign of the error. The last $\pi/2$-pulse then brings the Bloch vector the rest of the way up to the excited state. The resulting inversion is nearly ideal for a range of pulse areas and detuning. This is not the case for the naïve implementation, which would be the simple rotation 180_0.

A wide variety of composite pulses has been developed, to perform various rotations of the quantum state in a robust way [145,146]. In general, a more complex sequence of pulses is able to correct for more errors and some composite pulses consist of 10 or more different pulses with varying phase and duration. However, a more complex composite pulse places higher demands on the equipment generating the pulses and will also have a longer total duration, which means that the fidelity of the operation may be impaired by state relaxation. Although there are analytic tools for the construction of composite pulses, there is usually an amount of intuition and trial-and-error involved. One way of finding optimal pulses, to perform a desired rotation in a robust manner, is to use iterative numerical methods. The methods of *optimal control theory* have been applied successfully for automated design of pulses and quantum gates for quantum computing based on rare-earth-ion-doped materials [147].

Composite pulses can be divided into two classes [146]:
- Class A composite pulses produce a fully compensated rotation of the system for all initial states, over a particular range of imperfections.
- Class B composite pulses may only work for some particular initial states (usually the ground state) or may give an overall phase shift which depends on the pulse imperfections.

The $90_{90}180_090_{90}$ pulse, described above, belongs to class B, since it only works for atoms starting in either the ground or the excited state.

4.3.2 Frequency-chirped pulses

One way of achieving a specific quantum state operation on atoms with a wide range of resonance frequencies is by applying a brief pulse that is spectrally flat over the frequency range that is to be manipulated. The main problem with this is that high intensities (Rabi frequencies) are needed in order to change the state of the atoms in a short time. Basically, the requirement is

$$\Omega >> \Delta\omega \tag{4.27}$$

where $\Delta\omega$ is the bandwidth to be affected by for example a π or $\pi/2$ rotation. Another disadvantage is that a brief pulse may disturb other atoms or transitions, far off resonance, which should not be affected by the operation.

An attractive alternative is to use pulses that are continuously tuned through the resonance frequencies of the atoms that are to be manipulated. This has been explored, for example, in photon-echo-based signal processing, where π or $\pi/2$ pulses are used as reference fields and where it is usually desirable to use as large a bandwidth as possible [134,148,149]. By varying the intensity and chirp rate of the laser pulse, i.e. by varying the amount of energy per frequency interval, the level of inversion can be varied [150]. However, the trajectory of the Bloch vector and the final phase of the atomic states are more difficult to predict than for a pulse of fixed frequency.

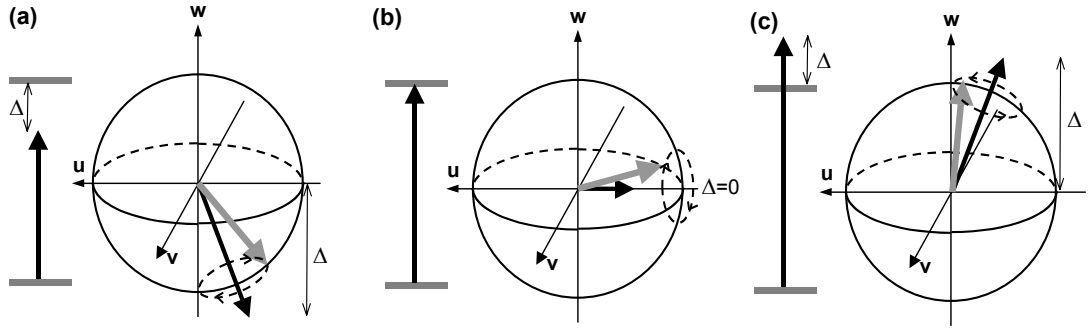

Figure 4.6. *Adiabatic following in the Bloch picture. The Bloch vector (grey) precesses rapidly around the pseudo-vector representing the applied laser field (black). (a) When the laser frequency is far detuned to lower frequencies, the pseudo-vector points almost straight down along the w axis. (b) As the frequency is tuned past resonance, the pseudo-vector moves up through the u-v plane, bringing the Bloch vector with it. (c) When the frequency has been tuned far past resonance, the Bloch vector has been brough to point up along the w axis, resulting in a complete population inversion.*

4.3.3 Adiabatic following

An extreme example of the application of frequency-chirped pulses is the use of *adiabatic following* (or *rapid adiabatic passage*) [114,151,152] to achieve complete inversion of the atomic population. Here, a strong laser field is slowly tuned through the resonance frequency of the atoms, which will bring all atoms in the ground state to the excited state and vice versa. The tuning rate should be slow enough for the state of the atoms to change adiabatically, i.e. the atomic state should always be approximately an equilibrium state, in this case an energy eigenstate of the total Hamiltonian including the interaction with the field. The whole process should also take place before any dephasing of the atomic state occurs, which gives us the following condition for adiabatic following [110]:

$$\frac{\Omega}{\pi T_2} << r << \frac{\Omega^2}{2\pi} \tag{4.28}$$

where Ω is the Rabi frequency, as usual expressed as an angular frequency and r is the chirp rate, in units of frequency/time.

In the Bloch picture, adiabatic following can be visualised in the following way: when the field is detuned very far from resonance (large Δ), the pseudo-vector will point almost completely down along the w axis and an atomic state starting in the ground state will precess in small circles around it. As the laser frequency is brought closer to resonance, the pseudo-vector will move up and at resonance (Δ=0) it will point along the u axis. If the rate of frequency change is small compared with the Rabi frequency (cf. the right-hand side of the inequality in Eq. 4.28), the Bloch vector will rotate rapidly around the pseudo-vector and follow it closely as the angle to the w axis changes. When the laser frequency is far beyond resonance (large negative Δ), the pseudo-vector will point up, almost parallel to the w axis, and the atomic state will have followed it, ending up close to the excited state.

Another way of describing the process is in terms of *adiabatic states*, which are instantaneous eigenstates of a Hamiltonian that includes the interaction with the field. The adiabatic states are time-dependent superpositions of the two unperturbed states $|g\rangle$ and $|e\rangle$,

with a mixing angle that is determined by the interaction with the laser field. As the detuning between the laser frequency and the atomic transition changes through $\Delta=0$, the state $|e\rangle$ adiabatically changes into $|g\rangle$ and vice versa, which means that an originally excited atom will end up in the ground state and an atom that is originally in the ground state will end up in the excited state.

Adiabatic following provides a very robust method for achieving state-to-state population transfer, for a group of atoms with inhomogeneous frequency broadening. In principle an arbitrarily large spectral interval can be inverted. The technique is also almost insensitive to variations in Rabi frequency, since the process will create complete inversion for all atoms experiencing a Rabi frequency above a certain threshold. A disadvantage is that conventional adiabatic following has poor frequency selectivity, as the frequency chirp should start very far detuned to higher (lower) frequencies and end up far detuned to lower (higher) frequencies.

4.3.4 Complex hyperbolic secant pulses

One type of tailored pulse that has the advantages of adiabatic following, while still being frequency selective, is pulses that take the form of a *complex hyperbolic secant function* (sech). During the work on quantum computing using rare-earth ions, presented later in this thesis, these pulses emerged as the best way to achieve robust manipulation of quantum bits, while at the same time permitting frequency-selective addressing of qubit ions [153].

In 1984, Silver et al. suggested the use of complex hyperbolic secant pulses for selective spin inversion, based on analogies to coherent optics, in particular the phenomenon of self-induced transparency [154]. The Rabi frequency of such a pulse, including a complex phase, can be described by

$$\Omega(t) = \Omega_0 \left[\sec h\left(\beta\left(t - t_0\right)\right)\right]^{1+i\mu} \tag{4.29}$$

where μ is a real constant related to the amount of frequency modulation of the pulse, Ω_0 is the maximum Rabi frequency and β is related to the duration of the pulse. This can be expressed as an amplitude and frequency modulation according to

$$\begin{aligned} \left|\Omega(t)\right| &= \Omega_0 \sec h(\beta(t - t_0)) \\ \Delta\nu(t) &= \mu\beta \tanh(\beta(t - t_0)) \end{aligned} . \tag{4.30}$$

The amplitude FWHM of the pulse is $2.6/\beta$. If μ is non-zero, the instantaneous frequency of the pulse changes with time and the laser can induce rapid adiabatic passage between the two energy levels of the driven system. Once $\mu \geq 2$ and provided that $\Omega_0 \geq \mu\beta$, the inversion is essentially independent of the maximum Rabi frequency, and hence robust against inhomogeneity in the field amplitude. The population inversion is highly selective, with an increasing sharpness as μ is increased and β decreased. Fig. 4.7 shows the probability of excitation as a function of detuning, for parameters chosen to invert a ± 0.5 MHz interval without affecting anything outside a ± 5 MHz interval, with a pulse of limited duration (3 μs).

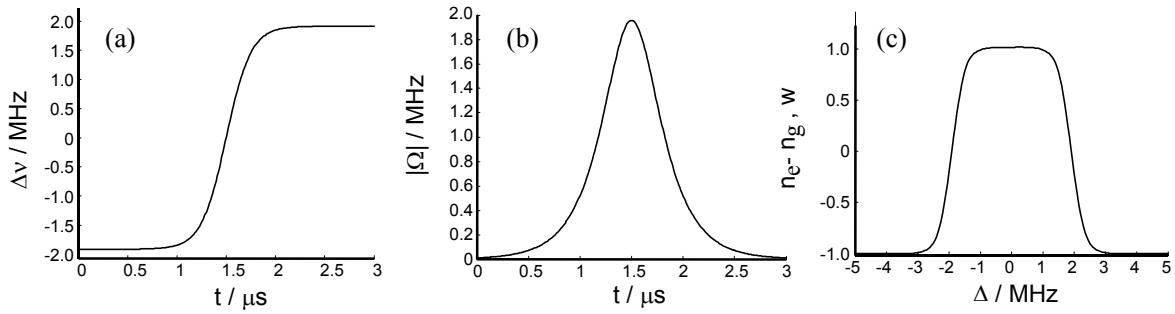

Figure 4.7. *Example of population inversion using complex hyperbolic secant pulses. (a) Instantaneous frequency of the pulse. (b) Instantaneous Rabi frequency, Ω. (c) Resulting population inversion, w, as a function of detuning from the centre frequency of the pulse. Absorbers with resonance frequencies within ±1 MHz experience complete transfer between the energy levels, whereas absorbers outside a ±4 MHz interval are completely unaffected by the pulse.*

The tailoring of pulses and composite pulses using the principles of adiabatic following have continued within the field of NMR, see e.g. Refs. [155] and [156]. As some of these pulses can produce adjustable, broadband, selective and phase-uniform excitation, they are likely to be used in many different applications, including quantum computing, where various types of field and frequency inhomogeneities must be overcome.

4.3.5 Manipulating hyperfine states using optical transitions

In the schemes for quantum information processing explored in this work, the information-carrying two-level system is in general not two energy levels connected by an optical transition, but two hyperfine levels in the ground state of a rare-earth ion. In principle, the hyperfine state of the atoms can be manipulated by using radio-frequency radiation to drive the transition between the two hyperfine levels, as is done in NMR. Population transfer, or arbitrary rotation of the quantum state between the hyperfine levels, can then be achieved using the methods described above. However, we would like to manipulate the atomic hyperfine state using laser light, because optical manipulation can in general be performed on much faster timescales, and because we want to use the optical resonance frequency to address different groups of ions.

This can be done by applying laser light at two frequencies, resonant or nearly resonant with optical transitions going from each of the two hyperfine levels to a common excited state. We thus leave our model of an atom as a two-level system, in favour of a Λ (lambda) system, i.e. two lower lying energy levels, both connected to a higher lying level. Coherent superpositions of atomic states in three-level systems can give rise to many interesting phenomena, such as *electromagnetically induced transparency*, *coherent population trapping, slow light* and *lasing without inversion* [116].

If only one of the transitions is driven at a time, the driven transition can be percieved as a two-level system and the formalism outlined above can be applied. For example, it is possible to move probability amplitude from one hyperfine level to the other by first applying a laser pulse to one optical transition, which transfers probability amplitude from one of the ground state hyperfine levels to the excited state, and then applying a laser pulse to the other transition, driving the atoms down into the other hyperfine level. A transition of this type can be seen as a resonantly driven *Raman transition* where the fields are

separated in time. A Raman process is usually described in terms of absorption of a photon on one transition and simultaneous emission of a photon from another transition. This induces coherence or population transfer between the two states not connected by the two optical transitions.

A *bichromatic pulse*, i.e. a pulse containing two frequencies, which simultaneously drives both optical transitions, can be called a *Raman pulse* [62]. Such a pulse can directly perform a rotation of the atomic state between the hyperfine levels and induce coherence between the levels. Intuitively this can be seen by noting that two fields at frequencies ω_1 and ω_2 will produce beats at the difference frequency ω_1-ω_2, when combined. If the difference frequency matches the resonance frequency of the hyperfine transition it will be coherently driven and the effect will be enhanced when the fields are nearly resonant with a third state. This description is somewhat oversimplified, since the atomic state usually evolves into a new hyperfine state via the excited state, when interacting with the two fields. A discussion of three-level effects in terms of coherent Raman processes and Raman excitation can be found e.g. in Ref. [117].

In general, the lower two levels of a Λ system interacting with resonant Raman fields can be described in terms of two new states, $|-\rangle$ and $|+\rangle$, defined as

$$\begin{aligned} |-\rangle &= \frac{1}{\Omega}\left(\Omega_2|1\rangle - \Omega_1|2\rangle\right) \\ |+\rangle &= \frac{1}{\Omega}\left(\Omega_1|1\rangle + \Omega_2|2\rangle\right) \end{aligned} . \tag{4.31}$$

Here $|1\rangle$ and $|2\rangle$ are the two lower states and Ω_1 and Ω_2 are the Rabi frequencies of the fields connecting them to the excited state, with $\Omega = \sqrt{\Omega_1^2 + \Omega_2^2}$. The states $|-\rangle$ and $|+\rangle$ are known as *dark states* and *bright states*, respectively, since only $|+\rangle$ couples to the excited state. Thus, atoms can be excited from state $|+\rangle$ and relax to state $|-\rangle$, where they are trapped – a process known as *coherent population trapping* [157]. This can be used as a way to create coherent superpositions of hyperfine levels [62].

Although arbitrary manipulation of the quantum hyperfine states can be achieved by using optical fields, the work related to quantum computing in rare-earth-ion-doped materials has, so far, focused on achieving efficient population transfer between hyperfine levels. In Paper III, population transfer was demonstrated, using tailored (sech) pulses to first excite atoms and then drive them down into a new hyperfine state. A fundamental limit on the efficiency of the process is decoherence and decay during the time the atoms spend in the excited state, which is significantly more prone to relaxation than the ground state hyperfine levels. For rare-earth ions in crystals the operations typically take a few μs, whereas the excited state lifetime is several hundred μs to a few ms.

A technique for transferring atoms between two ground state sublevels which avoids placing any atoms in the excited state is *stimulated Raman adiabatic passage (STIRAP)* [152,158]. By simultaneously driving both transitions in a Λ system and smoothly changing the relative intensity of the driving fields, the state of the atoms can be adiabatically changed from one of the two lower states, into a superposition of the two lower states, to finally end up in the other ground state sublevel.

SUMMARY

- An atom driven by a laser field close to resonance with one of its transitions can be modelled as a two-level system. The state of the system is described by the three-dimensional Bloch vector (u,v,w) within a unit sphere. The poles of sphere (w=-1 or 1) correspond to the ground state and the excited state, respectively. States in the equatorial plane correspond to equal superpositions of the ground state and the exited state, oscillating with a phase given by the azimuthal angle.
- The interaction of the atom with the field causes the Bloch vector to precess around a pseudo-vector ($-\Omega$, 0, Δ), where the Rabi frequency, Ω, is a measure of the strength of the interaction and the detuning, Δ, is the difference between the laser frequency and the resonance frequency of the atom.
- The pulse area, $\theta=\Omega \cdot t$, corresponds to the angle through which the Bloch vector is rotated around the pseudo-vector.
- Any rotation of the state vector can, in principle, be achieved by applying a laser pulse with a specific intensity, duration and phase.
- An atom in a superposition state, i.e. with a non-zero component in the u-v plane, has an oscillating electric dipole moment. An ensemble of atoms can give rise to a macroscopic oscillating polarisation, which will emit radiation.
- An echo is a temporary rephasing of the oscillations of an ensemble of atoms, which can result in coherent transient emission of radiation.
- An ensemble of atoms with an inhomogeneously broadened absorption line, i.e. with a spread of resonance frequencies, can be programmed to emit light at specific times, by preparing atoms oscillating with specific frequencies and phases.
- Composite or tailored pulses can be used to manipulate the state of an ensemble of two-level systems with high precision, even in the presence of unknown errors such as varying detunings and Rabi frequencies.
- Frequency-chirped pulses can be used to create a specific level of inversion of the atomic population within a wide spectral range. In particular, frequency-chirped pulses in the regime of adiabatic following can be used to create complete population inversion, in a robust and frequency selective manner.
- The hyperfine, or spin, state of an atom can be manipulated using laser light by driving the optical transitions connecting the hyperfine states to an excited state.
- Rare-earth-ion-doped inorganic crystals are well suited for experiments and applications using optical coherent transients or the quantised nature of optical transitions.

CHAPTER 5

STORAGE AND PROCESSING OF INFORMATION USING PHOTON ECHOES

This chapter will briefly review how coherent transient phenomena, such as photon echoes, are used to store and process classical information. Although this was not a main topic for the investigations in the present work, it has provided an important background, and much inspiration and insight have been gained from this field. Experiments involving photon-echo-based data storage, pulse compression and temporal pattern recognition were routinely performed in the lab during the course of this work, and in Paper VI a basic photon echo data storage application was used to demonstrate the long-time storage mechanism found for Tm:YAG in a magnetic field. A major part of current research concerning optical storage and processing using photon echoes is performed in rare-earth-ion-doped inorganic crystals at liquid helium temperatures.

In conventional optical data storage, the maximum storage density is limited by diffraction, since each bit must use at least an area equal to the size of the laser focus. A similar condition holds for volume (holographic) data storage, in three dimensions. In the 1970s it was suggested that frequency (colour or wavelength) could be used as an extra addressing dimension [97,98] to bring optical memories closer to the ideal limit, where only a few atoms are used to store each data bit. In particular, it was realised that any material with an inhomogeneously broadened absorption profile could be used for this purpose. By irradiating the sample with light of several different narrowband frequencies within the inhomogeneous absorption profile, many data bits could be stored at each spatial location. Different bits of data are actually stored by different atoms, absorbing at different frequencies, at a particular location.

A fundamental limitation on frequency domain addressing is that in order to address a very narrow frequency channel, the addressing laser pulse has to be very long ($\Delta\nu \sim 1/\Delta t$), which means that the data rate will be limited. The photon echo approach circumvents this by being a *time-domain* approach – a temporal sequence of data pulses is created by amplitude modulating a laser field and the Fourier transform of this pulse sequence will be recorded in the inhomogeneously broadened absorption line. In the time-domain approach, the data rate will be limited by the inhomogeneous linewidth, Γ_{ih}, and the maximum spectral storage density is given by the ratio between Γ_{ih} and the homogeneous linewidth, Γ_h. In other words, the shortest data pulses that can be stored have a duration of the order of $1/\Gamma_{ih}$ and the data sequence can at most have a duration of the order of $T_2=1/\pi\Gamma_h$. In addition to data storage, the photon echo process has the property of intrinsically being able to recognise and process temporal information.

All-optical information processing tasks that have been demonstrated with photon echoes include storage of 4000 bits of data at a single spatial location [159], recognition of temporal data [160], high-speed image processing [161] and realisation of a complete set

of Boolean operators [162]. Storage and recall of data at THz rates have been performed [163] and storage densities of the order of Tb/cm^2 has been projected [164,165]. Pulse compression and data rate conversion have also been demonstrated [166-168], as well as spatial routing and selection of beams based on their temporal information contents [103,160,169].

The majority of these applications can be understood as special cases of the three-pulse photon echo process (see Section 4.2.3). Three fields, described by $E_{ref}(t)$, $E_{data}(t)$ and $E_{read\text{-}out}(t)$, interact with the material. The fields interact sequentially, in the order given, with ions absorbing at each particular frequency, which elicits a coherent transient response – a three-pulse photon echo. When the electromagnetic fields of the three inputs are far from saturating the optical transition and the time separation between the pulse sequences is smaller than the transition relaxation times, the photon echo process can be expressed as

$$E_{echo}(t) \propto \int E_{ref}(\omega)^{*} E_{data}(\omega) E_{read-out}(\omega) e^{-i\omega t} d\omega \tag{5.1}$$

where $E_i(\omega)$ is the frequency Fourier transform of $E_i(t)$, * denotes the complex conjugate and $E_{echo}(t)$ is the electric field of the photon echo output signal. One can see that if the product $E_{ref}^{*}(t)E_{read\text{-}out}(t)$ is constant (up to a linear phase shift) over the frequency range where $E_{data}(t)$ is non-zero, the echo will be a (time-delayed) replica of the data field. This can be achieved by using reference pulses that are sufficiently brief to be spectrally flat over the full bandwidth of $E_{data}(t)$. The time-domain analogue to Eq. 5.1 is

$$E_{echo}(t) \propto E_1(t) \otimes \left[E_2(t) * E_{read\text{-}out}(t)\right] \tag{5.2}$$

where $\otimes$ represents correlation and $*$ represents the convolution operator. For experiments on address recognition, data are normally encoded in the first pulse, $E_1(t)$, while the second pulse, $E_2(t)$, is a brief pulse. In this case, $E_{echo}(t)$ is the correlation of the inputs $E_1(t)$ and $E_{readout}(t)$. If these two fields are identical then the resulting output is a perfect auto-correlation peak, and if they are mismatched a cross-correlation peak is emitted. In a three-pulse photon echo, the effect of the first and second field is to create a frequency-dependent excitation of ions in the medium (see Section 4.2). If it takes a long time for some excited ions to return to the ground state, i.e. in a hole-burning material, the result is a frequency-dependent modulation of the population in the ground state – a *spectral grating*. The population grating can be used to encode both temporal information, such as time delays, or spatial information, such as angles.

One issue that is being addressed within the field of photon-echo-based information processing, is how to achieve optimal reference pulses over a large bandwidth. In a three-pulse photon echo, the reference (write) pulse and the read-out pulse should give a pulse area of $\pi/2$, over the bandwidth of the data pulse, in order to give a maximal output signal. This can be difficult to accomplish using brief pulses, if the available laser power is limited, since the rare-earth ions typically have low transition strengths. One way of obtaining optimal reference pulses is to use temporally long pulses that are frequency-chirped. Such pulses can be used to obtain a flat spectrum in the frequency region where the data field is non-zero [148,150] . This is the basis of many successful experimental

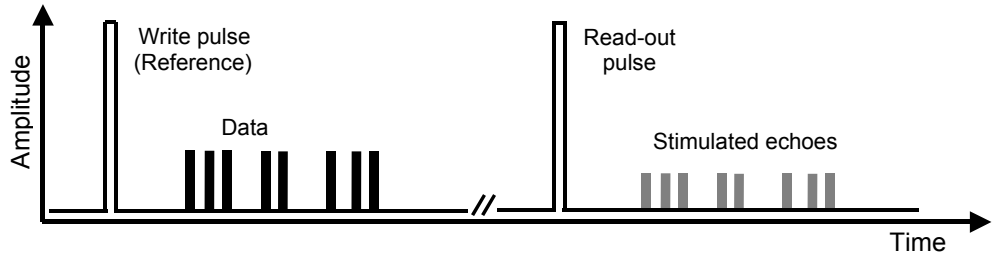

Figure 5.1. *Principles of photon-echo (time-domain) data storage. The second pulse in a three-pulse photon echo is replaced by a sequence of data pulses. The Fourier transform of the data is stored as a spectral population grating. The third pulse stimulates the emission of an echo, replicating the input data pulses. The reference (write and read-out) pulses should be equivalent to π/2-pulses for all atoms within the bandwidth used for data storage.*

implementations of information processing using photon echoes, as will be described later. Another way of creating suitable reference fields is to use long, appropriately phase-modulated pulses [170-172]. In the case of photon echo data storage, the requirement for faithful retrieval of the stored information is that the product $E_{ref}^{*}(\nu)E_{readout}(\nu)$ (where $E_{ref}(\nu)$ and $E_{read\text{-}out}(\nu)$ are the spectra of the reference (or write) and read-out pulses as described earlier) is constant over the spectral region used for information storage, or equivalently that the correlation of E_{ref} and $E_{read\text{-}out}$ is a single sharp peak (cf. Eqs. 5.1 and 5.2).

Frequency-chirped or phase-modulated pulses can also help alleviate the problem of *coherent saturation*. Coherent saturation can occur if a data sequence consists of a long sequence of pulses, e.g. N pulses, with the same optical frequency. For ions absorbing on the carrier frequency, the total pulse area will be N times the area of a single bit data pulse. Since the total pulse area should be much less than π/2, to avoid non-linearities, this places an upper limit on the number of bits that can be used before the transition is saturated. The peak power at the centre frequency, resulting from a coherent superposition, is proportional to N^2, and the longer the sequence, the more concentrated the optical power will be to the carrier frequency. The ions absorbing within the data bandwidth will be poorly utilised and the output power will be limited. One suggested solution to this problem is to introduce phase noise, allowing the data bits to have random or alternating phases, thereby spreading the power more evenly [170,173]. Another solution, suggested by Shen and Kachru [174], is to chirp the laser frequency so that no single dipole oscillates in phase with every data pulse.

5.1 Photon echo spectroscopy, decoherence and relaxation

In spectroscopy, one of the main applications of photon echoes is in measuring homogeneous dephasing and population relaxation between atomic states. These parameters are also relevant in applications using coherent transients for storage or processing of information. The output signal in a photon echo application will decrease due to decoherence, if the time between the reference pulse and the data pulses is comparable to the coherence time, T_2. The echo intensity in a two- or three-pulse echo decreases with the separation between the first and the second pulse, τ, according to

$$I = I_{\infty} \cdot e^{-4\tau / T_2} \tag{5.3}$$

where I_∞ would be the intensity if $T_2 \to \infty$. Eq. 5.3 can be understood intuitively by noting that the number of ions which are still phase coherent after a time t decreases as $\exp(-t/T_2)$, and that the echo intensity is proportional to N^2, where N is the number of contributing ions. The ions spend a time $2\cdot\tau$ (the time between the interaction with the first pulse and the emission of the echo) in a coherent superposition which gives an additional factor 2 in the exponent. By varying the time between the first and the second pulse and recording the intensity of the photon echo, the dephasing time of the optical transition, under the experimental conditions, can be inferred. This was used to measure T_2 and excitation induced spectral diffusion in $Pr:KY(WO_4)_2$ (Paper VII).

After the first two fields have interacted with the material, information is stored as a frequency-dependent modulation of the population in the ground and excited states. The number of ions contributing to the echo signal will decrease as ions relax back to the ground state. Thus, the echo output will decrease when the storage time, T, is of the order of the lifetime for spectral features (holes) created in the absorption line, T_1^{hole}, according to

$$I = I_\infty \cdot e^{-2T/T_1^{hole}} . \qquad (5.4)$$

Here I_∞ is the intensity if $T_1^{hole} \to \infty$. Thus, the lifetime of the states that are used for persistent storage can be measured by studying how the echo intensity depends on the separation between the second and third pulses (data and read-out pulses) in a three-pulse photon echo experiment.

5.2 Information storage using photon echoes

5.2.1 Sequential data storage

The fact that the shape of a photon echo can be highly correlated to the shape of one of the excitation pulses was perhaps first discussed by Elyutin et al. [175] and in 1980 by Zuikov et al. [176], who also mentioned the possibility of technical applications. Around the same time, it was also pointed out, and demonstrated independently by Hesselink et al. [140] and Mossberg et al. [122], that all relevant information of a stimulated photon echo can be stored in the population of only one specific state, and that in some cases this information can persist for a very long time. Consequently, in 1981 Mossberg described time-domain frequency-selective optical data storage [100], where stimulated photon echoes are used to store both the temporal and the spatial behaviour of a laser pulse, in the spatial and spectral distribution of population in the ground state of an inhomogeneously broadened absorbing material. The idea is closely related to the *spin echo serial memory* suggested in 1955 by Anderson et al. [177].

Within the next few years, more discussions and demonstrations of photon echo optical data storage appeared, where metal vapours (Yb) [178] or ruby [138] were used as the storage medium. In 1987 Babbitt et al. demonstrated data storage in a rare-earth-ion-doped crystal ($Eu^{3+}:Y_2O_3$) at cryogenic temperatures, and they were able to store a complex optical pulse shape (a pattern consisting of six pulses) and reproduce it after delays of up to a minute [179]. The ion-doped inorganic crystals were already being investigated as possible candidates for frequency-domain memories and were now also studied with regard to the properties relevant for time-domain frequency-selective memories, e.g. Refs. [58,180].

An important step was taken when pulse-shape storage using frequency-swept excitation pulses was introduced and demonstrated, first in Yb vapour [148] and later in an inorganic solid (Pr^{3+}:$YAlO_3$) [181]. Frequency-swept excitation pulses can be longer and of lower intensity than fixed frequency pulses and are thus easier to generate. The problem of coherent saturation of ions absorbing at the carrier frequency is also alleviated by the use of chirped pulses.

Using a tuneable laser source it is also possible to create a time- and frequency-domain hybrid optical memory, where a short temporal data sequence is stored using photon echoes, and then the laser carrier frequency is moved to another spectral location, where a new sequence of data can be stored. This has the advantage of random access to the spectral storage locations/addresses, but the technique is only interesting when the bandwidth of the data streams is much less than the inhomogeneous width of the absorption profile of the storage medium, i.e. when the bit rate is $<< \Gamma_{ih}^{-1}$. In 1991 Mitsunaga et al. used the technique to store 1.6 kbit data in a single spot [101]. At each spectral position the time-domain data were stored bit-by-bit using accumulated photon echoes, but all data bits stored could be recalled using a single read-out pulse, and the storage time was up to hours in the material used (Eu^{3+}:Y_2SiO_5), see Ref. [182].

A more general approach to hybrid time-/frequency-domain optical data storage was introduced in 1992 by Mossberg – the swept-carrier time-domain optical memory [134]. In this approach the frequency of the reference (write) field and the amplitude-modulated data field are swept in a continuous manner over the bandwidth where data are to be written. Both fields are applied simultaneously but with a slight frequency off-set, so that the data field interacts with atoms absorbing at a particular frequency some time τ_d after they have interacted with the write field. If τ_d is less than the phase memory time T_2 of the material, an echo will be produced with an additional delay τ_d after a data pulse. If the material has a mechanism for long-time storage of a spectral population grating (e.g. a metastable level) it is possible to stimulate an echo, recalling the data sequence after some time (limited by the lifetime of the metastable level), by applying a frequency-swept laser field that mirrors the original reference field. The swept-carrier time-domain optical memory was demonstrated in 1994, in Tm^{3+}:YAG [183], and in 1995 a storage density of 1.2 Gbit/cm^2 was demonstrated [159]. At most, 4 kbit in a single spatial location was demonstrated. The set-up used co-propagating data, and reference beams and output data pulses were identified using heterodyne detection.

Later investigations of photon-echo time-domain optical memories have focussed on circumventing some of the more serious process limitations, finding suitable materials and developing necessary technology such as frequency-agile lasers emitting light at the right wavelengths. Coherent saturation and the practical problem of generating suitable reference pulses (equivalent to powerful, brief pulses) have been addressed by introducing the use of phase-modulated and frequency-swept reference pulses, as was mentioned above. Excitation-induced frequency shifts [36,49-51,80-83,184] have proved to be a serious obstacle in realising the full spectral storage capacity of inorganic ion-doped crystals, but it has been shown that this problem can be overcome by using spatial modulation (scanning) of the writing beams while storing data, such that the density of excited ions is always low [185].

Several authors have addressed the issue of optimisation of the storage density of a two-dimensional storage device [164,165]. For given material parameters, one of the main

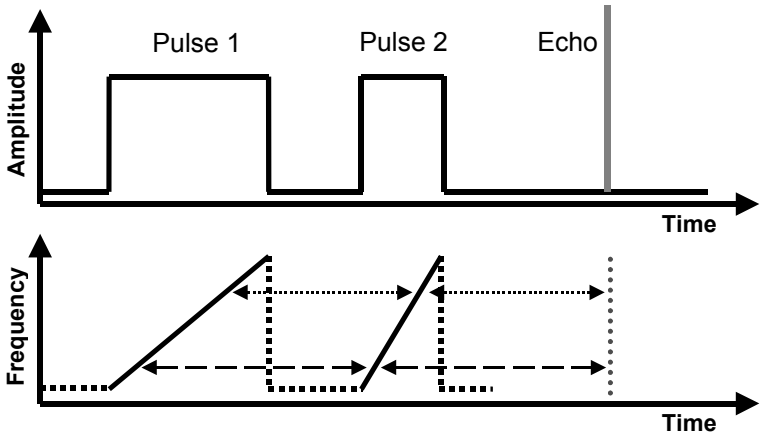

Figure 5.2. *Pulse compression using the two-pulse photon echo process. The second pulse is chirped twice as fast as the first. Atoms absorbing at each particular frequency will emit an echo after a time equal to the time between their interaction with the first and the second pulse. The result is a strong, brief (broadband) echo. If the first pulse is amplitude modulated, the echo will take the form of a Fourier transform of this input waveform.*

parameters that should be optimised is the absorption of the sample, where the optimum is generally found to be $\alpha L \approx 1$, or $\sigma n L \approx 1$, where σ is the absorption cross-section of the active ions and n is the concentration of ions. Another parameter is the diameter of a storage cell, which must be large enough for each cell to contain a sufficient number of ions to achieve a resonable signal strength. Development of materials for use in these applications has mainly focused on achieving a long dephasing time, T_2, and a high ratio between the homogeneous and inhomogeneous linewidths, Γ_{ih}/Γ_h, which gives a high capacity for spectral storage and processing [39,46,53].

5.2.2 Image storage

In photon-echo-based data storage, the medium stores information about both the temporal/spectral shape of the input pulses and spatial information such as beam direction. In the terminology of holography, information is stored as spatial as well as spectral gratings. This implies that storage and read-out of different data sets can be associated with different directions and that a complete image can be encoded onto a light wave and stored in a single spatial and spectral location. Time-domain holographic image storage was first demonstrated by Carlson et al. in 1983 [186], and in 1987 Kim and Kachru demonstrated the storage of multiple images at a single spatial location in an inorganic crystal (Pr^{3+}:LaF_3) [187].

Holographic data or image storage has been studied extensively and when persistent spectral hole-burning began attracting interest the two were combined in holographic frequency-domain storage. In a given spatial location it is, in principle, possible to store one image per spectral channel and to retrieve any individual image or play them back sequentially, within the spectral hole lifetime. Holographic hole-burning has been demonstrated by Wild and Holiday in dye-doped polymers [188] and in crystals [26], and in 1993 Mitsunaga et al. made a real-time recording of a moving object using persistent spectral hole-burning in cryogenic Eu^{3+}:Y_2SiO_5 [189]. In that demonstration the laser frequency was continuously scanned (by 200 MHz in 20 s) within the material absorption line, while holographically recording images. This meant that the recording was mainly in the frequency domain and each image could be seen as a separate spectral-spatial hologram. However, it is possible to use the data storage techniques described above, such

as the swept-carrier time-domain approach, for recording fast-moving objects, using the full bandwidth of the materials. For inorganic crystals doped with rare-earth ions this means timescales of ~1 ns or less.

Time-domain holographic image storage was impressively demonstrated by Shen and Kachru [102,190], who stored 100 pages of data, each containing 3360 bits, in a single spatial location in a rare-earth-ion-doped crystal. The images were encoded by sending a laser beam through a spatial light modulator (SLM) and then focusing it onto the storage medium, where it was overlapped with a reference beam. Each page was written as a three-pulse photon echo, with a write pulse from the reference beam followed by the data pulse and, at a later time, by a read pulse from the reference beam. The shortest pulse duration (also the shortest access time) was 11.2 μs and the pages were stored in distinct frequency channels, 800 kHz apart.

5.3 Optical signal processing

The many degrees of freedom in a general photon echo process offer many possibilities for applications in optical signal processing. Information can be processed on the basis of temporal information, frequency content or the angle of incidence of the optical fields. Photon-echo materials such as rare-earth-ion-doped crystals promise high bandwidths (Γ_{ih} can be up to 200 GHz) and high data through-puts. The ability to engrave spectral gratings in the inhomogeneously broadened spectrum of absorption frequencies means that the material can be temporally or spectrally programmed, or used to detect and accumulate weak optical signals based on frequency or phase. General signal processing using optical coherent transients have been discussed by Babbitt and co-workers in Refs. [160,191] and [107].

One straightforward aspect of the photon echo process is the ability to create or record a delay between optical pulses. Applying one or more pairs of pulses, with a separation τ between the pulses, records the time-delay, τ, in the form of a spectral grating in the material with a period $\Delta\nu=1/\tau$. So-called *true time delay* generation is interesting in radar applications using a phased array antenna and has been investigated in a number of experiments [149,192,193]. Merkel et al. have recently demonstrated radar range processing, using photon echo technology, at bandwidths of several GHz [194], with excellent signal-to-noise ratios.

Temporal pattern recognition and spatial routing of optical beams depending on the temporal structure of the signal has been proposed and demonstrated [139,195]. In demonstrations of the extraction of optical header information [103,196], the headers are programmed into the photon-echo material at different angles, before the data stream is sent into the material. If one of the pre-programmed headers occurs in the data stream, an echo will be emitted in a direction characteristic for the particular header.

Temporal compression of optical pulses using photon echoes was proposed by Bai and Mossberg in 1984 [197] and demonstrated two years later in a gaseous medium [198]. Later, the same technique was demonstrated using a rare-earth-ion-doped material and optical bit-rate conversion was studied [166]. The principles of pulse compression can be understood by considering a two-pulse photon echo created with two relatively long, frequency-chirped pulses (see Fig. 5.2). The two pulses are chirped over the same bandwidth, but the chirp rate of the second pulse is twice that of the first and is thus only

half as long. Interaction between the pulses and ions absorbing light at different frequencies takes place at different times, and for each frequency channel an echo will be emitted after the second interaction, with a delay equal to the time between the two interactions. The chirp rates, $2r_1=r_2$, are chosen such that all ions will emit their echo at the same time. The duration of the echo is determined by the bandwidth that has been excited, in theory $T_e \approx 1/\Delta\nu_{chirp}$. Optical pulses have been compressed from 10 μs to 22 ns, using a rapidly tuneable diode laser to excite ions in Tm-doped YAG [167]. Compression of a sequence of pulses can be performed by amplitude modulating the first of the two chirped pulses used in the compression. In this case, the output echo will basically be a Fourier transform of the input pulse sequence. The possibility of using chirped pulses in the photon echo process to implement Fourier transforms has been investigated by Menager et al. [136].

SUMMARY

- A major part of the research concerning coherent interactions in rare-earth-ion-doped crystals has addressed the use of coherent transients for all-optical storage and processing of (classical) information. Applications that have been demonstrated include high-density data storage, temporal pattern recognition, spatial-spectral routing, spectral filtering, all-optical logic operations, data rate conversion and pulse compression.
- The applications use the fact that the individual ions only absorb light within a very narrow frequency interval, Γ_h, and thus act as a kind of narrowband spectral filter, whereas the useful bandwidth of the full ensemble of ions, Γ_{ih}, can be many orders of magnitude larger.
- In the time-domain (photon-echo) approach to data storage in frequency-selective materials, the Fourier transform of temporally modulated input fields is stored in the form of a frequency-dependent modulation of the population of absorbing ions, within the inhomogeneously broadened absorption profile of an optical transition.
- The coherence properties of the rare-earth ions that are used in these applications and the techniques for manipulation of ensembles of rare-earth ions in the frequency or time domain can also be useful for quantum information processing.
- The development of materials for use in these applications has mainly focused on achieving a long dephasing time, T_2, and a high ratio between the homogeneous and inhomogeneous linewidths, Γ_{ih}/Γ_h, which gives a high capacity for spectral storage and processing. Since ion-ion interactions and spectral diffusion are detrimental to most applications, efforts are being made to minimise these effects.
- The reference pulses used within the field of photon-echo-based information processing must affect ions within a broad range of resonance frequencies with a specific pulse area, usually $\theta=\pi/2$ or $\theta=\pi$. This can be achieved, for example, using brief, strong pulses or using pulses with a linear frequency chirp.
- As part of the effort to maximise the photon-echo signal in these applications, ion-ion interaction and spectral diffusion caused by optical excitation of ions has been studied in some detail in various rare-earth-ion-doped materials, mainly using photon echoes. These interactions can be used for quantum logic operations in a quantum computer based on rare-earth-ion-doped crystals.

CHAPTER 6

EQUIPMENT

Several different experiments were performed in the work described in this thesis. This chapter contains a brief out-line of the elements that were common to the different experiments and some comments on technical issues that were found to be of particular importance when using rare-earth ions for quantum information science. Most of the experimental set-ups contained the following equipment:

- a laser, producing coherent light at a suitable wavelength,
- a modulation system, shaping the frequency, phase and amplitude of the light to perform the desired operation on resonant ions,
- a sample, containing rare-earth ions with suitable optical properties (the sample is contained in a cryogenic system, at temperatures of a few K), and
- a detection system – photo detectors, connected to an oscilloscope and a computer for recording the results of the experiment.

In addition to the equipment discussed below, a typical experimental set-up will contain a large number of standard optics components, such as mirrors, lenses, quarter- and half-wave plates, beam splitters, colour filters, and so on, and ancillary electronics for control and measurement. Background material can be found e.g. in Refs. [17,199,200] and general information about optical equipment can also often be found in catalogues from companies producing lasers and optical components.

6.1 Lasers

The main tool used in our experiments is laser light, i.e. coherent optical radiation. A first requirement is therefore one or more laser sources that produce light at a wavelength matching the absorption wavelength of the atoms we are working with, in a single mode and with sufficient output power. Here, lasers with a continuous (CW) output were used and the output was externally amplitude modulated to create pulses of appropriate durations. Typical optical powers used were 1-100 mW and typical pulse durations were 10 ns to 100 μs. Pulsed lasers, such as mode-locked or Q-switched lasers [17] can produce much higher peak intensities than CW lasers, but the pulses cannot be modulated arbitrarily and are often unnecessarily short, even if the full inhomogeneous bandwidth of an RE material (a few GHz) is used in the experiments.

For Tm^{3+}-doped materials, absorbing around 793 nm on the $^3H_6$-$3H_4$ transition, a Ti:Sapphire laser (MBR-110) or external cavity diode lasers [201], were used. The Ti:Sapphire laser can produce several hundred mW output power and can be tuned from 700 nm to 1050 nm. The laser cavity is a butterfly-shaped ring cavity and the lasing crystal is pumped by green light from an Ar-ion laser or a Nd laser. The frequency is actively stabilised and locked to a reference cavity which gives a linewidth of less than 100 kHz. Diode lasers are easier to operate but give less output power (<50 mW) and do not have as

high beam quality. The external laser cavities are fitted with electro-optical crystals, which allow very rapid frequency tuning within several GHz, which is useful for changing the laser frequency between different spectral positions within an inhomogeneous absorption profile [202].

For crystals doped with Eu^{3+} or Pr^{3+}, absorbing around 580 nm (the $^7F_0$-$^5D_0$ transition in Eu^{3+}) and 605 nm (the $^3H_4$-$^1D_2$ transition in Pr^{3+}), dye lasers (Coherent 699-21) were used. No high-power laser diodes are available at these wavelengths and although optical parametric oscillators (OPOs) or frequency doubling could be used, so far sufficient output powers and frequency stability have not been achieved. Dye lasers can produce several hundred mW output power and can be used for any wavelength in the visible range, by choosing an appropriate dye. However, they are intrinsically somewhat unstable, mainly because the lasing medium in this case is a jet of liquid dye, spraying through open air in the centre of the laser cavity. The commercial version of the dye laser used is actively frequency stabilised, using an intra-cavity piezo-mounted movable mirror, which gives a linewidth of less than 1 MHz. A modified version of this laser, with a linewidth of less than 50 kHz, was also used. In that laser system, an intra-cavity electro-optic crystal was used to further stabilise the optical path length of the cavity and the frequency was locked to a highly stable cavity using the Pound-Drever-Hall method [203]. The design follows that of the laser described in Ref. [204].

The $^4I_{15/2}$-$^4I_{13/2}$ transition of Er^{3+} occurs around 1.5 μm, which makes it interesting since this is in the telecommunications band, where lasers and other equipment are readily available. One example is fibre lasers, using a length of Er-doped fibre, pumped by laser diodes, as the laser oscillator. Er^{3+}-doped materials were not used in the experiments presented here, but are used by many other groups working with rare-earth-ion-doped crystals.

It is a technical challenge to construct laser systems with the required frequency and amplitude stability for precise coherent manipulation of quantum systems. Since the rare-earth ions can have transition linewidths of less than 1 kHz, corresponding to coherence times of more than one ms, lasers used for driving rare-earth ions should ideally have as good or better coherence properties [205]. To achieve this, active stabilisation of the laser frequency is needed. This is done by using a fast element, such as an electro-optic modulator or a piezo-mounted mirror, inside the laser cavity, which can adjust the optical length of the cavity to counteract any disturbances. The frequency of the laser is locked to a stable reference, through an error signal which changes if the phase or frequency of the laser drifts relative to the reference. One commonly used reference is the transmission fringes of a Fabry-Perot etalon, which should be thermally and vibrationally insulated to achieve high stability. The error signal can be obtained by sending some of the laser light through the etalon and monitoring the transmission or by the more sophisticated Pound-Drever-Hall technique [203], where the cavity is used in a reflective mode. Atomic resonance lines are also often used as frequency references. In the work presented in Paper IV, the laser frequency was locked to a transition in iodine molecules, to prevent thermal drift during the hour-long experiments. Rare-earth ions themselves provide good frequency references, as they have narrow homogeneous linewidths, and lasers have been locked to transitions in RE-doped materials with good results [40,41,99].

In order to access the full inhomogeneous absorption profile of rare-earth doped crystals, which can be tens of GHz, it is an advantage if the laser is frequency agile, i.e. if it can be

tuned over a large bandwidth in a short time. However, since it can be difficult to achieve both tuneability and frequency stability at the same time, the easiest solution is often to frequency modulate the output from a stable laser using an external frequency modulator.

High output powers are always an advantage. The speed with which the ions can be optically manipulated can be limited by the available laser power if the power is not high enough. In this case the laser light can be amplified, e.g. using fibre or diode amplifiers.

6.2 Modulators

After the laser, the continuous laser beam is modulated to obtain the required pulses. Here, mainly acousto-optic modulators (AOMs) were used, but also to some extent electro-optic modulators (EOMs) and mechanical shutters.

The requirements on amplitude modulation are high efficiency, i.e. when the modulator is open the losses should be low, and good suppression when the modulator is closed. This is especially important when working with weak pulses and weak signals, as in the experiments described in Paper IV, where an on/off ratio of $1{:}10^8$ was required.

Frequency modulation is needed to create chirped pulses, but also to access different transitions or ions with different inhomogeneously shifted resonance frequencies. As the frequency difference between transitions from different hyperfine states can be several hundred MHz, and as the inhomogeneous absorption profiles are often several GHz wide, it can be dificult to achieve sufficient bandwidth using a single modulator. In this case several modulators or more than one laser may be necessary to access all required frequencies.

The spectral purity of the light will be important when a small number of ions, or a weak transition, is to be studied at frequencies that are spectrally close to a bulk of absorbing ions. It is important that the modulator does not add harmonics, spurious frequencies or noise to the light. The *spurious free dynamic range* (SFDR) is defined as the ratio between the largest unwanted spectral component and the energy of the carrier frequency, measured in dB. If care is taken to use only low-noise components, high-resolution DA converters, power amplifiers with small frequency intermodulation (non-linearities), and so on, it is possible to achieve an SFDR of -50 dBc (relative to the carrier), or better, in a modulation system capable of generating arbitrary pulses [206,207].

The speed of the modulator should be sufficient to allow pulses to be applied within the coherence time of the laser and the ions. In most cases, a modulation bandwidth of 10 MHz, or pulses with a duration down to 100 ns, was sufficient for the present work.

6.2.1 Acousto-optic modulators

In an AOM, an acoustic wave sent through a crystal generates a periodic modulation of the refractive index and light is diffracted off this acoustic grating. In the Bragg regime, the first order of diffracted light will be deflected by an angle

$$\theta = \frac{\lambda F}{v} = \frac{\lambda}{\Lambda} \tag{6.1}$$

where $\lambda=\lambda_0/n$ is the optical wavelength inside the crystal, v is the acoustic velocity, F is the acoustic frequency and Λ is the wavelength of the acoustic wave. The diffracted light can be separated from the non-diffracted beam using a pick-off mirror or an aperture, and the light is amplitude modulated by turning the acoustic wave on and off. The diffracted light will pick up the properties of the acoustic wave: the frequency of the sound is added to that of the light ($\nu_{diffracted}=\nu_{laser}+m\cdot F$, where m is the order of diffraction), and the phase of the light changes if the phase of the sound is changed. The acoustic wave is generated from an RF signal, which is first amplified to 1 W or more. The intensity of the diffracted light, I_1, is related to the incident light intensity I_0 by

$$\frac{I_1}{I_0} = \sin^2\left(\frac{\pi}{2}\sqrt{\frac{P}{P_0}}\right) \tag{6.2}$$

where P is the acoustic power and P_0 is the optimal power, given by the dimensions of the acoustic beam and by the acousto-optic material. By modulating the RF signal input to the AOM, the light can be arbitrarily modulated. Typical RF/acoustic frequencies used are between 50 MHz and 500 MHz. Although the efficiency of the modulator is maximal for a certain frequency and diffraction angle, the carrier frequency of the modulator (and thus the frequency of the diffracted light) can often be tuned within an interval of ±25% around the centre frequency, with less than 3 dB loss of efficiency. Using several AOMs in series, or a single AOM in a multiple-pass configuration, a frequency range of several hundred MHz can be accessed. The modulation speed of an AOM is dependent on how fast the acoustic wave can traverse the laser beam. With a typical acoustic velocity of 4200 m/s in TeO_2 and a beam waist diameter of 0.2 mm, the light can be modulated on timescales of ~50 ns.

A standard method of generating a variable RF signal to drive an AOM is to use a voltage-controlled oscillator (VCO) followed by an RF switch or a variable attenuator. However, the VCO may have a limited tuning rate, which gives the system a limited frequency agility, and arbitrary phase shifts are not readily achieved. The dynamic range and suppression of the RF attenuator/switch may also be a concern. An alternative technique, which gives greater flexibility is direct generation of the RF pulses using a digital arbitrary waveform generator (AWG). In combination with computer programs controlling the waveform generator, this makes it possible to generate very complex pulses and pulse sequences consisting of hundreds of different pulses. This approach was used in the experiments presented in Papers II and III.

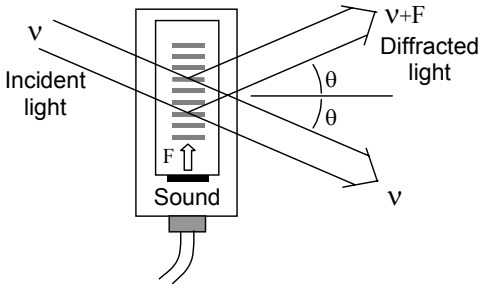

Figure 6.1. *Acousto-optic modulator, aligned to maximise the first-order diffraction. The intensity of light diffracted into the output beam is dependent on the power of the acoustic beam, which in turn is dependent on the modulation signal input to the driver. The frequency and phase of the sound wave is added to that of the diffracted light.*

6.2.2 Electro-optic modulators

In an electro-optic modulator, the refractive index of the electro-optic material is changed by applying a voltage across it. A laser beam passing through the EOM will experience a variable phase shift. By applying an oscillating voltage, with frequency F, to the EOM, sidebands can be added to the laser light, with frequencies $\nu_{laser} \pm F$. By varying the frequency and amplitude of the electric modulation, the sidebands can be frequency and amplitude modulated. A sideband can then be used to drive atomic transitions, but some thought must be given to the effect of the light at the carrier frequency and in the additional sideband. For an RE material, the carrier and one sideband may be positioned outside the inhomogeneous absorption profile, if the modulation frequency is higher than a few GHz. Alternatively, in a material where spectral hole-burning occurs (see Chapter 3), the carrier frequency may be allowed to burn a hole in the inhomogeneous absorption profile, after which it will no longer interact with any ions.

An EOM can also be used as a polarisation switch, if it is rotated so that one polarisation component is phase retarded when an electric field is applied over the electro-optic material. If a polariser is placed after the EOM, the transmitted light can be amplitude modulated. The modulation speed can be very high (several GHz), but the on/off ratio is usually limited to 10^2-10^3:1.

6.2.3 Mechanical shutters

A mechanical shutter "amplitude modulates" light by simply moving a non-transparent object into the path of the laser beam. Using a fast-moving sharp edge (e.g. >100 m/s near the edge of a rotating disc) and narrow beam diameter at the shutter (e.g. <0.1 mm in a beam focus) a rise/fall time down to 1 μs can be achieved. The obvious advantages of a mechanical shutter are that the suppression of the light can be nearly perfect when the shutter is closed and that there are no losses or distortions when the shutter is open. The disadvantage is that mechanical shutters usually only work at low repetition rates.

6.3 Crystals

The samples used were inorganic insulating crystals, doped with rare-earth elements. The samples were *single crystals*, i.e. there is only one crystal domain, so the crystal lattice has the same orientation throughout the sample. Typical transverse dimensions of the sample range from a few mm to slightly more than one cm. The length, L, of the crystal, i.e. the thickness in the direction of light propagation, can be selected according to the required optical depth, αL, and is typically between 0.5 mm and 10 mm. Since the laser beam is focused in the sample, only a small part of the crystal volume is actually used in an experiment. Two or more sides of the crystal are polished to optical quality, to allow the laser beam to be transmitted and to allow collection of fluorescence.

The optimal optical density of the sample varies depending on the experiment. It can be shown that a standard photon-echo sequence gives the highest output signal when $\alpha L \approx 1$. On the other hand, propagation effects in combination with pulses that invert the medium ($\theta \approx \pi$) can give stronger (although distorted) echoes, in a sample with $\alpha L >> 1$. In experiments with "slow light" [208] or where light is to be "stored" in the sample (see Chapter 7 and Paper V), it is usually advantageous to have $\alpha L >> 1$, to ensure that the incoming light interacts sufficiently with the medium. In applications such as quantum computing, where all ions should experience the same laser field, propagation effects should be avoided and $\alpha L << 1$, otherwise ions at the end of the crystal will experience a

weaker, or at least distorted, laser field compared with ions near the front of the crystal. A disadvantage of a sample with low absorption is of course that the signal will be weak if absorption measurements are used to study the atomic state.

The optical properties of the sample will vary depending the on rare-earth dopant, host material and dopant concentration. They may even vary from sample to sample, depending on the method used to grow the crystal and how successful the process was. There is an ongoing search for new rare-earth-ion-doped materials for various applications, such as lasers, scintillators, optical signal processing or quantum information processing. During the course of the work presented here, various materials were analysed regarding their suitability for use in quantum information processing, and high resolution spectroscopy were performed on previously unstudied materials (Paper VII).

The narrow homogeneous linewidths of RE materials are a prerequisite for many applications and it is important not to lose this property while trying to optimise the other parameters. A strong optical transition is advantageous, because it enables fast driving of the transition, without the need for very intense laser fields. However, a strong transition also implies faster spontaneous decay. A large inhomogeneous linewidth may be useful for signal processing or data storage applications, where a large bandwidth is desired, but in ensemble-based quantum computing schemes it is more desirable to have the ions concentrated to a narrower spectral interval. Ion-ion interaction is detrimental to many applications because it causes dephasing and thus increases the homogeneous linewidth. However, for continued development of quantum computing using RE materials, it may be advantageous to find materials with much stronger ion-ion interactions than in the materials used today.

6.4 Cryogenic systems

The materials used must be kept at very low temperatures in order to maintain their favourable optical properties. Above a certain temperature – usually of the order of 4-10 K – the homogeneous linewidth and the rate of spectral hole relaxation increase dramatically. Somewhat below this temperature, the relaxation is usually relatively independent of temperature. Thus, the samples are cooled and kept in a cryostat, around or below 4 K.

The cryostats used were cooled with cryogenic liquids, such as liquid helium and nitrogen. The helium is kept in a reservoir near the centre of the cryostat, surrounded by a nitrogen-cooled shell and evacuated shells for insulation. Glass or quartz windows give optical access to the central sample chamber. In a *bath cryostat* the sample is immersed in liquid helium, whereas in a *continuous flow cryostat* small amounts of helium gas or superfluid helium are continuously pumped over the sample. One disadvantage of a bath cryostat is that bubbles may form in the liquid helium, which distort the laser beam going to the sample. In a flow cryostat, there is not necessarily an internal helium reservoir but the helium can also be pumped through the cryostat from an external helium dewar. The sample may be mounted on a thermally conducting *cold finger*, which is cooled by the helium. By evacuating the helium container, the boiling point of the helium and thus the temperature can be lowered until, at a pressure of 50 mbar and a temperature of 2.7 K, the helium becomes superfluid. By varying the pressure, the temperature can be continuously adjusted and temperatures below 1.7 K can be reached, mainly limited by the capacity of the vacuum pump.

There are also closed-cycle cryostats, which do not require a supply of cryogenic liquid. In these, a compressor continuously compresses a cooling medium which circulates through the system, as in a conventional refrigeration system. Advanced closed-cycle cryostats can reach temperatures below 4 K, although with limited cooling power. One disadvantage of closed-cycle systems is that the compressors produce relatively large vibrations, which may be difficult to remove completely.

Many experiments involve applying a magnetic field to the sample and for this purpose the cryostat may be fitted with magnets. Magnetic fields of several T can be produced by using superconducting coils, which can be conveniently cooled together with the sample.

6.5 Detectors

After the sample, the transmitted light and the light emitted by the ions is detected using some type of photo detector. Various types of *photo diodes* and *photomultiplier tubes* (PMTs) were used. The relevant properties of the detector are speed, sensitivity and noise and there is often a trade-off between these properties. The detectors used had bandwidths from 500 MHz down to around 0.5 MHz. Typical optical powers detected were 10 μW to 10 mW using photo diodes, and down to a few nW (a few hundred photons per pulse) using a PMT.

Photo diodes are semiconductor devices which produce a current proportional to the incident light [209]. In principle, one electron-hole pair can be generated for each incoming photon, if the photon energy is greater than the energy gap between the valence band and the conduction band in the active region of the diode. In practice, the quantum efficiency, i.e. the probability of a photon generating an electron, varies between 50% and 90% depending on material and wavelength. However, it can approach 100% e.g. for a silicon diode at around 800-900 nm. The signal is often electronically amplified, near the diode, to the required voltage levels. In an *avalanche photo diode* (APD) the diode is operated under a reverse-bias voltage that is sufficient to enable avalanche multiplication, which results in an internal current gain. In this way, signals consisting of few or single photons can be detected.

In a photomultiplier tube, the light first hits a photo-sensitive material, the *photocathode*, which releases electrons. The electrons are accelerated by a high voltage between the photocathode and an anode, via a chain of *dynodes*. As accelerated electrons hit a dynode, more electrons are released and the result is a multiplicative current gain. The gain increases with increasing voltage over the PMT. Typical voltages are 1-2 kV which results in gains of up to 10^6-10^7. If the electron multiplier has a long chain of dynodes (e.g. 14 dynodes) and a high voltage is used (e.g. 3 kV), the gain can exceed 10^8. A low-noise PMT can be used to detect single-photon events, i.e. when a single photoelectron is released from the cathode. Typical response times are a few ns, set by the geometry of the dynode chain, as the travel time of the electrons from cathode to anode varies. The quantum efficiency of a PMT is determined by the spectral response of the photocathode material. Typically, the maximum efficiency is between 5% and 25% for materials working in the visible and ultra-violet spectral range and less than 10% in the (near) infra-red [210].

One of the most useful detectors in the lab is, of course, the naked eye. If a rare-earth-ion-doped material fluoresces in the visible range, the fluorescence can often be detected by

viewing the laser focus in the sample through a filter, which is a good aid in finding the optical resonance line. Alignment of modulators etc. can be done by direct inspection of the attenuated laser beam or, when working in the infrared, with the aid of an IR viewer. It is interesting to note that the eye is a very sensitive detector, in principle capable of detecting single photons. However, it only has a time resolution of the order of 20 ms and it is easily damaged.

SUMMARY

Technological advances are likely to make it increasingly easy to manipulate the world on the quantum level, using coherent radiation or otherwise. Many of the tools required for advanced quantum information science have already been developed and are now maturing. The unanswered questions mainly concern the quantum systems themselves – how do we find or build systems that will allow us to easily explore and exploit their world? This is also true for quantum information processing in rare-earth-ion-doped crystals – new materials and a better understanding of their properties will be essential if they are ever to be used for quantum computing. In the present context, the equipment outlined above can be seen as the interface between the quantum world and the everyday world – and in quantum science many mysteries lie at this interface.

Any list of state-of-the-art technology is doomed to become outdated all too soon, so no attempt will be made to give one here. Instead, some examples will be given of technological advances, which in the author's opinion are likely to be important for the future of quantum information science based on optical interactions. However, these areas lie outside the scope of this thesis and references are provided only as examples.

- Coherent radiation can be produced at almost any frequency from radio waves up to ultraviolet light and beyond [15,211-213].
- Lasers have been phase and frequency stabilised to extremely narrow linewidths for extended periods of time [214,215].
- Light can be modulated in space, time and frequency with ever-increasing precision and speed.
- Pulses of coherent radiation can be produced on almost any timescale, down to less than one fs [216-218].
- The radiation from single quantum systems, such as a molecule or a quantum dot, can be measured and characterised. [219-225].
- The techniques for isolating quantum systems from unwanted interactions, such as vibrations, collisions or stray photons, are constantly being improved. Vacuum technology and low-temperature physics are old but are still being improved on. Commercially available refrigerators can cool matter to below 10 mK [226] and nuclei in solids have been cooled to below 0.1 nK [227].
- Atoms can be trapped and cooled to below 20 nK [228,229]. Using nanostructured devices, cold atoms can be confined and controlled on spatial scales smaller than 100 nm [230].

CHAPTER 7

QUANTUM OPTICS IN RARE-EARTH-ION-DOPED CRYSTALS

When a system with long-lived coherences between energy levels interacts with coherent light, some very quantum and often counter-intuitive optical phenomena can occur. These include *self-induced transparency* [124], *coherent population trapping* [157], *electromagnetically induced transparency* (EIT) [231,232], *lasing without inversion* [233] and refractive index enhancement via quantum coherence *(slow light)* [234]. Sometimes, the effects can be related to exotic states of the quantised electromagnetic field, such as *single photons* or *squeezed* or *entangled states* (see e.g. Ref. [116]). Some of these phenomena are likely to become important for future technology, e.g. within quantum information science or in laser technology, and it is also interesting to study the effects because they give fascinating demonstrations of the workings of quantum mechanics. This chapter concerns the possibility if performing quantum optical experiments in rare-earth-ion-doped materials (RE materials). Two examples are discussed – the demonstration of *single-photon self-interference* (Paper IV) and schemes for storing the quantum state of light in a solid (Paper V).

Most quantum optics experiments have been performed in gases, i.e. in free atoms, rather than in solids or liquids. Quantum optics in solids can be difficult, because the number of states and transitions is usually overwhelming, due to the large number of interacting particles, and because coherence times are often extremely short. However, it is still interesting to look for suitable systems for solid-state quantum optics, because the thermal movement of atoms in a gas cause problems in many experiments, and because solid-state implementations of practical applications can often be made robust and compact. Effects caused by the movement of atoms in gases, e.g. so-called *flight-out-of-view effects*, can be reduced by cooling or trapping atoms, and research in this area has been highly rewarding. Impurities in solids can be seen as a kind of naturally occurring "trapped atoms", if interactions with the host material can be reduced. RE-doped materials constitute one example of such systems.

A complete description of the interaction between light and atoms must include the quantum state of the electromagnetic field, as well as the state of the atoms. A result of such a description is that the energy of the field can only change in discrete steps and that it can be described both as a stream of particles, *photons*, and as a wave [116,235]. The wave-particle duality of light (and matter) has been an important issue in the development of quantum mechanics. *Young's double-slit experiment* illustrates the possibility for single quantum objects to interfere with themselves and *Gedanken* experiments of this type are often used in discussions of, for example, quantum measurements or quantum interference.

Some intriguing questions arise if the experiments discussed below are described in the language of non-linear optics, where the radiation fields are usually treated classically while the atoms they interact with are treated quantum mechanically. The processes considered in non-linear optics involve several optical fields interacting with atoms, or a single field acting in more than one way on the atoms, often eliciting an output field. Each field causes partial transfer of population and coherence between two energy levels and the resulting fields can be calculated from the sum of all possible quantum mechanical paths [115]. A process is often visualised using an energy level diagram, with arrows representing the effect of each field, where each arrow is usually thought of as representing one photon. Unless absorption or emission takes place, the initial and the final state of the atoms will be the same, i.e. the arrows form a closed path. In a material with long-lived coherences between energy levels, such non-linear optical processes can occur even if the fields are separated in time. Intuitively we can say that, in many ways, a long phase memory (narrow resonance width) implies an uncertainty about the exact time of events. One example is the three-pulse echo, which can be described in terms of degenerate four-wave mixing, where the excitation pulses correspond to three input fields and where the fourth field is the echo. Some very fundamental issues arise if we move to the realm of quantum optics and replace two of the fields with a single photon, in addition to separating them in time. For instance, it is no longer possible to interpret each arrow in the level diagram describing the process as representing one photon.

7.1 Delayed single-photon self-interference

7.1.1 Single-photon states

Many experiments proposed within quantum optics concern the properties of single photons. For example, the experiment described in this section investigates the interaction of single photons with a macroscopic number of ions, in a photon echo process. Within quantum information science a single photon can be used to encode one bit of information, e.g. as the absence/presence of a photon, or in the polarisation of the photon.

However, experimentally it is non-trivial to realise states of the quantised electromagnetic field with a definite number of photons – so-called *number states* or *Fock states*. Although it is easy to identify processes that generate a single photon, e.g. the fluorescence from a single absorber, it can be difficult to control the timing and the mode (direction/frequency) of the photon. Much research has been directed towards the question of how to create single photons "on demand" and sources producing single photons have recently been demonstrated in different systems [236-238].

Highly attenuated laser pulses are often used instead of true single-photon wave packets. The output from a laser source, operating far above threshold, is a *coherent state* of the electromagnetic field, characterised by its amplitude and phase rather than by the number of photons. The probability of finding a specific number of photons in a coherent pulse is given by a Poisson distribution, see Fig. 7.1. If the amplitude of the field is sufficiently attenuated, the probability of finding more than one photon can be made arbitrarily small and any signal can be considered to be caused by single photons. Of course, there will also be a large probability of finding zero photons in the field. Even if there is a non-negligible probability of finding two or more photons in the pulses, effects due to single photons can still be deduced by using knowledge about the photon number distribution. This was used in the implementation of the delayed single-photon self-interference experiment described below.

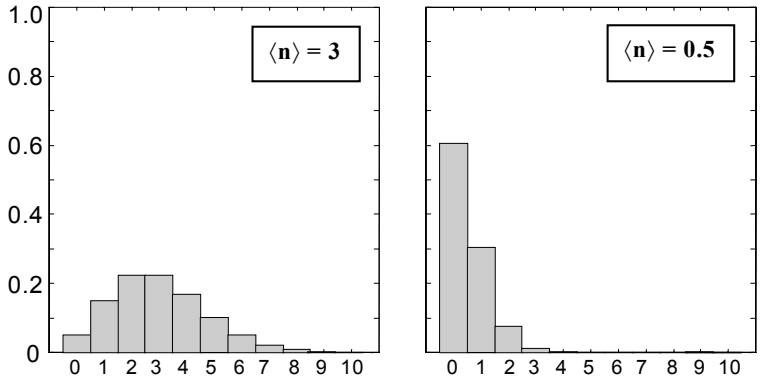

Figure 7.1. *The probability distribution for finding different numbers of photons in a coherent state with an average photon number ⟨n⟩=3 (left) or ⟨n⟩=0.5 (right).*

The so-called *squeezed coherent states* [239] are relatives of the coherent states. In a squeezed state, the quantum fluctuations in one variable are reduced at the expense of increased fluctuations in the conjugate variable. The product of the uncertainties in the two conjugate variables can never be lower than a certain value, given by the uncertainty relation. For example, an *amplitude squeezed state* of the electromagnetic field has a reduced uncertainty in the amplitude at the expense the uncertainty in the phase of the electric field. Such a field will have a different photon number distribution from the Poissonian described above. Squeezed states may become important for metrology, in order to circumvent the quantum zero-point noise, which otherwise sets the ultimate limit on the resolution of any measurement of an observable. They may also be important for the transmission and processing of quantum information.

7.1.2 Echoes of single photons

In Ref. [240] Kessel and Moiseev suggest a three-pulse photon echo experiment where the first two pulses consist of a single, shared photon. A single-photon wave packet is split using a beam splitter and sent along two paths with a path difference longer than the duration of the wave packet. The two paths are overlapped in a photon-echo material, i.e. a material with an inhomogeneously broadened absorption line and long coherence times, where the photon is absorbed. It is shown that there will be interference between the two quantum paths, even though one can think of the photon as being in a superposition of the wave packets that never overlap in space and time. The third pulse stimulates the emission of an echo, which occurs after a delay equal to the time difference between the two paths that the first photon can take and in a direction determined by the angle between the two paths. The echo shows that interference has taken place and that this has resulted in a spectral and spatial interference pattern. The medium has absorbed only one photon from the first two pulses, but atoms at different spatial positions and with different resonance frequencies have different probabilities of having absorbed the photon, and this modulation of probability amplitude has the form of an interference pattern. The experiment can be thought of as a time analogue to Young's double-slit experiment, where a single photon interferes with itself, and it has been called *delayed single-photon self-interference*. The terms *one-photon echo* [241] and *Zen echo* [242] have also been used.

If only a single photon is used for two of the fields in a three-pulse photon echo experiment, the signal will of course be very weak. In fact, is has been shown that the expectation value of its intensity will be zero, whereas the expectation value of the field amplitude is non-zero [240,242]. This highly non-classical field could, in principle, be

detected by using phase-sensitive detection and performing the experiment many times while accumulating the signal. However, for the purpose of demonstrating delayed single-photon self-interference, a stronger signal can be achieved by accumulating many interference events in the material, i.e. by sending in many pulse pairs, each containing only one photon, before sending in a strong *read-out pulse* to stimulate an echo (see Fig. 4.4). This washes out the non-classical properties of the echo, but scales favourably as the signal scales with the square of the number of single-photon events, according to the non-linear nature of the photon echo process.

A formal analysis of the experiment, involving the interaction between a quasi-stationary quantised field and a large number of absorbers, can be found in Refs. [240] and [242]. The experiment can be intuitively understood using the same picture as in the semi-classical description of a three-pulse photon echo (Section 4.2.3). Although not strictly correct, in this picture one thinks of the photon wave packet as being split in two "halves" by the beam splitter, where each "half" contains part of the probability amplitude of finding the photon at a particular position at a particular time. The first "half" of the photon wave packet excites the atoms with some probability, rotating the Bloch (state) vector slightly up from the ground state. Because of their different resonance frequencies, the atoms will accumulate phase at different rates after the pulse, corresponding to a rotation, at different speeds, around the w-axis of the Bloch sphere. When the second "half" of the photon arrives, some atoms will be close to their original phase and will be further excited by the field, i.e. their probability of having absorbed the photon will be increased. Atoms with other resonance frequencies may have the opposite phase and will be brought back to the ground state by the second pulse, i.e. their probability of absorbing the photon will be close to zero. In this way the probability of excitation will vary sinusoidally in the frequency domain, with a period equal to the inverse of the delay, τ_{12}, between the two paths of the photon wave packet. The width of the spectral interval affected by the photon is given by the inverse of the wave packet duration. If many events are accumulated, a spectral grating with many excited atoms will form. If there is a mechanism for persistent spectral hole-burning, the population grating in the ground state can be read out even after a long time. The position of the grating will be determined by the relative phase of the two wave packets. For example, if there is no phase difference between the two "halves" of the photon, atoms absorbing at the centre frequency of the field will have a large probability of being excited. If there is a phase difference of π there will be destructive interference at this frequency and these atoms will be left in the ground state, corresponding to a shift of the spectral grating by half a period. In an accumulated experiment it is thus important that the difference between the two paths the photon can take is stable during the accumulation of interference events. If the two photon paths cross at an angle in the material, the phase difference will be different for atoms at different positions and a spatially varying population grating will form, in addition to the spectral grating.

7.1.3 Experimental implementation

Paper IV describes the first experimental demonstration of delayed single-photon self-interference. An attenuated laser beam was used to produce pulse pairs with, on average, less than one photon per pair, and a rare-earth-ion-doped material was used as the absorbing photon-echo material. After accumulation of more than $7 \cdot 10^9$ interference events, a read-out pulse was sent into the material, which produced a detectable echo. By comparing the signal with the signal expected if delayed single-photon self-interference

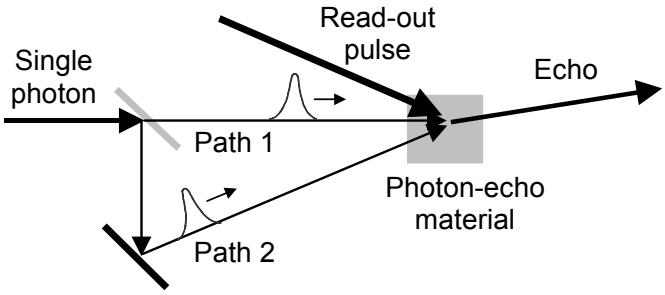

Figure 7.2. *The set-up originally proposed for the study of delayed single-photon self-interference. Single photons impinging on a beam splitter can travel along two possible paths to a material with resonant absorbers, where the paths overlap spatially. The difference between the path delays is longer than the duration of the photon wave packet, which means that no interference would be detected using a conventional photo-detector, since the paths do not overlap in both space and time. However, when the paths overlap in a medium with long-lived coherences, a spatial and spectral interference pattern can form. This can be detected by applying a read-out pulse, producing a stimulated photon echo.*

should not occur, it could be deduced that single photons had interfered with themselves. The experiment can be perceived as single photons "interacting with the medium at two different times", in the same sense that single particles "pass through both slits" in a double-slit experiment.

Attenuated laser light, i.e. coherent states, were used instead of single-photon states, since the development of single-photon sources is still in its early stages, and the demands on wavelength and pulse duration were very specific in the experiment. This made the experiment a slightly less clean demonstration of the delayed single-photon self-interference effect, since some pulse pairs could be said to contain two or more photons. It might then be claimed that the observed interference was due to one photon being absorbed from the first pulse and another photon being absorbed from the second pulse. However, by lowering the average number of photons to less than one and observing the scaling of the signal, it was possible to eliminate the contribution from the occasional pulse pairs with more than one photon. As the photon echo process is non-linear, it is possible to clearly distinguish the contribution from single photons already when the average number of photons is lowered to around 0.5 photons per pulse pair [242].

A material with a mechanism for persistent spectral hole-burning (see Chapter 3) was used to efficiently build up a signal from the interference events. Each absorbed photon excites and removes one ion from the ground state, which successively builds up a spectral population grating. When the grating is probed by the read-out pulse, the coherently emitted photon echo will be proportional to the square of the number of contributing ions and thus to the square of the number of accumulated single-photon events. This is far more efficient than accumulating the signal after detecting the photon echo in repeated experiments.

In Ref. [243], the dependence of the signal on different material parameters is calculated. The material should preferably have a large oscillator strength while still having a phase

memory considerably longer than the separation between the two pulses in each pulse pair. The number of photons in the signal, S, scales as

$$S \propto N^2 M^2 T \tag{7.1}$$

where N is the number of photons in each excitation pulse pair, M is the number of accumulated pulse pairs and T is the duration of each pulse. Several different materials were considered for the implementation to find the best trade-off between pulse duration, oscillator strength and accumulation time and efficiency. Dye-doped polymers were considered due to their high oscillator strengths. However, the short coherence times in these materials meant that picosecond pulses had to be used and it was difficult to achieve read-out pulses with a pulse area $\pi/2$ using these short pulses. Eu-doped Y_2SiO_5 was a likely candidate because of the demonstrated long coherence times (2.6 ms [52]) and efficient long-lived storage of spectral features. Finally, the experiment was performed using Pr^{3+}:Y_2SiO_5, which has a higher oscillator strength than Eu^{3+}:Y_2SiO_5. In both materials, spectral features are stored by redistribution of ions between the long-lived hyperfine states. In Pr^{3+}:Y_2SiO_5, the lifetime of these states is only around 100 s, but this could be increased by placing the material in a magnetic field, which enabled accumulation times longer than 1000 s. As can be seen from Eq. 7.1 it is preferable to have many short pulses rather than a few long pulses. The duration of the excitation pulses was set to slightly more than 40 ns, mainly determined by the speed of the available modulators and by the need to produce read-out pulses with a sufficient pulse area ($\pi/2$) using the available laser power. The delay between the two pulses in a pulse pair was 175 ns, which was considerably shorter than the coherence time of Pr^{3+}:Y_2SiO_5, which is 152 μs under the experimental conditions [36].

An important difference between the experiment performed and the originally proposed experiment is that only the time-frequency part of the interference was demonstrated, not the spatial part. In the original version, a photon was proposed to be split using a beam splitter and sent along two spatially separated paths into the absorbing medium. In the experimental implementation, a pair of excitation pulses containing on average less than one photon was carved out of a continuous laser beam and sent along the same path. The experiment shows that even if the two excitation pulses, containing a single shared photon, propagate through the material at different times, they interfere and create a spectral interference pattern, leading to an echo. However, since they propagate along the same path there is no spatial interference pattern and the final photon echo will propagate in the same direction as the excitation pulses. Making the two possible photon paths spatially colinear is experimentally advantageous, because this makes it much simpler to maintain a fixed phase relation between the two pulses. In the originally proposed experiment it would be necessary to keep the relative length of the two possible photon paths stable within less than a wavelength for the duration of the accumulation (up to one hour). In an implementation using co-propagating excitation pulses, this condition is transferred to a condition that the light source is coherent during the 175 ns between the pulses and that the path length is stable during this time, so that the phase relation between the two pulses is stable. When the pulses are attenuated to the single-photon level, the photon can be said to exist in a superposition of being in the first pulse and being in the second pulse. This is analogous to the *time-bin qubits* used in some experiments within quantum cryptography [244], where a logical 1 is represented by a photon in the first pulse and a logical 0 by the photon in the second pulse, and where the quantum bit can also be in a superposition of these two states.

The experiment was performed using a ring dye laser, Coherent model 699-21, lasing in a single mode. The laser system is frequency stabilised to a reference cavity and has a short-term frequency stability of around 1 MHz. On a timescale of a few minutes or hours the frequency drifts by around 50 MHz. This can be compared to the period of the spectral grating built up during the experiment, $\Delta\nu = 1/\tau = 1/175$ ns = 5.7 MHz (where τ is the time separation between the two "halves" of the photon). We see that the short-term linewidth of the source was good enough to resolve the interference. This could also be expressed by noting that the coherence time of the laser (a few hundred ns) is longer than the time between the pulses in a pulse pair. However, the long-term frequency stability had to be improved in order to ensure a coherent and constructive build-up of the spectral grating by successive photons. This was done by locking the laser frequency to an absorption line in iodine, which was probed using high-resolution saturation spectroscopy [245].

Some observations can be made regarding the scaling of the signal with the number of pulse pairs, M. If the laser stability were insufficient and successive interference events were added with random phases, the process would scale as a *random walk* process. The "depth" of the population grating, i.e. the difference between the population at the most excited frequencies and the least excited frequencies, would increase as $\sqrt{M}$, and the echo signal strength, S, would increase linearly with M. Using a perfectly stable source, the signal scales as $S \propto M^2$. In the experimental implementation the signal scaled as $S \propto M^x$, where x could be brought very close to 2 by careful adjustment of the laser. The above can also be said to explain why we did not observe interference between pulses in different pulse pairs (when a large number of weak pulses are accumulated), even though the pulse pairs were generated with short time separations (470 ns). The laser phase is not stable enough for such interference to build up constructively. Expressed differently, the coherence of the laser field is not sufficient that it can be claimed that the same photon is present in different pulse pairs and, in the words of P. Dirac, "each photon interferes only with itself" [246].

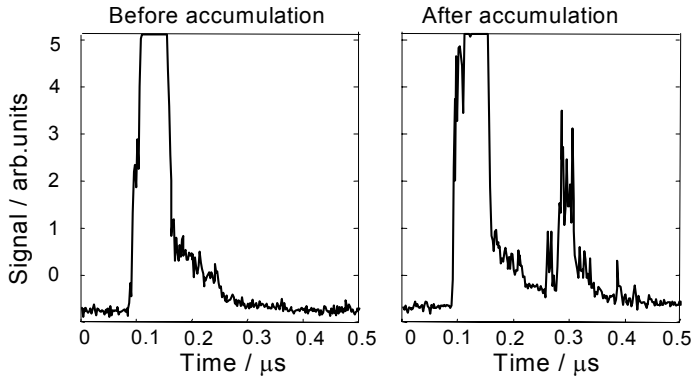

Figure 7.3. *Left: The result of sending a read-out pulse into the medium before accumulation. The strong signal to the left in both figures is the result of leakage of the strong read-out pulse through the closed detection gate. Right: Signal obtained after accumulation of $7 \cdot 10^9$ pulse pairs, containing on average 0.54 photons per pair, with a separation of 175 ns between the pulses in a pair.*

7.1.4 Implications of the experiment

The interpretation of the experimental results becomes problematic if we think of the photon as being absorbed *either* when the first pulse in a pair arrives at the photon-echo material *or* when the second pulse arrives. As in Young's double-slit experiment, where we can think of a photon as passing through *both* slits, we must think of the photon as being in *both* excitation pulses (with some probability) and acting on the material at two different times.

On the other hand, the results may seem obvious if we choose another way of describing the electromagnetic field. If the light in Young's double-slit experiment is described as a wave, the observation of an interference pattern is expected. Analogously, if the pulses in the delayed single-photon self-interference experiment are described in the frequency domain, the results are easy to accept. The spectral representation (Fourier transform) of two pulses, separated by a time τ, is a sinusoidally varying spectrum with period $1/\tau$. If the pulses only contain a single photon this can be interpreted as the probability of the photon having a particular frequency. The ions in the absorbing material have narrow absorption linewidths, which means that they act as narrowband filters and record the spectral content of the excitation pulses. Of course, in this picture there are some questions we are not allowed to ask. Asking *when* the interaction between the photon and the ions takes place is equivalent to requesting *which-path information* in a Young type experiment, which precludes interference. If we replace the narrowband ions with a high bandwidth (i.e. fast) photo detector, we will detect the photon either during the first pulse or during the second, but we will see no interference. Similarly, if we can measure the state of the ensemble of ions some time between the two pulses, we can determine if a photon has been absorbed, but this collapses any superposition of states and destroys the interference.

Many people find it disturbing not to be able to analyse the outcome of an experiment and at the same time tell what happens at each step of the experiment. One can argue that we must give up the notion of an objective reality, as we may only consider a limited set of aspects of the world at a time. More formally, we can only make observations which are compatible with the modes of our detector. If we believe in quantum mechanics, complete knowledge about the physical world (the state of a physical system) is only available in the form of a quantum state and never in the form of an answer to all the questions we might ask (every measurement we can make on the system).

Quantum mechanically, the experiment is described as starting from a state with all ions in the ground state and with a photon in a superposition of two pulses. When the first pulse hits the sample, the state changes to a superposition of a state with one excited ion and no photons and a state with no excited ions and a photon in the second pulse. Finally, after the second pulse has interacted with the sample, we have a state with no photons and one excited ion, with the probability of being excited distributed among the many ions in the sample. In Ref. [247], Moiseev makes a connection between the formation of the time-delayed single-photon interference – in particular the formation, evolution and decay of macroscopic coherence in the medium – and the interesting problem of the transition from quantum to classical [248].

The photon echo process can been seen as a case of degenerate four-wave mixing. In the experiment discussed here, this non-linear process was performed with two of the fields attenuated to the single-photon level. It may no longer be appropriate to refer to the process as a multi-photon process. For instance, the wave vector constraints usually

described as a requirement of momentum conservation may be more correctly phrased as a pure wave propagation effect.

7.1.5 Related experiments

An extension of the experiment performed would be to implement the originally proposed experiment, with the two possible photon paths spatially separated. This might be a more convincing demonstration of delayed single-photon self-interference to anyone who is not comfortable with the idea of tailoring or splitting a photonic wave packet using an amplitude modulator. This implementation would require the construction of a highly stable interferometer, but would on the other hand be simplified by the fact that the intense read-out pulse and the photon echo would propagate in slightly different directions, which would make detection of the weak signal easier.

Another experiment that would be interesting to attempt is to investigate the non-classical echo produced by a single pulse pair containing a shared photon and a strong read-out pulse, i.e. to perform the experiment without accumulation in the photon-echo material. This would involve phase-sensitive detection of the small rephasing in the electric field amplitude, corresponding to the one-photon echo, within the fluorescence emitted after the read-out pulse. A very large number of measurement results would have to be averaged, due to the low efficiency of the process. It is likely that this experiment would be very difficult to perform, at least in the form it has been presented in the literature.

Other versions of the experiment, utilising a three-level system, have also been proposed [241,249,250]. These schemes make the detection of the non-classical echo field somewhat easier. The excitation scheme can be arranged so that a single photon, in the first two pulses, interacts with atoms in the ground state on one transition, while the strong read-out pulse interacts with the probability grating created in the excited state, using another transition. In this way the background of fluorescence from atoms excited by the read-out pulse can be avoided.

The single-photon self-interference experiment can been seen against the background of many other interference experiments that have been performed using single photons or single excitations of atoms. One interesting example is an experiment where a photon from a single excited atom was split by a beam splitter and sent along a path much longer than the "length" of the photon ($c \cdot \tau$, where τ is the lifetime of the excited atomic state), before the wave packets were overlapped and the photon interfered with itself [251]. This experiment is interesting with regard to the issue of local realism and the non-local nature of measurements, and it demonstrated that optical interference effects persist at arbitrarily low intensities and over arbitrarily large distances.

Another experiment with some connection to the single-photon self-interference experiment is one where spin echoes were measured using a single electron spin [252]. In this experiment, a single molecular electronic spin was repeatedly submitted to a two-pulse echo sequence (two microwave pulses with pulse areas $\pi/2$ and π, respectively) and the spin state was measured, after a variable delay, using optically detected magnetic resonance (ODMR). Between the echo sequences, the resonance frequency of the spin transition changed randomly by a small amount, because of spin diffusion in the surrounding material. In this way, repeated probing of a single system replaced the ensemble of spins with a distribution of resonance frequencies.

7.2 Photonic quantum state storage

Most types of information can be conveniently transmitted over large distances in the form of optical pulses. This includes bits of quantum information, qubits, which can be encoded, for example, in the states of single photons. Photonic wave packets are generally seen as good carriers for quantum states, partly because they are fast and easy to create. However, when it comes to storing or processing the information, atoms are usually preferred, as they are stationary and have controllable interactions. Thus, it is of interest to find a reliable method to transfer to quantum state of light to atoms and back. This would be directly useful, e.g. within the field of quantum cryptography and in quantum repeaters. Several schemes for a "quantum memory for photons" have been proposed [253-256] and proof-of-principle experiments have been performed [257-259].

Storage of classical information is not problematic, in the sense that there is nothing fundamental to prevent amplification or copying of the information. In quantum mechanics, on the other hand, there are limits on how well one can measure and "amplify" variables describing the state and it is a proven fact that an unknown quantum state cannot be cloned. Quantum state storage necessarily implies that all information about the relevant properties of the state is destroyed in the transmission system. A requirement on an ideal quantum state storage process is that it can achieve complete transfer of an unknown quantum state from a carrier system onto the state of the storage system. This implies lossless transfer of properties of light such as phase and amplitude, to properties of an atom or an ensemble of atoms, and vice versa.

7.2.1 Photon-echo-based quantum state storage

Moiseev and Kröll have described a scheme for quantum state storage where a light pulse is completely absorbed and subsequently re-emitted by atoms on a Doppler broadened transition in a gas [255]. Through the action of reference fields (laser pulses), the quantum state of the absorbed light is transformed into a coherent superposition of the sublevels (e.g. hyperfine or Zeeman levels) of the atomic ground state, where it is stored, and later transferred back to the optical transition, such that the light is re-emitted. The field to be stored is absorbed by a macroscopic ensemble of atoms and if the field is a single-photon wave packet the probability of absorbing the photon will be distributed throughout the medium. The reference pulses make absorbers with different resonance frequencies and at different positions rephase at the correct time to produce a field replicating the originally absorbed light.

The proposed scheme is inspired by methods of pulse-shape storage using two- or three-pulse photon echoes [176,178,260] (see Chapter 5) and it can be discussed using the same language. Below, a description is given of how one may hope to achieve re-emission of absorbed light using the coherent rephasing process of a conventional two-pulse photon echo, followed by an attempt to explain why this process can never give perfect reconstruction of an absorbed wave packet.

A two-pulse echo can be said to achieve absorption and re-emission of a light pulse in the following way (see Section 4.2). The first pulse is absorbed on an inhomogeneously broadened transition and places the absorbers in superpositions of the ground and excited states, which evolve and accumulate phase according to the transition frequency of the individual absorbers. After some time, τ, a π-pulse inverts the phases of the atomic states (flips the u-v-plane of the Bloch sphere), which leads to rephasing and coherent emission

of light. If the only effect of the π-pulse was a flipping of the u-v plane of the Bloch sphere (e.g. v→-v), the evolution during the rephasing would be a *time reverse* of the evolution during the absorption process, up to a constant phase shift. However, the effect of the π-pulse is a 180° rotation of the Bloch sphere, which also flips the w component, i.e. the level of population inversion. Thus, the emission of the two-pulse echo is only a perfect time-reverse of the absorption process for atoms that were placed exactly in the u-v plane (50/50 superposition states) by the first pulse. This will not be the case if the first pulse is a general wave packet to be stored, e.g. a weak pulse or a pulse with an uneven spectral envelop (in which case atoms absorbing at different frequencies will experience different pulse areas).

In order to achieve efficient storage, the medium must have a large optical depth, so that all of the incoming light is absorbed. However, this also means that some of the re-emitted light will be re-absorbed, which will limit the re-emission efficiency in a conventional two-pulse photon echo. Phase matching requires the pulses to propagate in (approximately) the same direction. High absorption also means that the π-pulse will be attenuated while propagating through the medium, although this effect can be compensated for, to some extent, by letting the reference beam be slightly convergent. Even so, the photon echoes emitted in conventional photon-echo-based data storage can at most have an intensity of a few percent of the input pulses. Echo amplitudes larger than one of the input pulses ("greater-than-unity efficiency") can be achieved in an optically thick medium, if one of the reference pulses creates a population inversion which acts as an energy reservoir and amplifies the echo [261,262]. This comes at the price of more noise and distortion of the echo.

The scheme described in Ref. [255] also relies on temporal and spatial rephasing of coherently emitting absorbers, in order to achieve re-emission of absorbed light, but manages to circumvent the limitations described above. In this scheme rephasing is achieved after the absorption of a photonic wave packet, through the application of two π-pulses, one propagating in the forward direction and one in the backward direction, on a transition from the excited state to a third, previously unpopulated level. For example, the wave packet is absorbed on the optical transition between states $|1\rangle$ and $|3\rangle$ and the π-pulses are applied on the transition between the excited state $|3\rangle$ and the lower, metastable state $|2\rangle$. Rephasing and phase matching are achieved in the backward direction (the direction from which the absorbed wave packet originally came) because of the fact that the Doppler shifts of the optical transition are effectively inverted for waves propagating in opposite directions. The originally absorbed photonic wave packet will be re-emitted, although with an inverted temporal and spectral profile, on transition $|1\rangle$-$|3\rangle$. Between the two π-pulses, the state of the absorbed wave packet is stored as a superposition of the two lower states, $|1\rangle$ and $|2\rangle$. The procedure described above can, in principle, achieve complete reconstruction of the absorbed wave packet.

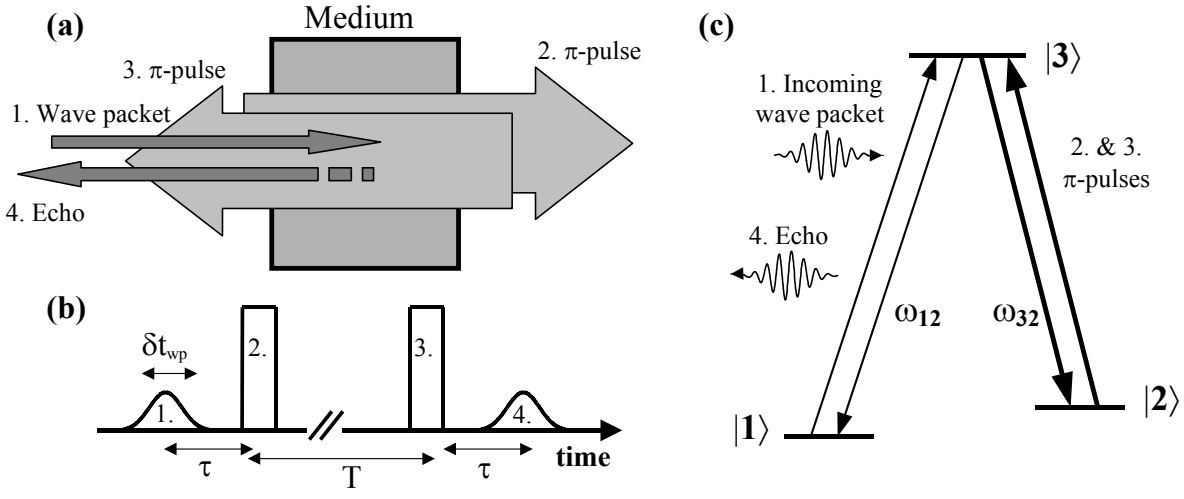

Figure 7.4. *The principles of the scheme for photonic quantum state storage, proposed in Ref. [255].(a) Geometry, (b) timing of the different pulses, (c) energy levels used in the scheme – the storage levels* $|1\rangle$ *and* $|2\rangle$ *and an optically excited state* $|3\rangle$.

A formal analysis of the scheme can be found in Refs. [255,263] and [264], and a brief outline is given in Paper V. Some general requirements on the process and the storage medium, which can be extracted from Refs. [255] and [263], will be given below. The approximations and assumptions that are introduced are relevant for an experimental implementation of the scheme and are also of interest for a comparison with other schemes for quantum state storage.

- The pulses must be considerably shorter than the coherence time of the optical transition, i.e. $\delta t_{wp} << T_2$ and $\tau << T_2$, where δt_{wp} is the duration of the photon wave packet that is to be stored and τ is the time between the absorption of the wave packet and the first π-pulse, which drives the probability amplitude down from the excited state to the storage levels. This requirement can also be formulated as a requirement that the homogeneous linewidth, Γ_h, should be narrow enough for the sharpest spectral features of the stored field to be resolved.
- The inhomogeneous broadening of the transition should be large enough to accommodate the full spectrum of the wave packet, i.e. $\delta\omega_{wp} \approx \delta t_{wp}^{-1} << \Gamma_{ih}$. A Doppler broadened line in a gas has a Gaussian profile with a FWHM of

$$\Delta\nu_D = \frac{2\nu_0}{c}\sqrt{2\ln 2\frac{kT}{m_0}}, \tag{7.2}$$

  where ν_0 is the centre frequency, m_0 is the particle mass and T is the temperature. If we require that the absorption varies by less than 10% over the spectral interval used for storage, this gives a useful bandwidth of approximately $\Delta\nu \approx 400$ MHz, for optical frequencies, temperatures around $T \approx 500$ K and absorbers with a mass of the order of $m_0 \approx 100$ u.
- The medium must be optically thick enough for the wave packet to be completely absorbed, i.e. $\alpha L >> 1$ or $\exp(-\alpha L) \approx 0$, where α is the absorption coefficient and L is the

total length of the absorbing medium. The absorption takes place within a distance $z \approx \alpha^{-1}$. In order for all spectral components to be properly phase matched, this distance must be small compared with the difference in wavelength between the highest and the lowest spectral component of the wave packet. This gives the condition $\delta\omega_{wp} << c\alpha/2$ or alternatively $\delta t_{wp} >> 2/c\alpha$.

- Dephasing on the storage transition must be small, i.e. the storage time, T, must be less than the coherence time of the transition, $T << T_2^{(12)}$.
- Additionally, the small Doppler broadening of the storage transition causes dephasing that is not compensated for by the storage scheme. We obtain the criterion $\omega_{12}(v_z/c)T << 1$, where T is the storage time. This can also be seen as a requirement that the atoms move considerably less than a wavelength of the storage transition $(2\pi c/\omega_{12})$ – a requirement that is shared by other information storage schemes utilising gases [258].
- There should be no initial absorption on the transition $|2\rangle$-$|3\rangle$, to which the reference laser pulses (storage and recall π-pulses) are applied, i.e. state $|2\rangle$ should initially be empty. In combination with the requirements above – that the storage states $|1\rangle$ and $|2\rangle$ should be spectrally close – this indicates that level $|2\rangle$ must be emptied, e.g. by optical pumping, before storage.
- The π-pulses should affect only transition $|2\rangle$-$|3\rangle$, which means that they should be made frequency and/or polarisation selective.
- It is assumed that the light propagates essentially as a plane wave, so that diffraction and Doppler shift due to curvature of the wave front and transverse motion of the atoms are negligible. This will probably always be the case, since the beams will have to have a large diameter, in order to avoid flight-out-of-view effects (see below).
- Atoms escaping from the storage volume during the storage time, T, will lead to a decrease in storage efficiency. In its simplest form, this gives $v \cdot T < a$ and $v \cdot T < 1/\alpha$, where v is the velocity of the atoms, a is the mode radius of the radiation fields (of the π-pulses) and $1/\alpha$ is approximately the longitudinal distance over which the absorption takes place.

The requirements above place considerable restrictions on which atomic species and optical transitions can be used in an experimental realisation of the storage scheme. One possibility which has been considered would be to implement the scheme in Yb vapour (^{171}Yb or ^{173}Yb), using the $^1S_0$-$^3P_1$ transition and Zeeman levels for storage. Using pulses with a duration of the order of ~10 ns (T_1=875 ns for the transition) and beam radii of around 2 cm, it could be possible to store photons for a duration of ~10 μs, with an efficiency of 80-90%. The main experimental difficulties would be to achieve sufficient intensity in the brief (~2 ns) reference pulses to obtain a pulse area of π, and to achieve sufficient selectivity in driving only atoms absorbing on the correct transitions.

7.2.2 Quantum state storage using artificially broadened absorption lines

Since photon-echo-based data storage has been successfully implemented in rare-earth-ion-doped solids, it is reasonable to consider whether the scheme proposed in Ref. [255] can be implemented in these materials. However, the scheme relies on the fact that the inhomogeneous Doppler shift has opposite sign for waves travelling in opposite directions, and thus it cannot be directly implemented using stationary absorbing impurities in a solid.

One way to implement the scheme in solids, for storage of photons with sub-millimetre wavelengths, has been suggested by Moiseev, Tarasov and Ham [264]. This proposal assumes a medium where a spin transition in paramagnetic dopant ions in a solid is inhomogeneously broadened by interaction with nuclear spins in the crystal lattice, and where this inhomogeneous broadening can be inverted by applying a π-pulse at the resonance frequency of the nuclear spins, inverting their nuclear magnetic moment.

In Paper V, a general method of creating a reversible artificial inhomogeneous broadening in RE materials, based on the interaction of the dopant ions with an external field, is proposed. A narrow absorbing line can be isolated within the inhomogeneously broadened optical absorption line of the RE material, using the hole-burning techniques described in Chapter 3 (Paper II). When a longitudinally varying electric field is applied to the material, the absorption line will effectively be broadened, as the resonance frequency of ions at different positions will be Stark shifted by various amounts. By changing the polarity of the applied field, this inhomogeneous broadening can be inverted, providing a method for implementing the protocol for photonic quantum state storage described in Ref. [255], in this class of materials.

This scheme for implementing storage of the quantum state of light in an RE material shares many of the requirements listed above for implementation in a gas, with the notable difference that atomic motion will not limit the storage duration. A practical problem when implementing the scheme in an RE material will be to achieve a sufficient absorption depth. Since the absorption line should have high absorption when it is artificially broadened ($\alpha L \approx 3$-5, sufficient to completely absorb the wave packet to be stored) it needs to have a very large absorption (e.g. αL=100-1000) before being broadened. The crystals used generally have an absorption coefficient α in the range 1-15 cm^{-1} and are fitted inside cryostat sample chambers with dimensions of the order of a few cm. One solution that has been suggested would be to use waveguides or crystalline fibres doped with rare-earth ions. If such fibres can be created, with properties similar to RE single crystals, they would also be useful in other applications of RE materials. Since the laser light interacting with the ions would be confined to a narrow region in the waveguide/fibre, the field would be strong and homogeneous for all ions, which is advantageous for coherent driving of the ions.

Only a small fraction of all RE ions in the medium – ions within a narrow region of the original inhomogeneous absorption profile – are selected for use in the storage process. Another significant obstacle for a practical implementation of the scheme is therefore how to optically drive the ions participating in the storage, without exciting *spectator ions*, i.e. ions that are not participating. Any excited spectator ions will contribute background spontaneous emission, which may drown the signal of interest, and absorption by these ions may attenuate the reference (π-) pulses (cf. Section 3.2). The problem could be alleviated by using a material with large separations between the hyperfine (spin) states, where broad spectral intervals can be emptied of absorption or where the hyperfine splitting is larger than the optical inhomogeneous linewidth.

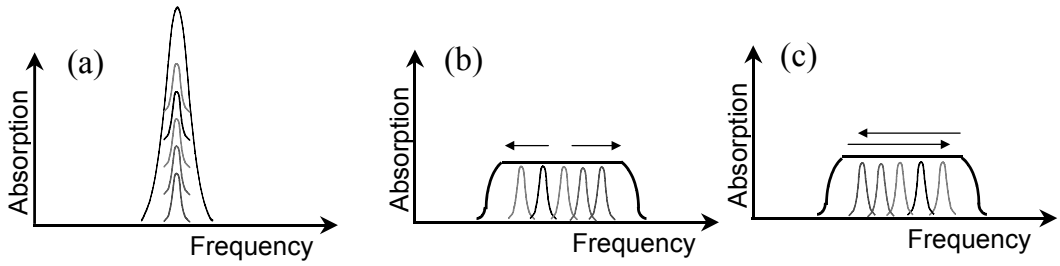

Figure 7.5. *Creating reversible inhomogeneous broadening. (a) Originally all atoms absorb at nearly the same frequency. (b) By applying an external field, the resonance frequencies of the atoms can be shifted by differing amounts, effectively increasing the bandwidth available for storage or processing of information. (c) If the field is reversed, the detunings of the individual atoms relative to the centre frequency are reversed.*

The technique of creating artificially broadened absorption lines may be applicable to many other systems, which would mean that photon echo-like quantum state storage could also be implemented in these systems. For example, it has been suggested [265] that the same effect can be produced using AC Stark shifts in a cloud of cold atoms, by applying a strong laser field with a spatially varying intensity. Controllable and invertible inhomogeneous line broadening may also be interesting for other quantum optical experiments, because inversion of a distribution of frequencies ($\omega \rightarrow -\omega$) leads to time reversal of the temporal evolution. Consider, for example, the following situation. An ensemble of atoms, with a distribution of resonance frequencies, $\Delta\omega$, around a centre frequency ω_0, is located within a small volume ($d<\lambda=2\pi c/\omega_0$, required for phase matching). If the atoms absorb a pulse of coherent radiation they will first emit radiation coherently, but the emission will decrease rapidly, as the oscillating atoms dephase relative to each other. However, if the inhomogeneous broadening $\Delta\omega$ can be inverted after some time T, the atoms will rephase and will emit a pulse of radiation which is a temporally reversed copy of the initially absorbed pulse. This is the essence of the proposed quantum state memory discussed above.

7.2.3 Quantum state storage using slow and stopped light

Another technique for storing the quantum state of light is based on the phenomena of electromagnetically induced transparency and slow light [256,257]. Although this technique has not been investigated in the present work, it is relevant for the discussion here because EIT and ultraslow and stored light have been demonstrated in RE materials, and because the techniques are related to the scheme described in the previous sections. In particular, Ham, Hemmer, Shahriar and co-workers have demonstrated these phenomena [208,266,267] and related applications [268-270], using Pr^{3+}-doped Y_2SiO_5 .

The principles of EIT and slow light can be summarised as follows [234]. A strong "control" field drives one of the transitions in a Λ system, i.e. a system where two lower energy levels, $|1\rangle$ and $|2\rangle$, are both connected to an excited state, $|3\rangle$, via optical transitions. This field drives the transition $|2\rangle$-$|3\rangle$ with Rabi frequency Ω and creates a quantum interference for a weaker "probe" field, which is tuned to the $|1\rangle$-$|3\rangle$ transition. In a storage application, this probe field would be the light that is to be stored. In the presence of the control and probe fields, the absorbing atoms will have a "dark" eigenstate, which is a coherent superposition of states $|1\rangle$ and $|2\rangle$. The coherences excited by the two fields will cancel and no absorption of the weak probe field will take place, even if the medium has a

large optical depth. The medium will be transparent near the resonance frequency ω_{13}, within a frequency window given approximately by [256]

$$\Delta\omega_{tr} \approx \frac{\Omega^2}{\Gamma}\frac{1}{\sqrt{\alpha L}} \tag{7.3}$$

where Γ is the linewidth of the optical transition and αL is the absorption in the absence of EIT. The group velocity of the probe light is approximately [234]

$$v_g \approx c\frac{\hbar\varepsilon_0}{2\omega_{13}}\frac{\Omega^2}{|\mu_{13}|^2 n} \tag{7.4}$$

where μ_{13} is the transition dipole moment between states $|1\rangle$ and $|3\rangle$ and n is the atomic density. The approximations made in Eq. 7.4 hold for $v_g << c$. One can see that for small values of Ω, the velocity of a pulse of light with frequency ω_{13} can be significantly less than the speed of light in vacuum, provided that the coherence of the atomic state is sufficient.

As the efficiency of EIT is limited by the macroscopic dephasing of the optical transition, it is advantageous to use media with a narrow inhomogeneous linewidth, e.g. an ultra-cold gas [234] or a narrow absorbing feature preapared in an RE material, using the methods described in Chapter 4. In the EIT experiments performed in the rare-earth-ion-doped material a narrow absorbing peak (FWHM≈1 MHz), prepared in Pr:YSO, was used [208,266]. In those experiments, group velocities of 45-100 m/s were reported, for coupling field intensities of the order of 30-100 W/cm^2 and the observed EIT transmission windows were 30-100 kHz wide.

One way of achieving "storage" of photons is to delay them using a medium with small but finite group velocity. In Ref. [256] it was calculated that the achievable delay/storage time will be limited to

$$T \leq \sqrt{\alpha L}\cdot\delta t_{wp} \tag{7.5}$$

where δt_{wp} is the initial duration of the photon wave packet. This is related to the maximum bandwidth of the stored wave packet, which is determined by Eq. 7.3. An additional condition is that $T << T_2^{(12)}$, where $T_2^{(12)}$ is the coherence time of the transition between states $|1\rangle$ and $|2\rangle$ (the storage transition).

By reducing the intensity of the coupling light on transition $|2\rangle$-$|3\rangle$ to zero, the light can be brought to a full stop. Such *stored light* has been demonstrated in clouds of ultra-cold gas [258], in rubidium vapour [257] and in rare-earth-ion-doped solids [208]. The light is converted into a collective atomic excitation of the transition between states $|1\rangle$ and $|2\rangle$ (usually a spin transition). When the control fields are turned back on, the light is restored and continues to propagate through the medium.

The process, and its application as a quantum memory for photons, has been analysed in detail in Ref. [256], where it is described in terms of quasiparticles called *dark-state*

polaritons, which are mixtures of electromagnetic and collective atomic excitations. The mixing angle between the two components, and the propagation velocity, are determined by the strength of the coupling to the control field. This allows adiabatic passage from a pure photon-like state to a pure atomic excitation.

EIT-based quantum state storage shares many of the aspects of the photon-echo-based storage protocol discussed in previous sections, such as the need for high absorption depths and strong coupling to reference/control fields. In both schemes the photonic wave packet is resonantly "absorbed" on optical transitions and stored as superpositions of ground state (spin state) levels. The study of similarities and differences between EIT-based and photon-echo-based quantum state storage could be an interesting topic for further investigations.

SUMMARY

- The properties of the optical transitions in rare-earth-ion-doped crystals make them suitable for solid-state implementation of quantum optical experiments and applications. For example, electromagnetically induced transparency and slow and stopped light have been demonstrated in Pr^{3+}:Y_2SiO_5 [208,266]. In this chapter some comments have been made on two experiments that have been investigated by our group:
- In an experiment using an RE-doped material, it was shown experimentally that the photon echo process can be performed with, on average, less than one photon in each pair of excitation pulses. The experiment can be interpreted as a form of delayed self-interference for photon wave packets that do not overlap in both space and time.
- The spectral absorption profile of a material such as a rare-earth-ion-doped crystal can be manipulated to efficiently absorb and subsequently re-emit a wave packet, in a photon-echo-like process. Using such techniques it would be possible to store and retrieve the quantum state of a single-photon or a weak classical or non-classical optical wave packet, in a solid-state medium.

CHAPTER 8

QUANTUM COMPUTING IN RARE-EARTH-ION-DOPED CRYSTALS

In this chapter, efforts to make materials doped with rare-earth ions work as quantum computer hardware are described. The chapter begins with an introduction to the general ideas of quantum computing, followed by details on how to perform quantum logic operations using rare-earth ions in a crystal. After this, some comments are made on implementation issues and expected performance.

Most of the work on quantum computing using rare-earth-ion-doped materials (REQC) presented here has been performed as part of a European research project, going under the acronym REQC hardware ("Development of quantum computer hardware based on rare-earth-ion-doped inorganic crystals"), and its expanded successor, the ESQUIRE network ("Experimental realisation of quantum gates and development of scalable quantum computer schemes in rare-earth-ion-doped inorganic crystals"). The network involves researchers in Lund (LTH) [271], Caen (CIRIL) [272], Orsay (LAC) [273], Paris (LCAES) [274] and Aarhus (QUANTOP) [275]. Significant work concerning the implementation of quantum gates using rare-earth-ion-doped materials is also being performed in Canberra (ANU/LPC) [276], by M.J. Sellars and co-workers, and research along the same lines is currently being initiated in the USA.

Although a completely unified view of quantum information science has yet to emerge, the book by Nielsen and Chuang [13] has become something of a standard work, with a thorough discussion of the ideas and theory of quantum information. The work by Bouwmeester, Ekert and Zeilinger [14] has a more physical/experimental perspective and the book by Stolze and Suter [277] can be recommended for a short course in quantum computing. An impressive amount of introductory material is available on the internet (see e.g. www.qubit.org) and many scientific results in this field are in fact first (or only) published in electronic form (www.arxiv.org).

8.1 Introduction to quantum computing

For many years after the first realisation of machines capable of performing calculations, it was assumed that the exact physical implementation of the computing machine was of no great importance. Indeed, the work of Church and Turing had shown that any model of computation could be simulated on a (probabilistic) Turing machine, with at most a polynomial increase in the number of elementary operations required. This meant that attention could be restricted to the Turing machine model of computation and that a problem which could be solved efficiently on one computing machine could be solved efficiently by all other computing machines, or alternatively, that any computing machine could be efficiently simulated by any other computing machine. *Efficiently solvable* means that the amount of resources needed to solve a problem increases at most polynomially,

$O(p(n))$, with the input size of the problem, n, as opposed to a *hard* or *intractable* problem, where the best possible algorithm requires an exponentially increasing amount of resources.

This view would change in the 1980s, as people started investigating the idea of using quantum mechanics in information processing. Benioff [278] and Peres [279] studied reversible logic and quantum computers, and it was shown that a quantum system could be used to solve all computational tasks that could be solved by a classical computer. Feynman was the first to indicate that quantum computers could be more powerful than classical computers, by showing that a classical computer can not efficiently simulate a quantum system [280], and in 1985 Deutsch showed that a quantum computer can perform certain computational tasks using fewer steps than a classical computer, by employing *quantum parallelism* [1]. The quantum equivalent of the Church-Turing thesis, i.e. the conjecture that any universal quantum computer can be programmed to simulate any other local quantum system, was finally proven in 1996 [281].

Quantum computers require the design of quantum algorithms, i.e. calculating procedures that make use of the potential of quantum parallelism and quantum interference, and produce a result that is accessible to the "classical world". Shor's algorithm [2] for finding the prime factors of large integers, and Grover's algorithm [3] for quantum searching are probably the most well-known quantum algorithms. Shor's factoring algorithm is an example of how quantum computers can efficiently solve problems for which there are no known efficient solutions using classical computing. The factoring problem belongs to a large class of *hidden subgroup problems*, which can be solved efficiently on a quantum computer. These problems can be said to have some underlying structure, i.e. the problem can be formulated along the line of "the function f(x) is known to have a given property – characterise that property". On the other hand, it can be shown that for a completely unstructured problem, a quantum computer can at most achieve a speed-up by a factor $\sqrt{n}$, compared with a classical computer [13], which is the case for Grover's algorithm.

8.1.1 The building blocks of a quantum computer

Constructing a quantum computer can be formally described as constructing a quantum mechanical system evolving according to a Hamiltonian which describes a computation. This Hamiltonian, H(t), should generate a dynamical evolution of the quantum state of the system according to the prescriptions of some quantum algorithm. The requirements on any implementation of quantum computing are often stated as a form of what is known as the *DiVincenzo criteria* [12,282] and the description below is organised according to these criteria.

- **Qubits:** The quantum computer consists of a definite number of interacting quantum systems, each with a given number of quantum states involved in the computation. The quantum systems are often particles, such as atoms, electrons or photons, but they can also be, for example, field modes in a cavity, or vibrational modes in a string of coupled particles.

In analogy to the classical unit of information, the *bit*, which can take two distinct values, 0 or 1, the basic unit of quantum information is called a *qubit*. A qubit can exist in any superposition of two quantum states, $|0\rangle$ and $|1\rangle$ and the state of a qubit can, for example, be written

$$|\psi\rangle = \sin\frac{\theta}{2}|0\rangle + e^{i\varphi}\cos\frac{\theta}{2}|1\rangle . \quad (8.1)$$

Thus two real numbers are needed to describe the qubit state, which would in principle require an infinite amount of classical bits. The qubit state can be conveniently represented using a Bloch vector within a unit sphere (see Chapter 4), in which case θ would be the angle between the Bloch vector and the axis connecting the two poles ($|0\rangle$ and $|1\rangle$), and φ would be the azimuthal angle. Another often used representation of a qubit is a 2×2 density matrix. Convenient quantum systems that can be used to represent a single qubit are, for example, spin-1/2 particles or two energy levels in an atom.

A set of qubits in a quantum computer is sometimes called a *quantum register*. To give an explicit example, the state of a register with two qubits A and B, in states $|\alpha\rangle_A=|0\rangle$ and $|\beta\rangle_B=|1\rangle$ respectively, can be written $|\psi\rangle_{AB}=|0\rangle_A|1\rangle_B=|01\rangle_{AB}$. Usually the subscripts are dropped and the position within the brackets is used to indicate the different qubits. Thus, the state $|\psi\rangle=|0110\rangle$ refers to a set of four qubits, in states $|0\rangle$, $|1\rangle$, $|1\rangle$ and $|0\rangle$, respectively.

In the examples above, the state of the quantum register could be given by specifying the state of each qubit independently. However, an important feature of quantum computers is that the qubit registers can also be in so-called *entangled states*, which can not be described as a product of the states of the individual qubits. A simple example of two qubits in an entangled state is the state $|\psi\rangle=(|00\rangle+|11\rangle)/\sqrt{2}$. Entanglement is usually seen in the form of a correlation between the results of measurements on the states of different qubits. In the example, the two bits will always be found to be in the same state, 0 or 1, even though a measurement on one of the qubits will give the results 0 and 1 with equal probability. This state is said to be *maximally entangled*.

▪ **Initialization:** Before the quantum computation begins, the computer must be initialized in some standard state, e.g. the state $|00\ldots000\rangle$. This is usually expressed as the requirement that it should be possible to prepare qubits in a given pure state, e.g. in an energy ground state. The exact formulation of this requirement is being debated, as the starting state in some implementations of quantum computing (e.g. in NMR quantum computing) is actually a high-entropy thermal state, from which an "effective pure state" is prepared.

▪ **Unitary transformations:** Our next requirement is that it should be possible to perform operations on the qubits, i.e. change the state of one or more qubits according to some prescription. The property of *unitarity* can be formulated mathematically, for example, the operators can be represented by *unitary matrices*, but loosely it means that the qubits should be rotated between pure states without losses or decoherence. The fundamental operations in a quantum computer are called *quantum gates*, in analogy to logic gates in a classical computer. Examples of gates changing the state of a single qubit are the *NOT* gate and the *Hadamard* gate, and examples of gates acting on two qubits are the *controlled-NOT* gate and the *controlled-phase* gate. The program (algorithm) followed by a quantum computer is given as a sequence of quantum gates – a *quantum circuit* or *quantum network*. In a quantum circuit diagram, each qubit is represented by a line/wire running from left to right in the diagram. The gate operations, represented by blocks or connections between the qubit wires, are applied to the qubits in the order they occur, from left to right. See Fig. 8.1.

In principle, there are an infinite number of single-qubit gates, corresponding to all the possible transformations that can be made on the state of a two-level quantum system. Perhaps the intuitively most simple is the NOT gate, which takes a qubit in state $|0\rangle$ to state $|1\rangle$ and a qubit in state $|1\rangle$ to state $|0\rangle$. Note that this also implies that a qubit in state $(|0\rangle-|1\rangle)/\sqrt{2}$ will end up in state $(|1\rangle-|0\rangle)/\sqrt{2}$ after being subjected to a NOT operation. The NOT operation can be represented in matrix form or by its quantum circuit symbol, as shown below.

$$\begin{pmatrix} 0 & 1 \\ 1 & 0 \end{pmatrix} \qquad \text{X}$$

Another important single-qubit gate is the Hadamard gate, which can be described as taking qubits from a computational basis state ($|0\rangle$ or $|1\rangle$) into a superposition of these states and vice versa. E.g. $|0\rangle\rightarrow(|0\rangle+|1\rangle)/\sqrt{2}$ and $|1\rangle\rightarrow(|0\rangle-|1\rangle)/\sqrt{2}$. The matrix representation and the quantum circuit symbol of the Hadamard gate are:

$$\frac{1}{\sqrt{2}}\begin{pmatrix} 1 & 1 \\ 1 & -1 \end{pmatrix} \qquad \text{H}$$

All single-qubit gates can in principle be achieved using a maximum of three elementary rotations of the Bloch sphere [13], e.g. rotations by an angle θ around the u, v and w axes ($\hat{\mathbf{x}}$, $\hat{\mathbf{y}}$ and $\hat{\mathbf{z}}$). For two-level systems coupled to the electromagnetic field, such rotations can be performed by driving the system with coherent radiation, resonant with the transition between the states corresponding to $|0\rangle$ and $|1\rangle$ (see Chapter 4). For example, a Hadamard operation can be performed by applying a $\pi/2$-pulse, followed by a π-pulse, phase shifted by 90°.

Two-qubit gates can usually be described as operations where the state of one qubit determines what will happen to the other qubit. Thus, the controlled-NOT, or C-NOT, operation acts on two qubits, where one qubit acts as the *control qubit* and the other as the *target qubit*. The target bit is subjected to a NOT operation if the control bit is in state $|1\rangle$, otherwise nothing happens. Of course, the operation is slightly more difficult to analyse when the control qubit is in a superposition of $|0\rangle$ and $|1\rangle$. In classical computing, the corresponding operation is also known as an XOR gate. Another way to specify the gate is by saying that it performs the following transformations: $|00\rangle\rightarrow|00\rangle$, $|01\rangle\rightarrow|01\rangle$, $|10\rangle\rightarrow|11\rangle$ and $|11\rangle\rightarrow|10\rangle$, where the first bit is the control bit and the second bit the target. The matrix representation and the quantum circuit symbol for the C-NOT gate are:

$$\begin{pmatrix} 1 & 0 & 0 & 0 \\ 0 & 1 & 0 & 0 \\ 0 & 0 & 0 & 1 \\ 0 & 0 & 1 & 0 \end{pmatrix}$$

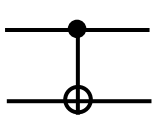

In the quantum circuit representation, the upper wire represents the control bit and the lower wire represents the target bit.

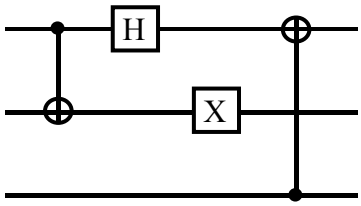

Figure 8.1. *Quantum circuit diagram, where each horizontal line represents a quantum bit. The following quantum gates are applied, from left to right: (1) a C-NOT operation, with the upper qubit as control and the middle qubit as taget, (2) a Hadamard transformation on the upper qubit, (3) a NOT operation on the middle qubit, and (4) a C-NOT operation with the lower qubit as control and the upper qubit as target. See the text for an explanation of the quantum gates.*

Although the number of possible quantum gates is infinite, it has been shown that only a limited number of basic gates are needed to build a universal quantum computer. For example, it can be shown that any unitary operation on n qubits can be constructed from only the C-NOT gate and single-qubit gates. Together, the C-NOT and the set of all single-qubit gates form a *universal set of gates* for quantum computing, i.e. a universal quantum computer can be constructed using only this set of gates. Furthermore, it can be shown that only a small number of basic single-qubit gates are needed to be able to approximate all other single-qubit gates to arbitrary precision. This is indeed good news for anyone trying to build a universal quantum computer, because only a limited number of gates have to be implemented.

- **Read-out:** After the execution of the steps of the quantum algorithm, the result should be read out, using measurements on the quantum systems that are used to represent qubits. As the quantum registers usually exist in highly complex superposition states during the course of the computation, an important part of the quantum algorithm is to transform the result of the information processing into a useful output. Quantum parallelism implies that a quantum computer can process input states that are a superposition of many different classical inputs, but the final measurement can only give a single result. The algorithms are often probabilistic, i.e. the algorithm only gives a correct answer with a certain probability, or, if there are many solutions to a problem, any of the solutions may be given with a certain probability. In this case it may be necessary to run the algorithm many times and measure the output after each completion of the algorithm.

Considerations regarding read-out of the state of qubits may involve noise introduced by the measurement process, or the choice of what basis to measure in. Since many quantum computing schemes use single particles as qubits, a typical qubit read-out can involve a measurement of the state of a single spin or a single photon, which can be very difficult. A different approach is to use *ensemble quantum computing*, by which we here mean that the same computation is performed, in parallel, on a large number of identical quantum computers. The qubit is then read out by performing an expectation value measurement on all systems representing the same qubit, which gives a stronger output signal. This type of quantum computing is also known as *expectation value quantum computing*.

A problem with the expectation value approach occurs when an algorithm can produce several possible answers. In many cases, the output from a quantum algorithm is a random number, whose distribution gives the solution to the problem. Different computers (*instances*) in the ensemble of quantum computers will then give different results upon

measurement and the read-out will result in an average (expectation value) of a mixture of answers. A quick way to answer this problem is to say that all information processing must be performed on the quantum computer, including the post-processing of results or the processing between different runs of a quantum algorithm. The result of any computation must eventually be formulated as a single classical answer, in order to be useful.

Another solution is to perform the read-out one qubit at a time, conditioning each measurement on the result of the measurements on previous qubits [283,284]. For example, suppose that there are two possible results in a quantum computation with two output bits, $|01\rangle$ and $|10\rangle$. A direct measurement on an ensemble quantum computer would find an equal mixture of 0 and 1, for each of the two qubits. The same result would be obtained e.g. if the two answers were $|00\rangle$ and $|11\rangle$, so no information would have been gained. We now repeat the computation, but before read-out we perform a bit flip on the second bit conditioned on the state of the first (a C-NOT with the first bit as control and the second bit as target). A measurement on the second bit will now find it in state $|1\rangle$ with probability 1, and a comparison with the first measurement tells us that the state $|01\rangle$ was one of the output states from the computation.

Some ensemble approaches to quantum computing, e.g. NMR quantum computing, have the additional problem that it is difficult to prepare all quantum computer instances in the ensemble in a pure initial state (cf. "Initialization", above). Although this is not necessarily the case for all implementations of quantum computing using an ensemble of quantum computers, working in parallel, the two issues are often discussed together.

- **Coherence:** The last requirement on a quantum computer is that it can be sufficiently isolated from the environment, so that the only interactions are initialisation, read-out, and controlled interactions between the qubits. If the quantum computer interacts with the environment in such a way that they are entangled or, equivalently, that the environment obtains information about the state of the quantum computer, this will result in decoherence. This means that superposition states of the quantum computer will be destroyed and that it will evolve towards a preferred mixed state which will result in errors in the final output from the computer. Relaxation towards an equilibrium state, e.g. spontaneous emission of photons by atoms or dampening of any harmonic oscillator, is also included among the processes that cause decoherence. An important figure of merit for any physical implementation of quantum computing is the ratio between the time required to perform a quantum gate operation, τ_{op}, and the average decoherence time, $\tau_c=T_2$. This ratio determines how many operations can be performed before decoherence makes the computation meaningless. Since a typical computational task may require thousands or millions of operations, this number must be very large.

A truly universal quantum computer should be able to perform an arbitrary number of operations, with an arbitrarily small probability of errors in the final output. This is in principle possible through the use of *quantum error correction*. If a single logic qubit is encoded using several qubits (e.g. $|0\rangle\rightarrow|000\rangle$ and $|1\rangle\rightarrow|111\rangle$), errors can be corrected by performing measurements and conditioned operations on these qubits, in analogy to error correction used in classical computing. As this method requires the use of more qubits, the probability of errors occurring will increase proportionally, and it is truly remarkable that it is in principle possible to perform fault-tolerant quantum computing, using error correction. The *threshold theorem* states that, under reasonable assumptions about the

noise in the underlying hardware, the probability of errors can be reduced arbitrarily, provided that the probability of failure in each component during an operation, p, is less than some constant threshold, p_{th}. Calculations of this threshold give different results depending on the underlying assumptions made, but typical values stated are of the order of $p_{th} \approx 10^{-5}$ [13].

8.1.2 Physical implementation

Many different physical systems have been proposed for use as quantum computer hardware. These include: trapped ions [285-287]; cold and trapped neutral atoms, interacting, for example, through electric dipole coupling [288,289]; cavity QED (photons in a high finesse resonator interacting with an atom or a quantum dot) [290-293]; photons controlled with linear optics [294], possibly using strong non-linearities for photon-photon coupling [295]; electron spins in quantum dots [296] or nuclear spins of phosphorus donors in solids [297,298]; and nuclear spins in molecules in liquid-state NMR [299-301]. Quantum information science has provided these different areas of physics with a common language. Techniques and solutions to problems encountered in one system will often also be useful in other fields. Many of the candidate systems mentioned above share features with the scheme for rare-earth-ion based quantum computing in solids discussed here. For example, in several proposals, spin states are used as qubits and optical fields are used to control the quantum computer. Although few-qubit quantum algorithms have been performed in some systems, research on many candidate systems for the implementation of quantum computing, including quantum computing in rare-earth-ion-doped crystals, is still aimed at creating a few qubits and demonstrating single- and two-qubit gates.

The proposals and demonstrations are often evaluated by their ability to fulfil the requirements on a quantum computer discussed above. This means that the following must be demonstrated: a scalable physical system with well defined qubits, the ability to initialise the qubits, decoherence times much longer than the gate operation time, demonstration of a universal set of quantum gates, and measurement of the state of individual qubits. The potential for scaling the systems to many qubits and the ratio between the qubit coherence time and the time required for a gate operation, τ_c/τ_{op}, are important benchmarks. For example, quantum computing in solid-state systems are yet in its early stages, but it has been suggested that the extensive manufacturing capabilities developed within the semiconductor industry may eventually make it easier to scale quantum computing schemes implemented in solids, than other schemes.

8.2 Quantum computing in rare-earth-ion-doped materials

The work presented here follows the scheme for quantum computing in rare-earth-ion-doped materials – in the following referred to as REQC – that was proposed by Ohlsson et al. in 2001 [96]. There have also been other, related, proposals: Ichimura suggested the use of nuclear spins in RE ions in crystals as qubits and the use of optical resonance frequency to address qubits [302]. In that proposal, the interaction between qubits was to be mediated by a single cavity mode of a high-Q cavity. Shahriar et al. proposed a scheme which combined spatial and spectral selectivity for qubit addressing, and which also used strong atom-cavity interaction to provide coupling between qubits [303]. Lukin and Hemmer suggested a scheme where dipole-dipole-induced “hopping” (resonant transfer of optical excitation) was used to manipulate collective metastable states in impurity-doped solids,

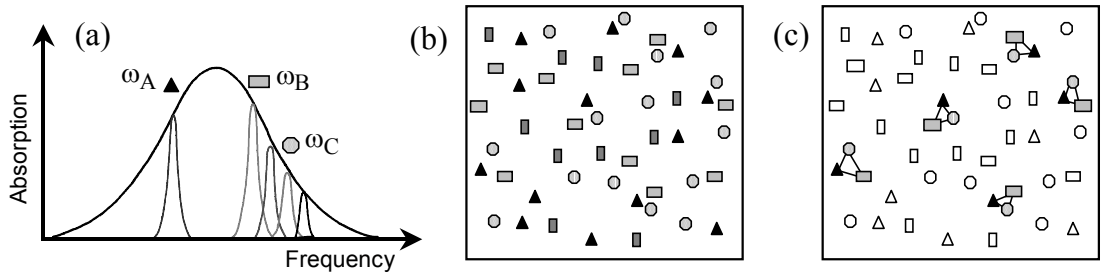

Figure 8.2. *(a) Ions absorbing at different frequencies can be used for different qubits. (b) The ions are randomly located in the crystal and interact with other ions in their surroundings. (c) Ions that are not useful for quantum computing are deactivated by optical pumping to an auxiliary state, where they no longer absorb at the original frequency. This includes ions with unsuitable resonance frequencies and ions that do not have strong interactions with an ion in each of the other qubits. After the distillation, only valid quantum computer instances are left.*

such as RE materials [304]. Jaksch et al. proposed a scheme for performing quantum gate operations on Rydberg atoms using *dipole blockade*, which is similar to the scheme described below [305].

The basic ideas in REQC are the following. Quantum information is stored in the state of rare-earth ions in a solid. Two of the hyperfine levels (nuclear spin states) in the ground state of the ions are used as qubit states $|0\rangle$ and $|1\rangle$. These levels have slow relaxation and long decoherence times (see Section 2.4). Different qubits are defined in the frequency domain, in the form of ions having different optical resonance frequencies. Due to the large difference in optical homogeneous and inhomogeneous resonance frequency, the number of separately addressable frequency channels (qubits) can in principle be very large. Qubit operations are performed by driving the optical transitions using laser light. Interaction between ions representing different qubits is mediated by (electrical) dipole-dipole interaction (see Section 2.7). The interaction can be "turned on" by transferring the ions to the excited state and is "turned off" by bringing them back to the ground state (qubit) levels. The proposed scheme uses an ensemble approach, since there will be many ions with the same optical resonance frequency representing the same logical qubit. An important characteristic of the scheme is the possibility to deactivate ions that are not suitable for use in quantum information processing, by transferring these ions to an auxiliary storage state, where they no longer absorb on their the original optical resonance frequency and do not affect the quantum computation. The rare-earth ions are randomly distributed throughout the crystal and no attempt has been made to organise them into quantum computer hardware. However, due to the large number of ions in the crystal, there will be groups of ions in the crystal which have suitable interactions and optical resonance frequencies for use as quantum computers (see Fig. 8.2). The key to REQC is to spectrally isolate these quantum computer instances from the rest of the ions in the material and to achieve efficient and precise manipulation of their quantum state.

8.2.1 Qubits

A qubit is prepared by selecting ions absorbing on a particular frequency, within the inhomogeneously broadened absorption line, and placing them in a specific ground state hyperfine level, using optical pumping and spectral hole-burning techniques (see Chapter 3).

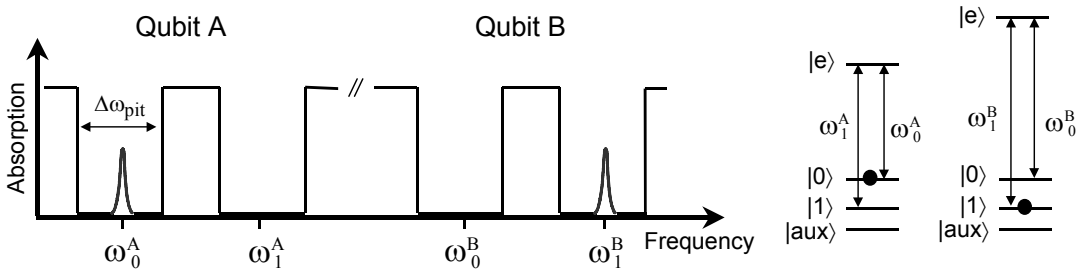

Figure 8.3. *Two qubits, A and B, have been prepared within an inhomogeneously broadened absorption line. The qubit ions are seen as absorbing peaks within pits that have been emptied of all other absorbing ions. The qubits have different optical resonance frequencies, ω^A and ω^B. Transitions from the two qubit states, $|0\rangle$ and $|1\rangle$, to the excited state, $|e\rangle$, can be addressed on frequencies $\omega^A{}_0$ and $\omega^A{}_1$ ($\omega^B{}_0$ and $\omega^B{}_1$), respectively. Qubit A is shown in state $|0\rangle$ and qubit B in state $|1\rangle$. Ions that cannot be used in a qubit are placed in an auxiliary level in the ground state.*

A typical qubit structure is shown in Fig. 8.3 (see also Figs. 3.5-3.7). The qubit ions form a sharp spectral feature, a *peak*, absorbing light at frequency ω_0 if they are in qubit state $|0\rangle$ and absorbing at frequency ω_1 if they are in qubit state $|1\rangle$. The spectral regions around these two frequencies are emptied of all absorbing ions, so that only the qubit ions will be affected when laser light is used to manipulate them. This forms two spectral *pits*, of width $\delta\omega_{pit}$, around frequencies ω_0 and ω_1. By repeating the procedure at several frequencies, many qubits can be prepared. Note that only a fraction of the ions absorbing a particular frequency can be used in the qubit, since we also require that these ions interact strongly enough with ions in the other qubits, i.e. be spatially close enough to an ion in the other qubit to be used for quantum logic.

The qubits are initialised in an energy eigenstate of the ions, i.e. in a pure state. This is relatively straightforward to achieve, since the optical pumping used in the preparation can be said to remove entropy from the ions and because thermalisation, in this case relaxation between the qubit levels, is very slow.

In the present work, performed mainly in Eu:YSO, Eu:$YAlO_3$ and Pr:YSO, the typical frequency width of a qubit peak was ~1 MHz and the typical width of the pit ~10 MHz. A broad qubit peak gives more ions in the qubit, which has advantages for signal strength and scaling. However, the variation in resonance frequency also causes problems in performing operations by driving the optical transition (see below). In this work, the laser linewidth set the lower limit on the peak width. The optical homogeneous linewidth, Γ_h, which would otherwise be the lower limit, is at most a few kHz in these materials.

The spectral distance between the qubit levels ($|\omega_0-\omega_1|/2\pi$) is of the order of 10-50 MHz in Eu:YSO and Pr:YSO. One might consider using materials with larger separations between the spin states, which can be more than 1 GHz in some cases, or using Zeeman levels, in which case suitable level separations can be chosen by applying a magnetic field with a particular strength.

8.2.2 Single-qubit gates

Single-qubit operations are performed by driving the ions resonantly between the ground state hyperfine levels and the optically excited state, $|e\rangle$. For example, a NOT operation can be achieved as shown in Fig. 8.4a. A π-pulse at frequency ω_0 transfers all probability

amplitude from state $|0\rangle$ to $|e\rangle$. The second π-pulse, with frequency ω_1, exchanges the amplitudes in states $|e\rangle$ and $|1\rangle$. Finally, a third pulse transfers the probability amplitude in the excited state down to the now empty state $|0\rangle$. The evolution of the quantum state can be expressed as $\alpha|0\rangle+\beta|1\rangle \rightarrow \alpha|e\rangle+\beta|1\rangle \rightarrow \alpha|1\rangle+\beta|e\rangle \rightarrow \alpha|1\rangle+\beta|0\rangle$.

The time required for a π-pulse depends on the available laser power, how tightly the laser is focused into the sample and on the strength of the optical transition. For typical values of the transition strength and laser power, Rabi frequencies of around ~1 MHz can be achieved, giving a π-pulse duration of 0.5 μs and gate times, τ_{op}, of the order of a few μs. For example, this was achieved using ~20 mW laser power, focused to a diameter of 50-100 μm, to drive the $^3H_4 \leftrightarrow {}^1D_2$ transition in Pr:YSO.

Coherent driving of the optical transitions in rare-earth-ion-doped crystals is routinely performed in investigations concerning coherent transients, e.g. photon echoes. Manipulation of the quantum states of rare-earth ions in the context of quantum logic gates has been demonstrated, e.g. in Refs. [306] and [85]. Although these demonstrations pertain to qubits based on a single optical transition, the same ideas can be used in the three-level system $|0\rangle$, $|1\rangle$, $|e\rangle$. Roos and Mølmer have suggested robust quantum gates for REQC, which involve two fields simultaneously coupling the states $|0\rangle$ and $|1\rangle$ to the excited state $|e\rangle$ [153]. The experiments presented in Paper III demonstrated tailored pulses for use in that scheme, and can also be seen as a demonstration of bit flips, as ions were repeatedly transferred between states $|0\rangle$ and $|1\rangle$ in Pr:YSO.

The width of the emptied spectral region, $\delta\omega_{pit}$, ultimately determines how fast an operation can be performed on the qubit ions, since the spectral content in the driving pulses is approximately given by the inverse of the pulse duration, t_p^{-1}, and we require that no ions outside the qubit are excited, i.e. $t_p > 1/\delta\omega_{pit}$. In addition, one can note that any quantum computer that uses frequency to address different qubits will be limited to gate times of at least $\tau_{op} > 1/\Delta\omega_{qubit}$, where $\Delta\omega_{qubit}$ is the spectral distance between two qubits, since this is the time required to address a qubit. Gate operations performed faster than this will affect neighbouring qubits.

8.2.3 Two-bit quantum gates

Controlled interactions between the qubit ions are achieved using the dipole-dipole coupling between the excited states. As was described in Chapter 2, rare-earth ions in a crystal can have a permanent electric dipole moment, which is different for different electronic states. When an ion is excited, its dipole moment and the electric field around it change, affecting nearby ions. The dipole-dipole interaction will cause the resonance frequency for transitions between the ground state and the excited state to shift, e.g. $\omega_{ge} \rightarrow \omega_{ge}+\delta\omega_{dd}$. If the interaction (frequency shift) is large enough, an ion close to an ion that has been excited may no longer be effected by light at its original absorption frequency, ω_{ge}. This effect is known as *dipole blockade* and is used for two-qubit gates in REQC. We require that ions representing different qubits in a quantum computer should interact strongly enough that the excitation of one of the ions will shift ions in the other qubits completely out of the spectral interval affected by the laser pulses used in a single-qubit gate, i.e. $\delta\omega_{dd} > \delta\omega_{pit}$. That is, when one qubit is excited, all ions in the other qubits should shift out of the pits that they are absorbing in. Ions that do not interact strongly enough are deactivated by pumping them to an auxiliary state, where they no longer interact with the laser light (cf. Section 8.2.4).

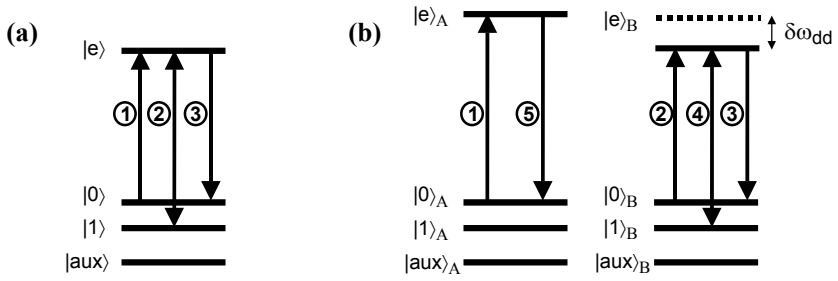

Figure 8.4. (*a) A NOT operation, i.e. an exchange of the states |0⟩ and |1⟩, using optical transitions. Pulse (1) transfers probability amplitude from state |0⟩ to |e⟩, (2) exchanges the amplitudes in states |1⟩ and |e⟩, and (3) brings the amplitude back from |e⟩ to |0⟩. (b) A controlled-NOT operation, with qubit A as control and qubit B as target. Pulse (1) brings the control qubit to the excited state, if it is originally in state |0⟩. Pulses (2)-(4) perform a NOT operation on qubit B, unless the resonance frequency of the B ions has been shifted because the A ions were excited, i.e. only if qubit A was originally in state |1⟩. Pulse (5) brings the control ions back to the qubit states.*

This interaction can be used to perform a C-NOT operation on ions representing two different qubits, a target (T) and a control (C) qubit, with different optical resonance frequencies (Fig. 8.4b). The pulse sequence that should be applied is the following:

(1) π-pulse on $|0\rangle_C \leftrightarrow |e\rangle_C$
(2) π-pulse on $|0\rangle_T \leftrightarrow |e\rangle_T$
(3) π-pulse on $|1\rangle_T \leftrightarrow |e\rangle_T$
(4) π-pulse on $|0\rangle_T \leftrightarrow |e\rangle_T$
(5) π-pulse on $|0\rangle_C \leftrightarrow |e\rangle_C$

Pulses 1 and 5 transfer the control ions from qubit state |0⟩ to the excited state |e⟩ and back, respectively. Thus, if the control ions were originally in state |0⟩ they will be in the excited state during pulses 2-4, but if they were in state |1⟩ they will remain there. Pulses 2-4 perform a NOT operation on the target ions, unless their resonance frequencies have been shifted because the control ions are excited, i.e. unless the control ions were in state |0⟩. In order to perform a C-NOT operation with several control qubits, a C^n-NOT, we need only repeat the first and the last step (pulses 1 and 5) for all qubits that are to act as control bits, since the excitation of any other qubit will block the not NOT operation on the target ions.

The C-NOT gate described above requires that the frequency shift experienced by an ion when ions in another qubit are excited is larger than a certain threshold value. The strength of the dipole-dipole interaction will be random and will depend on the relative positions of the randomly located ions. However, it is not necessary to know the spatial position of the ions or the exact magnitude of their interactions, only that the interaction between ions belonging to a particular quantum computer instance is sufficiently strong.

Longdell *et al.* have proposed, and partly demonstrated, a slightly different scheme for realising a two-qubit quantum gate between qubits based on rare-earth ions in a crystal [111,307]. The scheme performs a conditional phase shift, in a manner that is related to the technique of studying ion-ion interaction using *echo demolition measurements* [49,308]. A two-pulse echo sequence consists of a $\pi/2$-pulse followed, after some delay

τ_{12}, by a rephasing π-pulse (see Section 4.2.2). In an echo demolition measurement an additional perturbing pulse, resonant with some other frequency, is applied after the π-pulse. The ions excited by the perturbing pulse will interact with the ions contributing to the photon echo and shift their optical resonance frequencies, which will lead to a phase shift during the time τ_{12}. This partly destroys the echo rephasing and the intensity of the photon echo will decrease, in proportion to the strength of the ion-ion interaction and the density of excited ions. In the scheme of Longdell *et al.*, an ensemble of target ions is excited by a $\pi/2$-pulse, followed by a π-pulse after a time τ_{12}, as in a two-pulse photon-echo excitation sequence. Simultaneously with the rephasing π-pulse, an ensemble of control ions is excited. Some of the target ions will have just the right strength of coupling to the control ions to obtain a phase shift of $\pi/2$ during the rephasing time, τ_{12}. These ions are selected for use in a qubit, i.e. the ions that couple to the control ions with a coupling strength $\delta\omega_{dd}$ given by $\delta\omega_{dd}\cdot\tau_{12}=\pi/2+2\pi\cdot n$, where n is an integer. A quantum controlled-phase gate is possible, since the phase of the target ions will depend on whether the control ions were excited or not. In the proposal, the qubit levels are assumed to be the optical ground and excited states, but the scheme could be adapted to be applicable to qubits stored in the long-lived ground state hyperfine levels.

The scheme for performing a controlled phase shift described above has the advantage that much weaker interactions are needed than in the C-NOT scheme using dipole blockade. In principle, the frequency shifts caused by ion-ion interaction need only be greater than the homogeneous linewidth, Γ_h. However, a weaker interaction also means that the time required to perform a gate operation, τ_{op}, will be longer. Also, small interactions with ions far away in the crystal, e.g. ions belonging to other quantum computer instances, will become significant and may affect the gate operation.

8.2.4 Distillation

A key idea within REQC is that ions with suitable interactions with each other or with laser light can be selected, and unsuitable ions deactivated, in a process called *instance identification* or *distillation*. Ions that are unsuited for use in quantum computing are removed through spectral hole-burning (see Chapter 3). In the present work, they were optically pumped to an auxiliary hyperfine level in the ground state.

The study of ion-ion interaction and selection of strongly interacting ions in rare-earth-ion-doped crystals was an important part of the work presented in this thesis (Papers I and III). Strongly interacting ions, for use in a two-qubit gate, can be selected by using the procedure shown in Fig. 8.5 [96].

(1) Prepare two qubit structures at different optical frequencies, i.e. two ensembles of ions that are candidates for qubit ions, absorbing at frequencies ω_C and ω_T.
(2) Excite the ions in one of the qubits, the control ions, by applying a π-pulse at frequency ω_C. The resonance frequencies of the ions in the other qubit will now shift by varying amounts, depending on how strongly they interact with ions in the control qubit.
(3) Use spectral hole-burning to remove the target ions that have not shifted sufficiently, i.e. excite ions in a frequency region around ω_T.
(4) Bring the control ions back to the ground state with another π-pulse.
(5) Repeat the procedure with the roles of the qubits reversed. The result will be two sets of mutually controlling ions.

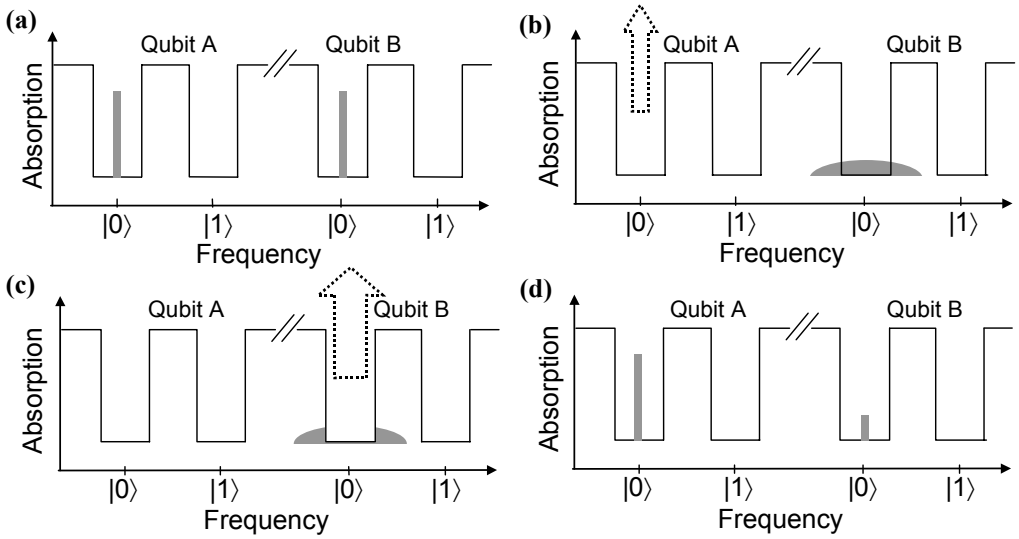

Figure 8.5. *Schematic description of the procedure for selecting strongly interacting ions. (a) Two qubit structures have been created and the ions representing qubits are prepared in their |0⟩ state. (b) The ions in qubit A are promoted to the excited state. The optical resonance frequencies of the ions in qubit B will shift by varying amounts, depending on how close they are to an excited ion in qubit A. (c) The ions that did not experience a sufficient shift are transferred to an auxiliary state using optical pumping or coherent transfer pulses. (d) The ions in qubit A are returned to the ground state and the resonance frequencies of the ions in qubit B return to the original frequency. All the remaining ions in qubit B have strong interactions with ions in qubit A, which makes it possible to implement gates where qubit A controls the state of qubit B.*

In order to create more qubits, another qubit structure can be prepared and the procedure above repeated for each pair of qubits that is to be used in two-bit gates. If non-interacting ions are removed by optical pumping, as was described above, steps (1)-(4) must be repeated several times before only strongly interacting ions remain, since only some of the ions relax to other states when they are excited. This can be inefficient, since some of the control ions are lost through spontaneous decay every time the procedure is performed. A more efficient technique is to use coherent pulses to drive the non-interacting ions to a previously empty state, with high efficiency. This type of distillation was performed and is described in Paper III.

An important question is how many of the ions we can expect to have sufficient interactions. This depends on the density of ions in the material and on how large a fraction of the ions absorbs within the frequency intervals selected for the qubits, which can also be expressed in terms of a spatial-spectral density of ions. For example, the number of ions absorbing within a 1 MHz interval of the inhomogeneous absorption profile, within a volume of 0.004 mm^3 (corresponding to the approximate size of the laser focus in the crystal), in a Pr:YSO crystal with 0.05 at.% doping, is of the order of $4 \cdot 10^9$. Dipole-dipole interaction is proportional to the square of the difference in static dipole moment between the ground and excited states ($|\Delta\mu|^2$), and inversely proportional to the cube of the distance between the interacting ions (see Section 2.7). For example, the average distance between two site-I Pr ions in a Pr:YSO crystal with 0.05 at.% doping is approximately 6 nm [71], which would give an interaction strength of the order of 5 MHz. However, two rare-earth ions that happen to be in neighbouring Y sites could have an

interaction strength of several GHz. Ion-ion interaction in RE materials has been experimentally measured and numerically simulated (Paper I). Under the conditions considered, it was found that, for ions within two randomly chosen 1 MHz intervals, the fraction of ions interacting strongly enough to shift each other's resonance frequencies by more than 5 MHz is of the order of 0.4%.

Distillation of ions with suitable interactions to perform the phase gate of Longdell *et al.* is discussed in Ref. [307]. In the experiments described in Ref. [111], partial distillation of ions fulfilling the requirement on the interaction between ions in different qubits has been performed, in addition to distillation of ions with a specific coupling to the driving laser field, i.e. a specific Rabi frequency.

8.2.5 Read-out

It is relatively straightforward to measure the state of a qubit in the hyperfine levels of an ensemble of rare-earth ions, by transferring the quantum state to the optical transition. One can then choose to measure fluorescence, absorption or coherent emission (FID) from the ions.

Fluorescence measurements are usually a very sensitive technique for measuring the population in a specific state. Ions are excited from one of the qubit levels $|0\rangle$ and $|1\rangle$, and the spontaneous emission on some optical transition is measured. The measured intensity will be proportional to the number of ions that were in the ground state level, or rather, the ensemble average probability of finding ions in that state. The photons will be emitted in all directions, which means that only a fraction of the fluorescence light can be collected. A problem with fluorescence measurements in RE materials is that the transitions that are used usually have low relaxation rates, which means that the read-out will be slow. Another difficulty is that the ions in general can relax to many different states, which means that it is difficult to find transitions that can be cycled many times, in order to get many photons out of each ion.

Absorption can be measured by sending light, resonant with either the transition $|0\rangle$-$|e\rangle$ or $|1\rangle$-$|e\rangle$, past the ensemble of rare-earth quantum computers, and detecting how much was transmitted. The experimental work described in the papers has mainly involved absorption measurements using frequency-swept pulses, which give a frequency-resolved measurement of how many ions are absorbing at each particular frequency. For weak and slowly chirped pulses, the average number of absorbing ions is proportional to the absorption, with a frequency resolution given by $\sim\Delta\nu=\sqrt{r}$, where r is the chirp rate. For a rapidly chirped pulse, the frequency-domain information can be reconstructed by performing a mathematical transform on the time-domain detector signal, $I_t(t)$ [309]. Absorption measurements are greatly improved by using a reference beam that propagates outside the sample and dividing the transmission signal by the reference signal, in order to remove noise and fluctuations in laser amplitude.

As was discussed in Chapter 4, ions in a coherent superposition of a ground and an excited state will emit light coherently on the optical transition. The amplitude of this light will be determined by the level of inversion (the w component in the Bloch vector formalism), with a maximum for an even superposition (w=0), and the phase will be given by the phase of the coherent superposition. Coherent transients, such as free induction decay, can be measured phase-sensitively by frequency shifting some of the laser light and mixing this with the light emitted by the ions, which gives heterodyne beating. Thus, by

transferring the qubit state from the qubit levels (hyperfine levels $|0\rangle$ and $|1\rangle$) to the optical transition, e.g. by applying a π-pulse to the transition $|0\rangle$-$|e\rangle$, a measurement can be made on the qubit by studying coherent emission from the ions.

If the qubit state is rotated before measurement, e.g. using a $\pi/2$-pulse, this will correspond to measuring in different bases. Using several measurements in different bases in a method known as *quantum state tomography*, it is possible to map out the complete quantum state of the qubit, in contrast to a projective measurement in a single basis. Quantum state tomography on an optical transition in an RE material has been performed, using phase-sensitive measurements of coherent emission from the RE ions [85].

Suggestions have also been made [96] to use a single instance of the RE quantum computer, e.g. 10-100 ions doped into a small volume $(\sim 10\ \text{nm})^3$. In this case, read-out of the quantum bits may be more difficult. Single molecules, ions and quantum dots can be studied and single-ion fluorescence spectroscopy of Pr and Eu ions in nanoclusters has been performed [224,225]. If such schemes can be combined with selective excitation from one of the qubit states, read-out of a single-ion-based, rare-earth quantum computer could be feasible.

8.3 General considerations regarding REQC

8.3.1 Inhomogeneities

As in all other physical implementations of quantum computing, an implementation of REQC must be able to deal with several types of systematic errors in order to perform quantum gate operations with high *fidelity*, i.e. where the result is close to the intended operation. Such systematic errors may be small differences between different instances of the quantum computer or variations in the optical fields used to perform the operations.

One such systematic variation can arise from the fact that the intensity in a laser beam varies depending on the radial position in the beam. A standard assumption is that a laser focus has a roughly Gaussian intensity profile. This means that ions in different parts of the beam will experience different electric field amplitudes, and thus different Rabi frequencies and pulse areas. Experimentally, one can try to limit this problem by using one of the following techniques.

- Create a flat (top-hat) intensity distribution in the sample by passing the laser light through a pinhole and imaging this pinhole onto the sample with a lens.
- Place a pinhole directly next to the sample and allow only the centre of the laser focus to pass into the sample. Both this and the previous technique will be limited by diffraction and will work best for a thin sample.
- Try to detect only signals due to ions in the centre of the laser focus, where the intensity variations are small, e.g. by imaging the sample onto a pinhole on the detection side.
- Alternatively, use a probe beam with a smaller focal spot than the beam driving the ions to probe only ions at the centre of the control beam.

Another inhomogeneity that causes systematic errors is the spectral width of the absorbing qubit peak, i.e. the fact that different ions representing the same qubit absorb at slightly different frequencies. This can be tackled by requiring the optical pulses to be spectrally flat over the extent of the qubit peak, which can be achieved, for example, using brief

pulses. However, at the same time we require that the pulses are spectrally selective, i.e. that no spectator ions (ions outside the qubit) are affected by the pulse.

Inhomogeneities can be tackled by using composite and tailored pulses of the type briefly discussed in Section 4.3. Wesenberg and Mølmer have presented a quantum gate for REQC, based on composite pulses, which is tolerant to variations in coupling strengths between ions, pulse lengths and frequency shifts [310]. It can achieve worst-case fidelities of 0.999 with relative variations in coupling strength as high as 10% and frequency shifts up to several percent of the Rabi frequency of the driving laser field. Roos and Mølmer proposed a class of composite Gaussian pulses and complex sech pulses for accurate π rotations of the qubit in the presence of variations of the resonance frequencies [153]. They also describe how arbitrary qubit rotations and a C-NOT quantum gate can be produced by sequences of π-pulses between the excited state and coherent superpositions of the qubit states. The proposed scheme involves two fields which simultaneously couple the states $|0\rangle$ and $|1\rangle$ to the excited state $|e\rangle$, and the operation is analysed in terms of dark states and bright states of the ions.

Frequency-chirped pulses, in particular pulses with the form of a hyperbolic secant, have been used to achieve population inversion by single adiabatic transfer [205]. In the present work, sech pulses were used to efficiently manipulate the state of a narrow absorbing feature (qubit peak) in the presence of variations of field intensity and a distribution of resonance frequencies (Paper III).

A general way to tackle inhomogeneous broadening of the qubit transition or of the optical transition in an ensemble qubit, is to use *refocusing*. This technique is known from NMR and consists of a periodic flip of the inhomogeneously broadened transition (e.g. $|0\rangle \leftrightarrow |1\rangle$), for example by applying a π-pulse. This changes the sign of the phase accumulated by a member of the ensemble relative to the centre frequency ($\Delta\varphi \leftrightarrow -\Delta\varphi$) and after some time the ensemble will rephase. The process is obviously the same as in a two-pulse echo, where the second pulse rephases the inhomogeneously broadened ensemble of atoms excited by the first pulse. Refocusing might be used in REQC, for example, to counter the inhomogeneous broadening of the hyperfine transitions that are used as qubits.

The approach to the problem of inhomogeneities which is most in line with the general ideas of REQC, is to use distillation to select a sub-set of ions with small variations in coupling strengths and resonance frequency and deactivate the other ions in the original ensemble. This approach is very general and can be applied without detailed knowledge about the source of the inhomogeneities. For example, Pryde *et al*. have demonstrated a technique for selecting a set of ions with a homogeneous Rabi frequency from an ensemble of ions with a distribution of different strengths of the coupling to the driving field [108]. The technique is to repeatedly apply a pulse with pulse area 2π followed by a delay of the order of the excited state lifetime. An ideal 2π-pulse will bring ions through the excited state and back to the ground state, while ions that experience stronger or weaker coupling to the field will be left slightly excited and may relax to the auxiliary hyperfine level. In a similar manner the echo sequence constructed by Longdell et al. returns target ions with the appropriate control ion interaction back to the ground state, while other ions are left partly excited and will be pumped to auxiliary levels. In practice, this type of distillation occurs implicitly in any manipulation of the ions where an imperfect operation results in a probability that the ions will be left excited, e.g. the

quantum gates described in the previous sections and in the experiments described in Papers II and III.

8.3.2 Operation time vs. decoherence

A fundamental limit on the performance of a quantum computer is set by the relation between the average time required to perform quantum gate operations, τ_{op}, and the rate of loss of coherence, $1/\tau_c$ ($1/T_2$). For small values of the ratio τ_{op}/τ_c, the probability of an error is $p_e \approx \tau_{op}/\tau_c$ per gate operation and the average number of operations that can be performed is of the order of τ_c/τ_{op}. Ideally, we would like the probability of errors to be smaller than the theoretical threshold for fault-tolerant quantum computing using quantum error correction. In this section the possibility of optimising this ratio in REQC, by carefully choosing which material and optical transition to use, will be briefly discussed.

In the ideal case, for an atom interacting only with the electromagnetic field, the coherence time is determined by the radiative lifetime, $\tau_c=2T_1$. For some optical transitions in RE materials, the coherence time approaches this value. If we consider only a single transition, the spontaneous radiative lifetime is connected to the transition dipole moment, μ_{ge}, according to [66]

$$T_1 = \frac{1}{A_{ge}} = \frac{3\varepsilon_0 hc^3}{2\omega_{ge}^3 \boldsymbol{\mu}_{ge}^2} \tag{8.2}$$

The time required to perform a general rotation of the quantum state on an optical transition is determined by the inverse of the Rabi frequency, which is directly proportional to the amplitude of the applied field and to μ_{ge}. The single-qubit operations in REQC all involve taking the qubit ions to a new state via the excited state, and we can thus write

$$\frac{\tau_c}{\tau_{op}} \propto \frac{T_1}{1/\Omega} \propto \frac{1}{\boldsymbol{\mu}_{ge}} \tag{8.3}$$

which means that, for a fixed laser intensity, it is favourable to use a weak optical transition, if other dephasing processes are absent or slower than the spontaneous decay of the excited state.

The interaction used for two-qubit gates takes the form of coupling between the excited states of the rare-earth ions, which means that there must always be some probability of finding an ion in the excited state at some point during the gate operation. In Ref. [283] it is shown that, under general conditions, any two-qubit gate capable of generating one unit of entanglement, e.g. a C-NOT gate, must necessarily suffer a time-integrated excitation approximately given by

$$\int P_e^{(tot)}(t)dt > \frac{2}{\delta\omega_{dd}} \tag{8.4}$$

where $P_e^{(tot)}(t)$ is the total probability of finding an ion in the excited state during the operation and $\delta\omega_{dd}$ is the ion-ion interaction strength, expressed as an angular frequency

shift. This result is perhaps not so surprising, but it shows clearly why it is necessary to use qubit systems with mutual interactions that are many orders of magnitude larger than the relaxation rate on the transitions used in qubit gates. For example, for an interaction strength (frequency shift) equal to five inhomogeneous linewidths, $\delta\omega_{dd}/2\pi=5\cdot\Gamma_h$, the probability of an error due to spontaneous decay during a two-qubit operation is at least of the order of 6%. For REQC this implies that even if it is possible to construct qubit gates that make use of ions with moderate interaction strengths [111], only gate implementations using strong interactions (e.g. the dipole blockade gate) can be pushed to perform several operations with low error rates.

The dipole-dipole interaction strength is proportional to the square of the difference in static electric dipole moments between the ground and the excited states of the ions, $|\Delta\mu|^2=|\mu_{gg}-\mu_{ee}|^2$. One may hope to increase the qubit-qubit interaction strength in REQC by finding materials where this value is large. However, the general trend in the materials studied in the present work was for the transition dipole moment $|\mu_{ge}|$ and the difference in static dipole moments, $|\Delta\mu|$, to change in roughly the same way for different choices of rare-earth ions and host materials. Although this has not been rigorously shown, it seems intuitively possible, since the same effect (interaction with the crystal field and mixing of electronic levels) contributes both to the occurrence of a static dipole moment and to making the forbidden optical transitions weakly allowed. Since the time required for a two-qubit gate is proportional to $1/|\Delta\mu|^2$ and the spontaneous decay rate is proportional to $|\mu_{ge}|^2$ it could turn out that the ratio τ_c/τ_{op} cannot be increased significantly by looking for RE materials with large static dipole moments. In this case, the best way to increase the general performance of quantum gates in REQC would be to decrease the distance between qubit ions.

8.3.3 Scaling and strongly interacting ions

The scheme for REQC discussed here relies on distilling working quantum computers from a set of randomly located ions. An important issue is how the number of working computers in the ensemble scales with the number of qubits that are implemented. Consider two sets of ions, A and B, e.g. the ions absorbing around frequencies ω_A and ω_B. For each ion in set A, there is a certain probability, p, that the ion is close enough to an ion in set B to be used in one of two mutually controlling qubits. That is, after qubit distillation, a fraction p of the ions will be left in each of the two sets. If we want three qubits, we introduce a third set of ions, C, and require that each of the ions in sets A and B is close enough to an ion in set C for mutual control. Assuming there are no correlations between the positions of ions and a relatively low level of doping, the fraction of strongly interacting ions in the three sets will be proportional to p^2. Continuing this argument, we find that the number of useful quantum computer instances, N_{QC}, decreases according to

$$N_{QC} \propto p^{n-1} \tag{8.5}$$

where n is the number of qubits. This gives a somewhat discouraging scaling, especially if the probability p is small, which has been the case for the materials studied so far ($p\approx 0.1$-1 %). However, p can be increased by increasing the density of ions, ρ, or by choosing to work with ions that have large static dipole moments, $|\Delta\mu|$, since the probability of finding strongly interacting ions scales as

$$p \propto \rho |\Delta\mu|^2 . \tag{8.6}$$

Increasing $|\Delta\mu|$ will increase the distance within which the ions can interact strongly, and increasing the density of ions will decrease the average distance between ions. Note that the latter implies increasing the density of ions within the spectral interval defining a qubit as well as increasing the number of ions within a certain volume, which can be difficult if the inhomogeneous linewidth increases with increasing dopant concentration (see Chapter 2). Increasing the probability of interaction, p, too much may also introduce some complications. For example, the probability that ions within the same frequency channel (potential qubit) are close enough to interact strongly will also increase, as does the probability that an ion will interact with two or more ions in another qubit, which would lead to incorrect quantum gate operation. Although this can be dealt with, by deactivating (burning away) ions in defect quantum computer instances, the improvement in scaling will be limited.

Wesenberg and Mølmer have suggested another architecture for REQC [310], which offers new possibilities for improved scaling. They propose the use of a *bus qubit*, which mediates all two-qubit operations between other qubits. This means that, instead of requiring that all qubits are coupled, we only require that every qubit is coupled to a central designated bus qubit. A bus-mediated two-qubit gate can be constructed from only a small number of single-qubit operations and two-bit gates between the bus and other qubits. The bus architecture gives direct improvement of the probability p by approximately a factor 8, which can be seen in the following way. In the original architecture, we require that all ions are within some maximum interaction distance, r, from each other, which means that the n ions belonging to a particular instance need to be within a sphere with diameter r. Using the bus architecture, the ions only need to be within a distance r of the bus qubit, which means that ions within a sphere with diameter 2r can be used in a quantum computer instance. The bus architecture also allows for the possibility of having an *asymmetric bus*, i.e. a bus qubit that is implemented differently from the other qubits. For example, one may consider using ions with larger static dipole moments for the bus qubit, which would increase the interaction with other qubits.

The potential of REQC is closely linked to finding structures in which rare-earth ions have strong interactions. One possibility is to use materials where rare-earth ions form pairs, or clusters, for example RE^{3+}:$CsCdBr_3$ [311,312]. Ions within a pair or cluster interact strongly and ensembles of such pairs could be candidates for quantum gates. Another interesting class of materials is *stoichiometric rare-earth compounds*, i.e. undoped materials where the rare earths are a main component of the crystal. Coherent transients and optical hole-burning have been seen in such materials [313,314]. However, since optical excitations in these materials may be delocalised, i.e. extend over several lattice sites [313], the schemes for performing quantum gate operations may have to be modified.

Finally, as has been mentioned previously, one way to develop REQC could be to abandon the use of randomly doped materials and use tailored structures, for example a large number of ions doped into a small volume. The qubit ions would be addressed in the frequency domain and qubit gate operations could be performed using the techniques described here.

Summary

- The development of quantum computers provides a structured way for learning how to fully control quantum systems and may provide new ways of solving computational problems.
- In the scheme for quantum computing discussed in this chapter, rare-earth ions, randomly doped into a solid, are used for quantum computing hardware.
- Qubits are addressed in the frequency domain, using the inhomogeneously shifted optical resonance frequencies of the rare-earth ions to define qubits.
- Hyperfine levels (spin states) in the ground state of the rare-earth ions are used as qubit states. The coherence times of these transitions can be extended to tens of seconds. The population lifetime in the qubit levels is minutes to days.
- Qubit gate operations are performed by driving optical transitions in the ions. The coherence time during operations involving a particular qubit, i.e. the optical coherence time, ranges from approximately 100 μs to 2 ms in the materials that have been used. Coherence times up 6 ms have been reported.
- The dipole-dipole interaction between ions is used for qubit-qubit control. The interaction can be turned on and off at will by exciting and de-exciting the ions.
- Groups of ions with suitable interactions are selected and used as quantum computer instances, in an ensemble of identical quantum computers. Other ions absorbing at the same optical frequencies as the qubit ions are removed by spectral hole-burning.
- Quantum state tomography, implemented for an ensemble of rare-earth ions, on one of the ions' optical transitions, has been reported.
- The quantum states of rare-earth ions in optical superposition states are routinely manipulated in experiments involving optical coherent transients. Rabi flopping and arbitrary rotations on the Bloch sphere have been demonstrated.
- The effects of inhomogeneities such as variations in resonance frequency, Rabi frequency, or qubit coupling strength, can be removed using tailored optical pulses and robust gate implementations.
- Qubit structures have been prepared using hole-burning techniques. Preparation and read-out of both qubit states has been demonstrated. Robust transfer of ions between qubit states has been demonstrated.
- Ion-ion interactions in rare-earth-ion-doped materials have been characterised and the selection of strongly interacting ions, for use in quantum gate operations, has been demonstrated. Rudimentary qubit-qubit control has also been demonstrated.
- Using the technology and materials available today, implementation of a few qubits and a C-NOT gate appears highly feasible.

COMMENTS ON THE PAPERS

Paper I describes the first steps in demonstrating the viability of quantum information processing in rare-earth-ion-doped crystals. A rudimentary qubit was created by preparing ions absorbing within a narrow frequency channel in a specific hyperfine level of the ground state. The interaction between groups of ions was studied in frequency-resolved measurements and characterised by numerical simulations.

I participated in the planning and in all experiments and wrote a major part of the manuscript. In particular, I was the person mainly responsible for the study of spectral hole broadening due to ion-ion interactions and the analysis of the experimental results. I also performed computer simulations of the qubit preparation.

Paper II reports new hole-burning techniques that can be used to reveal transitions between specific hyperfine levels, which are initially buried in an inhomogeneously broadened absorption line. This removes a significant limitation on the scope of experiments that could be carried out in materials such as rare-earth-ion-doped crystals, and makes it possible to use the narrow homogeneous linewidths in these materials for applications in quantum information science. Groups of rare-earth ions were prepared in specific ground state hyperfine levels, absorbing on specific transitions without any background absorption from other transitions. Coherent optical driving (Rabi flopping) of the transitions was demonstrated. New spectroscopic data on Pr^{3+}:Y_2SiO_5 are reported.

The experiments were performed using a laser system at Dortmund University. Lars Rippe and I jointly performed most of the experimental work. I had a major part in the preparation and planning of the experiments. In particular, I designed the program for generating tailored pulses and complicated pulse sequences and contributed to the design of the modulation system. I wrote the manuscript and evaluated the data presented in the paper.

Paper III presents experiments that were performed in connection with the experiments described in Paper II. We demonstrated how qubit structures in a rare-earth-ion-doped material can be manipulated in a robust and efficient manner using tailored pulses. Complex secant hyperbolic pulses were used to invert the population on an optical transition and to transfer ions between hyperfine levels. We also demonstrated qubit distillation, i.e. how strongly interacting ions can be selected and non-controllable ions deactivated.

I participated in all the planning, preparation and execution of the experiments. See also Paper II.

Paper IV describes an accumulated photon echo experiment in which the excitation pulses were attenuated so as to contain less than one photon on average. At such low light levels, effects due to the quantisation of the electromagnetic field have to be taken into account. The signal strengths are compared with theoretical predictions, for the case when at least one photon is required in each of the excitation pulses and for the case when a photon shared between the pulses is sufficient for the generation of a photon echo. The results support the suggestion that a single photon can act as two of the optical fields

involved in the photon echo process and can be seen as a demonstration of delayed self-interference for wave packets that do not overlap in both space and time.

I participated in the experiments and assisted in writing the manuscript. I performed the measurement of spectral hole relaxation of Pr in a magnetic field, which was used in order to enable hour-long accumulation times, and analysed these results.

Paper V describes a scheme for the implementation of storage of the quantum state of light using a photon-echo-like process, in a solid-state medium. A previously proposed scheme was based on the inversion of the Doppler shift in gases, for fields propagating in opposite directions, and we suggest that a similar effect can be obtained by creating artificial and externally controlled inhomogeneous broadening in a solid, by applying a reversible external field. We describe how the spectral absorption profile of a material such as a rare-earth-ion-doped crystal can be manipulated to efficiently absorb and subsequently re-emit a wave packet and analyse an implementation for a specific material.

I contributed to the development of the scheme, analysed the viability of an implementation and wrote the manuscript.

Paper VI presents a long-time storage mechanism for spectral features in the absorption line of thulium ions doped into YAG, when an external magnetic field is applied. Storage times of several tens of seconds were obtained, which is several orders of magnitude longer than those achieved without an external magnetic field. The mechanism enabling long storage time is Zeeman splitting of the ground state. The splitting of the ground and excited states was investigated as a function of the applied magnetic field, for field strengths up to 5 T.

I participated in all experiments, performed a substantial part of the data evaluation, and assisted in writing the manuscript.

Paper VII reports on high-resolution laser spectroscopy performed on Pr^{3+}:$KY(WO_4)_2$. The hyperfine structure and homogeneous linewidth are reported. The ion-ion interaction was studied in the form of excitation-induced dephasing in photon echo experiments.

I participated in the planning and assisted in some of the experiments and in the preparation of the manuscript. In particular, I had a major part in the spectral hole-burning experiments which are reported.

ACKNOWLEDGEMENTS

This work would not have been possible to perform without the help and support I have received from numerous people during the past four years. Here, I would like to express my gratitude to all my colleagues and co-workers, family, friends and girlfriend, who have contributed to this work in many different ways.

I am grateful to my supervisor, Stefan Kröll, for giving me the opportunity to work with interesting physics and for always taking the time to discuss problems or questions that I have encountered. I would also like to thank him for letting me take part in summer schools and conferences and for providing me with opportunities to meet and work with scientists from around the world.

I will remember my co-supervisor, Dan Hessman for his generous help with equipment, and my other co-supervisor Krishna Rupavatharam Mohan for interesting coffee-break discussions about everything from physics to exotic places around the world.

I would like to thank the people I have had the pleasure to work with in the Photon Echo Group, in particular Nicklas Ohlsson, for his humour and for the inspiration he has provided, Lars Rippe, for sharpening my debating skills during numerous discussions, and my roommates Ingela Roos and Andreas Walther. I have also enjoyed working with Huailiang Xu and others who have spent some time working with us and who have made the lab an interesting place. Thank you also for your patient waiting during lunches.

My fellow PhD students at the Atomic Physics Division have provided a friendly atmosphere and much fun during coffee breaks, football games and excursions. I am also grateful to them and the other scientists at the Division for sharing their knowledge and enthusiasm for physics with me. In particular, the enthusiasm of Sune Svanberg is a constant source of amazement and inspiration.

I am also grateful to other people at the department who have helped me in different ways. Laila Lewin, for help with administrative issues of all kinds. Åke Bergquist and Bertil Hermansson, for their help with all technical problems. Lennart Nilsson, and others at the teaching department, for giving me the opportunity to develop as a teacher. Furthermore, I am grateful to Leif Magnusson, who has always been ready to help with a few extra litres of liquid helium when needed, and to Elsie Nilsson, for making sure we drink enough coffee.

I would like to thank Robert Klieber at the University of Dortmund, for keeping his lab and laser constantly running for several weeks, for our benefit, and for not being too angry when we adjusted things that we should have left alone.

I would also like to thank our collaborators within the ESQUIRE network for interesting discussions and valuable exchanges of ideas, and Serguei Moiseev for valuable discussions during his visits to Lund.

To my friends and family, for your encouragement and for being there.

To Ulrica, for putting up with me and for being who you are.

BIBLIOGRAPHY

1. D. Deutsch, *Quantum-Theory, The Church-Turing Principle and the Universal Quantum Computer*, Proc.R.Soc.Lond.Ser.A **400**, 97-117 (1985)
2. P.W. Shor, *Polynomial-time algorithms for prime factorization and discrete logarithms on a quantum computer*, Siam J.Comput. **26**, 1484-1509 (1997)
3. L.K. Grover, *Quantum mechanics helps in searching for a needle in a haystack*, Phys.Rev.Lett. **79**, 325-328 (1997)
4. S. Wiesner, *Conjugate Coding*, SIGACT News **15**, 77 (1987)
5. Bennett, C.H. and Brassard, G. *Quantum key distribution and coin tossing,* Proceedings of IEEE International Conference on Computers, Systems and Signal Processing, 175-179, Dec. 1984
6. C.H. Bennett, G. Brassard, and A.K. Ekert, *Quantum cryptography*, Sci.Am. **267**, 50-57 (1992)
7. C.H. Bennett, F. Bessette, G. Brassard, L. Salvail, and J. Smolin, *Experimental quantum cryptography*, Lecture Notes In Computer Science **473**, 253-265 (1991)
8. J.A. Jones and M. Mosca, *Implementation of a quantum algorithm on a nuclear magnetic resonance quantum computer*, J.Chem.Phys. **109**, 1648-1653 (1998)
9. I.L. Chuang, N. Gershenfeld, and M. Kubinec, *Experimental implementation of fast quantum searching*, Phys.Rev.Lett. **80**, 3408-3411 (1998)
10. C. Monroe, D.M. Meekhof, B.E. King, W.M. Itano, and D.J. Wineland, *Demonstration of a Fundamental Quantum Logic Gate*, Phys.Rev.Lett. **75**, 4714-4717 (1995)
11. Los Alamos National Laboratory, Quantum Information Science and Technology Roadmap, http://qist.lanl.gov
12. D.P. DiVincenzo, *Quantum computation*, Science **270**, 255-261 (1995)
13. Nielsen, M.A. and Chuang, I.L., *Quantum Computation and Quantum Information*, Cambridge University Press (2000)
14. Bouwmeester, D. et al., *The Physics of Quantum Information*, Bouwmeester, D., Ekert, A. and Zeilinger A. (Eds.), Springer (2000)
15. T.H. Maiman, *Stimulated optical radiation in ruby*, Nature **187**, 493 (1960)
16. A.L. Schawlow and C.H. Townes, *Infra-red and optical masers*, Phys.Rev. **112**, 1940-1949 (1958)
17. Siegman, A.E., *Lasers*, University science books, Mill Valley, California (1986)
18. van der Krogt, P., Elementymology & Elements Multidict, www.vanderkrogt.net/elements/elem/yb.html
19. J.L. Marshall and V.R. Marshall, *Rediscovery of the elements: Ytterby Gruva (Ytterby Mine)*, Journal Of Chemical Education **78**, 1343-1344 (2001)
20. Macfarlane, R.M. and Shelby, R.M., *Coherent transient and hole-burning spectroscopy of rare earth ions in solids*, in *Spectroscopy of solids containing rare earth ions*, Kaplyanskii, A. A. and Macfarlane, R. M. (Eds.), North-Holland, Amsterdam (1987)
21. R.M. Macfarlane, *High-resolution laser spectroscopy of rare-earth doped insulators: a personal perspective*, J.Lumin. **100**, 1-20 (2002)
22. Henderson, B. and Imbush, G.F., *Optical Spectroscopy of Inorganic Solids*, Clarendon Press, Oxford (1989)
23. Yen, W.M., et al., *Laser Spectroscopy of Solids*, Yen, W. M. and Selzer P.M. (Eds.), Springer-Verlag, Berlin (1981)

24. Kaminskii A.A., *Laser Crystals - Their Physics and Properties, 2nd edition*, Springer-Verlag, Berlin (1990)
25. B.R. Judd, *Optical absorption intensities of rare-earth ions*, Phys.Rev. **127**, 750 (1962)
26. K. Holliday, M. Croci, E. Vauthey, and U.P. Wild, *Spectral hole-burning and holography in an Y_2SiO_5Pr3+ crystal*, Phys.Rev.B **47**, 14741-14752 (1993)
27. L.E. Erickson, *Optical Measurement of Hyperfine Splitting of D-1(2) Metastable State of Pr^{3+} in LaF_3 by Enhanced and Saturated Absorption Spectroscopy*, Phys.Rev.B **16**, 4731-4736 (1977)
28. R. Yano, M. Mitsunaga, and N. Uesugi, *Ultralong optical dephasing time in $Eu^{3+}Y_2SiO_5$*, Opt.Lett. **16**, 1884-1886 (1991)
29. W.R. Babbitt, A. Lezama, and T.W. Mossberg, *Optical dephasing, hyperfine structure, and hyperfine relaxation associated with the 580.8-nm 7F0-5D0 transition of Europium in Eu-3+-Y_2O_3*, Phys.Rev.B **39**, 1987-1992 (1989)
30. M. Yamaguchi, K. Koyama, T. Suemoto, and M. Mitsunaga, *Perturbed ion sites in Eu^{3+}:$YAlO_3$ studied by optical-rf double-resonance spectroscopy*, Phys.Rev.B **59**, 9126 (1999)
31. J.B. Gruber, M.E. Hills, R.M. Macfarlane, C.A. Morrison, G.A. Turner, G.J. Quarles, G.J. Kintz, and L. Esterowitz, *Spectra and energy-levels of Tm^{3+}-$Y_3Al_5O_{12}$*, Phys.Rev.B **40**, 9464-9478 (1989)
32. C. Li, A. Lagriffoul, R. Moncorgé, J.C. Souriau, C. Borel, and C. Wyon, *Luminescence properties of the Tm(3+) doped silicates Y_2SiO_5, $CaY_4(SiO_4)_3O$ and $SrY_4(SiO_4)_3O$*, J.Lumin. **62**, 157-171 (1994)
33. A. Lupei, C. Tiseanu, and V. Lupei, *Correlation between spectra and structural data of YAG-Tm^{3+} and YAG-Cr^{3+}, Tm^{3+}*, Phys.Rev.B **47**, 14084-14092 (1993)
34. Y. Zhang, X.A. Shen, and R. Kachru, *Observation of photon echo in Er^{3+}:YAG at 1.527 μm*, Opt.Lett. **22**, 1068-1070 (1997)
35. R.M. Macfarlane, T.L. Harris, Y. Sun, R.L. Cone, and R.W. Equall, *Measurement of photon echoes in Er:Y_2SiO_5 at 1.5 μm with a diode laser and an amplifier*, Opt.Lett. **22**, 871-873 (1997)
36. R.W. Equall, R.L. Cone, and R.M. Macfarlane, *Homogeneous broadening and hyperfine structure of optical transitions in Pr^{3+}:Y_2SiO_5*, Phys.Rev.B **52**, 3963-3969 (1995)
37. G.H. Dieke and H.M. Crosswhite, *The spectra of the doubly and triply ionized rare earths*, Appl.Opt. **2**, 675-686 (1963)
38. R.W. Equall, Y. Sun, R.L. Cone, and R.M. Macfarlane, *Ultraslow optical dephasing in Eu-3+-Y_2SiO_5*, Phys.Rev.Lett. **72**, 2179-2181 (1994)
39. Y. Sun, C.W. Thiel, R.L. Cone, R.W. Equall, and R.L. Hutcheson, *Recent progress in developing new rare earth materials for hole burning and coherent transient applications*, J.Lumin. **98**, 281-287 (2002)
40. N.M. Strickland, P.B. Sellin, Y. Sun, J.L. Carlsten, and R.L. Cone, *Laser frequency stabilization using regenerative spectral hole burning*, Phys.Rev.B **62**, 1473-1476 (2000)
41. G.J. Pryde, T. Bottger, R.L. Cone, and R.C.C. Ward, *Semiconductor lasers stabilized to spectral holes in rare earth crystals to a part in 10(13) and their application to devices and spectroscopy*, J.Lumin. **98**, 309-315 (2002)
42. R.M. Macfarlane and R.M. Shelby, *Magnetic-field dependent optical dephasing in LaF_3-Er^{3+}*, Opt.Commun. **42**, 346-350 (1982)
43. R.M. Macfarlane, *Photon-Echo Measurements On the Trivalent Thulium Ion*, Opt.Lett. **18**, 1958-1960 (1993)
44. J. Ganem, Y.P. Wang, D. Boye, R.S. Meltzer, W.M. Yen, and R.M. Macfarlane, *Nonexponential photon-echo decays pf paramagnetic-ions in the superhyperfine limit*, Phys.Rev.Lett. **66**, 695-698 (1991)

45. G.M. Wang, R.W. Equall, R.L. Cone, M.J.M. Leask, K.W. Godfrey, and F.R. Wondre, *Optical dephasing mechanisms in Tm^{3+}:$Y_2Si_2O_7$*, Opt.Lett. **21**, 818-820 (1996)
46. R.M. Macfarlane, *Photon-echoes in rare-earth-doped solids - A materials perspective*, Laser Phys. **5**, 567-572 (1995)
47. R. Orbach, *Spin-lattice relaxation in rare-earth salts*, Proc.R.Soc.Lond.Ser.A **264**, 458 (1961)
48. D.R. Taylor and J.P. Hessler, *Photon-echo decay in ruby - Electric dipole interactions and instantaneous diffusion*, Phys.Lett.A **A50**, 205-207 (1974)
49. J. Huang, J.M. Zhang, A. Lezama, and T.W. Mossberg, *Excess dephasing in photon-echo experiments arising from excitation-induced electronic level shifts*, Phys.Rev.Lett. **63**, 78-81 (1989)
50. G.K. Liu and R.L. Cone, *Laser-induced instantaneous spectral diffusion in Tb^{3+} compounds as observed in photon-echo experiments*, Phys.Rev.B **41**, 6193 (1990)
51. F.R. Graf, A. Renn, G. Zumofen, and U.P. Wild, *Photon-echo attenuation by dynamical processes in rare-earth- ion-doped crystals*, Phys.Rev.B **58**, 5462-5478 (1998)
52. F. Könz, Y. Sun, C.W. Thiel, R.L. Cone, R.W. Equall, R.L. Hutcheson, and R.M. Macfarlane, *Temperature and concentration dependence of optical dephasing, spectral-hole lifetime, and anisotropic absorption in Eu^{3+}:Y_2SiO_5*, Phys.Rev.B **68**, 085109 (2003)
53. R.L. Cone, R.W. Equall, Y. Sun, R.M. Macfarlane, and R. Hutcheson, *Ultraslow dephasing and dephasing mechanisms in rare-earth materials for optical-data storage*, Laser Phys. **5**, 573-575 (1995)
54. A.M. Stoneham, *Shapes of Inhomogeneously Broadened Resonance Lines in Solids*, Rev.Mod.Phys. **41**, 82 (1969)
55. R.M. Macfarlane, *Inhomogeneous broadening of spectral lines in doped insulators*, J.Lumin. **45**, 1-5 (1990)
56. M.J. Sellars, E. Fraval, and J.J. Longdell, *Investigation of static electric dipole-dipole coupling induced optical inhomogeneous broadening in Eu^{3+}:Y_2SiO_5*, J.Lumin. **107**, 150-154 (2004)
57. R.M. Macfarlane, A. Cassanho, and R.S. Meltzer, *Inhomogeneous broadening by nuclear-spin fields - a new limit for optical-transitions in solids*, Phys.Rev.Lett. **69**, 542-545 (1992)
58. R. Yano, M. Mitsunaga, and N. Uesugi, *Nonlinear laser spectroscopy of $Eu^{3+}Y_2SiO_5$ and its application to time-domain optical memory*, J.Opt.Soc.Am.B **9**, 992-997 (1992)
59. Moerner, W.E., et al., *Persistent spectral hole-burning: Science and applications*, Moerner, W. E. (Ed.), Springer-Verlag, Berlin (1988)
60. R.J. Elliott, *Theory of nuclear magnetic resonance in Eu*, Proc.Phys.Soc.Lond.Sect.B **70**, 119-123 (1957)
61. J.M. Baker and B. Bleaney, *Paramagnetic resonance in some lanthanon ethyl sulphates*, Proc.R.Soc.Lond.Ser.A **245**, 156-174 (1958)
62. B.S. Ham, M.S. Shahriar, M.K. Kim, and P.R. Hemmer, *Spin coherence excitation and rephasing with optically shelved atoms*, Phys.Rev.B **58**, R11825-R11828 (1998)
63. E. Fraval, M.J. Sellars, and J.J. Longdell, *Method of extending hyperfine coherence times in Pr^{3+}: Y_2SiO_5*, Phys.Rev.Lett. **92**, 077601 (2004)
64. E. Fraval, M.J. Sellars, J.J. Longdell, *Dynamic decoherence control of a solid-state nuclear quadrupole qubit*, quant-ph/0412061 (2004)
65. L.E. Erickson and K.K. Sharma, *Nuclear quadrupole resonance measurement of the anisotropic magnetic shielding and quadrupole coupling-constants of Eu-151(3+) and Eu-153(3+) dilute in YAlO3 single crystal*, Phys.Rev.B **24**, 3697-3700 (1981)
66. R.C. Hilborn, *Einstein coefficients, cross-sections, f values, dipole moments, and all that*, Am.J.Phys. **50**, 982-986 (1982)

67. B. Bleaney, *Enhanced nuclear magnetism*, Physica **69**, 317-329 (1973)
68. Goldner, P. and Guillot-Noel, O., personal communication, submitted for publication
69. P. Goldner and O. Guillot-Noel, *Magnetic interactions in Pr^{3+}:$LiYF_4$ for quantum manipulation: search for an efficient three-level Lambda system*, Mol.Phys. **102**, 1185-1192 (2004)
70. A.A. Kaplyanskii, *Linear Stark effect in spectroscopy and luminescence of doped inorganic insulating crystals*, J.Lumin. **100**, 21-34 (2002)
71. J.G. Wang, S.J. Tian, G.B. Li, F.H. Liao, and X.P. Jing, *Preparation and X-ray characterization of low-temperature phases of R_2SiO_5 (R=rare earth elements)*, Mater.Res.Bull. **36**, 1855-1861 (2001)
72. W. Kaiser, D.L. Wood, and S. Sugano, *Splitting of emission lines of ruby by an external electric field*, Phys.Rev.Lett. **6**, 605 (1961)
73. R.M. Shelby and R.M. Macfarlane, *Measurement of pseudo-Stark effect in Pr^{3+}-LaF_3 using population hole burning and optical free-induction decay*, Opt.Commun. **27**, 399-402 (1978)
74. A.J. Meixner, C.M. Jefferson, and R.M. Macfarlane, *Measurement of the Stark effect with subhomogeneous linewidth resolution in Eu^{3+}:$YAlO_3$ with the use of photon-echo modulation*, Phys.Rev.B **46**, 5912-5916 (1992)
75. Y. Sun, G.M. Wang, R.L. Cone, R.W. Equall, and M.J.M. Leask, *Symmetry considerations regarding light propagation and light polarization for coherent interactions with ions in crystals*, Phys.Rev.B **62**, 15443-15451 (2000)
76. G.D. Mahan, *Local-field corrections to Coulomb interactions*, Phys.Rev. **153**, 983 (1967)
77. C. Kittel and E. Abrahams, *Dipolar broadening of magnetic resonance lines in magnetically diluted crystals*, Phys.Rev. **90**, 238-239 (1953)
78. J.R. Klauder and P.W. Anderson, *Spectral diffusion in spin resonance experiments*, Phys.Rev. **125**, 912 (1962)
79. J. Huang, J.M. Zhang, A. Lezama, and T.W. Mossberg, *On the shifting of optical-transition frequencies in rare-earth doped insulators by resonant optical-excitation*, J.Lumin. **45**, 392-396 (1990)
80. S. Kröll, E.Y. Xu, and R. Kachru, *Influence of Excited-State Pr^{3+} On the Relaxation of the Pr^{3+}-$YAlO_3$ $^3H_4$-$^1D_2$ Transition*, Phys.Rev.B **44**, 30-34 (1991)
81. M. Mitsunaga, T. Takagahara, R. Yano, and N. Uesugi, *Excitation-induced frequency shift probed by stimulated photon echoes*, Phys.Rev.Lett. **68**, 3216 (1992)
82. J.M. Zhang and T.W. Mossberg, *Optically induced frequency shifts in the frequency of the H-3(4)-D-1(2) transition of Pr^{3+} in LaF_3*, Phys.Rev.B **48**, 7668-7671 (1993)
83. S.B. Altner, M. Mitsunaga, G. Zumofen, and U.P. Wild, *Dephasing-rephasing balancing in photon echoes by excitation induced frequency shifts*, Phys.Rev.Lett. **76**, 1747 (1996)
84. J.H. Wesenberg and K. Mølmer, *The field inside a random distribution of parallel dipoles*, Phys.Rev.Lett. **93**, 143903 (2004)
85. J.J. Longdell and M.J. Sellars, *Experimental demonstration of quantum-state tomography and qubit-qubit interactions for rare-earth-metal-ion-based solid-state qubits*, Phys.Rev.A **69**, 032307 (2004)
86. Persson, M., *Stark shifts and ion-ion interaction in Europium doped $YAlO_3$ - On the road to quantum computing*, Lund Reports on Atomic Physics, LRAP-279, Diploma paper, Lund, Sweden (2001)
87. A.J. Meixner, A. Renn, and U.P. Wild, *Spectral hole-burning and holography .1. Transmission and holographic detection of spectral holes*, J.Chem.Phys. **91**, 6728-6736 (1989)
88. A. Szabo, *Observation of hole burning and cross relaxation effects in ruby*, Phys.Rev.B **11** , 4512-4517 (1975)

89. A.A. Gorokhovskii, R.K. Kaarli, and L.A. Rebane, *Hole burning in contour of a pure electronic line in a Shpolskii system*, JETP Lett. **20**, 216-218 (1974)
90. B.M. Kharlamov, R.I. Personov, and L.A. Bykovskaya, *Stable gap in absorption-spectra of solid-solutions of organic-molecules by laser irradiation*, Opt.Commun. **12**, 191-193 (1974)
91. R.M. Macfarlane and R.M. Shelby, *Photoionization hole burning and nonlinear Zeeman effect in CaF_2-Sm^{2+}*, Opt.Lett. **9**, 533-536 (1984)
92. H. Devries and D.A. Wiersma, *Photophysical and photochemical molecular hole burning theory*, J.ChemPhys. **72**, 1851-1863 (1980)
93. A. Winnacker, R.M. Shelby, and R.M. Macfarlane, *Photon-gated hole-burning - A new mechanism using 2-step photoionization*, Opt.Lett. **10**, 350-352 (1985)
94. J. Brossel and A. Kastler, *La detection de la resonance magnetique des niveaux excites - l'effect de depolarisation des radiations de resonance optique et de fluorescence*, C.R.Acad.Sci. **229**, 1213-1215 (1949)
95. T.R. Carver, *Optical pumping*, Science **141**, 599-608 (1963)
96. N. Ohlsson, R.K. Mohan, and S. Kröll, *Quantum computer hardware based on rare-earth-ion-doped inorganic crystals*, Opt.Commun. **201**, 71-77 (2002)
97. Szabo, A., *Frequency selective optical memory*, U.S. Patent No. 3,896,420 (1975)
98. Castro, G., et al., *Frequency selective optical data storage system*, U.S. Patent No. 4,101,976 (1978)
99. P.B. Sellin, N.M. Strickland, J.L. Carlsten, and R.L. Cone, *Programmable frequency reference for subkilohertz laser stabilization by use of persistent spectral hole burning*, Opt.Lett. **24**, 1038-1040 (1999)
100. T.W. Mossberg, *Time-domain frequency-selective optical-data storage*, Opt.Lett. **7**, 77-79 (1982)
101. M. Mitsunaga, R. Yano, and N. Uesugi, *Time- and frequency-domain hybrid optical memory - 1.6- kbit data-storage in Eu^{3+} -Y_2SiO_5*, Opt.Lett. **16**, 1890-1892 (1991)
102. X.A. Shen, A.D. Nguyen, J.W. Perry, D.L. Huestis, and R. Kachru, *Time-domain holographic digital memory*, Science **278**, 96-100 (1997)
103. X.A. Shen and R. Kachru, *Optical header recognition by spectroholographic filtering*, Opt.Lett. **20**, 2508-2510 (1995)
104. M. Tian, E. Grelet, I. Lorgeré, J.P. Galaup, and J.L. Le Gouet, *Persistent spectral hole burning in an organic material for temporal pattern recognition*, J.Opt.Soc.Am.B **16**, 74-82 (1999)
105. T.L. Harris, Y. Sun, W.R. Babbitt, R.L. Cone, J.A. Ritcey, and R.W. Equall, *Spatial-spectral holographic correlator at 1536 nm using 30- symbol quadriphase- and binary-phase-shift keyed codes*, Opt.Lett. **25**, 85-87 (2000)
106. L. Menager, I. Lorgeré, J.L. Le Gouet, D. Dolfi, and J.P. Huignard, *Demonstration of a radio-frequency spectrum analyzer based on spectral hole burning*, Opt.Lett. **26**, 1245-1247 (2001)
107. K.D. Merkel and W.R. Babbitt, *Optical coherent transient continuously programmed continuous processor*, Opt.Lett. **24**, 172-174 (1999)
108. G.J. Pryde, M.J. Sellars, and N.B. Manson, *Solid state coherent transient measurements using hard optical pulses* , Phys.Rev.Lett. **84**, 1152-1155 (2000)
109. M.J. Sellars, G.J. Pryde, N.B. Manson, and E.R. Krausz, *50 kHz absorption line in Y_2SiO_5:Eu^{3+}*, J.Lumin. **87-9**, 833-835 (2000)
110. F. de Seze, V. Lavielle, I. Lorgeré, and J.L. Le Gouet, *Chirped pulse generation of a narrow absorption line in a Tm^{3+}:YAG crystal*, Opt.Commun. **223**, 321-330 (2003)
111. J.J. Longdell, M.J. Sellars, and N.B. Manson, *Demonstration of conditional quantum phase shift between ions in a solid*, Phys.Rev.Lett. **93**, 130503 (2004)

112. N.A. Kurnit, S.R. Hartmann, and I.D. Abella, *Observation of Photon Echo*, Phys.Rev.Lett. **13**, 567 (1964)
113. R.G. Brewer, *Optical Free Induction Decay*, Phys.Rev.A **6**, 2001 (1972)
114. Allen, D. and Eberly, J.H., *Optical resonace and two-level atoms*, Wiley, New York (1975)
115. Boyd, R.W., *Nonlinear optics*, Academic press limited, London, England (1992)
116. Scully, M.O. and Zubairy, M.S., *Quantum Optics*, Cambridge University Press (1997)
117. Suter, D., *The Physics of Laser-Matter Interactions*, Cambridge University Press (1997)
118. Shoemaker, R.L., *Coherent Transient Infrared Spectroscopy*, in *Laser and Coherence Spectroscopy*, Steinfeld, J. I. (Ed.), Plenum Press, New York (1978)
119. F. Bloch, *Nuclear induction*, Phys.Rev. **70**, 460-474 (1946)
120. I.I. Rabi, *Space Quantization in a Gyrating Magnetic Field*, Phys.Rev. **51**, 652 (1937)
121. G.B. Hocker and C.L. Tang, *Observation of the optical transient nutation effect*, Phys.Rev.Lett. **21**, 591 (1968)
122. T.W. Mossberg, R. Kachru, and S.R. Hartmann, *Echoes in gaseous media - generalized theory of rephasing phenomena* , Phys.Rev.A **20**, 1976-1996 (1979)
123. Mandel, L. and Wolf, E., *Optical Coherence and Quantum Optics*, Cambridge University Press (1995)
124. S.L. McCall and E.L. Hahn, *Self-Induced Transparency by Pulsed Coherent Light*, Phys.Rev.Lett. **18**, 908 (1967)
125. Cornish, C. S., *Highly efficient photon echo generation and a study of the energy source of photon echoes,* dissertation, University of Washington/Department of electrical engineering (2000)
126. G.W. Burr, T.L. Harris, W.R. Babbitt, and C.M. Jefferson, *Incorporating excitation-induced dephasing into the Maxwell-Bloch numerical modeling of photon echoes*, J.Lumin. **107**, 314-331 (2004)
127. R.H. Dicke, *Coherence in spontaneous radiation processes*, Phys.Rev. **93**, 99-110 (1954)
128. E.L. Hahn, *Spin Echoes*, Phys.Rev. **80**, 580-594 (1950)
129. R. Beach, S.R. Hartmann, and R. Friedberg, *Billiard-ball echo model*, Phys.Rev.A **25**, 2658-2666 (1982)
130. M. Mitsunaga and R.G. Brewer, *Generalized perturbation theory of coherent optical emission*, Phys.Rev.A **32**, 1605 (1985)
131. A.V. Durrant, J. Manners, and P.M. Clark, *Understanding optical echoes using Schrödinger's equation: I. Echoes excited by two optical pulses*, Eur.J.Phys. **10**, 291-297 (1989)
132. A.V. Durrant, J. Manners, and P.M. Clark, *Understanding optical echoes using Schrödinger's equation: II. Three pulse echoes and collision effects*, Eur.J.Phys. **12**, 234-239 (1991)
133. Y.S. Bai, W.R. Babbitt, N.W. Carlson, and T.W. Mossberg, *Real-time optical waveform convolver/cross correlator*, Appl.Phys.Lett. **45**, 714-716 (1984)
134. T.W. Mossberg, *Swept-carrier time-domain optical memory*, Opt.Lett. **17**, 535-537 (1992)
135. M. Mitsunaga, R. Yano, and N. Uesugi, *Spectrally programmed stimulated photon echo*, Opt.Lett. **16**, 264-266 (1991)
136. L. Menager, J.L. Le Gouët, and I. Lorgeré, *Time-to-frequency Fourier transformation with photon echoes*, Opt.Lett. **26**, 1397-1399 (2001)
137. L. Menager, I. Lorgeré, and J.L. Le Gouët, *Fresnel diffraction on the edge of causality*, Opt.Lett. **25**, 1316-1318 (2000)

138. S.O. Elyutin, S.M. Zakharov, V.A. Zuikov, E.A. Manykin, and V.V. Samartsev, *Spatial and temporal correlations of coherent optical pulses in the photon echo effect*, Sov.Phys.JETP **61**, 234-242 (1985)
139. W.R. Babbitt and T.W. Mossberg, *Spatial routing of optical beams through time-domain spatial- spectral filtering*, Opt.Lett. **20**, 910-912 (1995)
140. J.B.W. Morsink, W.H. Hesselink, and D.A. Wiersma, *Photon-echo stimulated from optically induced nuclear-spin polarization*, Chem.Phys.Lett. **64**, 1-4 (1979)
141. N.W. Carlson, Y.S. Bai, W.R. Babbitt, and T.W. Mossberg, *Temporally programmed free-induction decay*, Phys.Rev.A **30**, 1572-1574 (1984)
142. W.H. Hesselink and D.A. Wiersma, *Picosecond photon-echoes stimulated from an accumulated grating*, Phys.Rev.Lett. **43**, 1991-1994 (1979)
143. W.H. Hesselink and D.A. Wiersma, *Photon-echoes stimulated from an accumulated grating - theory of generation and detection*, J.Chem.Phys. **75**, 4192-4197 (1981)
144. G.J. Pryde, M.J. Sellars, and N.B. Manson, *Optical non-Bloch behaviour observed using an optical Carr- Purcell-Meiboom-Gill pulse sequence*, J.Lumin. **86**, 279-283 (2000)
145. H.K. Cummins, G. Llewellyn, and J.A. Jones, *Tackling systematic errors in quantum logic gates with composite rotations*, Phys.Rev.A **67**, 042308 (2003)
146. M.H. Levitt, *Composite Pulses*, Progress In Nuclear Magnetic Resonance Spectroscopy **18**, 61-122 (1986)
147. J.H. Wesenberg, *Designing robust gate implementations for quantum-information processing*, Phys.Rev.A **69**, 042323 (2004)
148. Y.S. Bai, W.R. Babbitt, and T.W. Mossberg, *Coherent transient optical pulse-shape storage recall using frequency-swept excitation pulses*, Opt.Lett. **11**, 724-726 (1986)
149. K.D. Merkel and W.R. Babbitt, *Chirped-pulse programming of optical coherent transient true- time delays*, Opt.Lett. **23**, 528-530 (1998)
150. T.L. Harris, M.Z. Tian, W.R. Babbitt, G.W. Burr, J.A. Hoffnagle, and C.M. Jefferson, *Chirped excitation of optically dense inhomogeneously broadened media using* Eu^{3+}*:*Y_2SiO_5, J.Opt.Soc.Am.B **21**, 811-819 (2004)
151. M.M.T. Loy, *Observation of population inversion by optical adiabatic rapid passage*, Phys.Rev.Lett. **32**, 814-817 (1974)
152. N.V. Vitanov, T. Halfmann, B.W. Shore, and K. Bergmann, *Laser-induced population transfer by adiabatic passage techniques*, Annu.Rev.Phys.Chem. **52**, 763-809 (2001)
153. I. Roos and K. Mølmer, *Quantum computing with an inhomogeneously broadened ensemble of ions: Suppression of errors from detuning variations by specially adapted pulses and coherent population trapping*, Phys.Rev.A **69**, 022321 (2004)
154. M.S. Silver, R.I. Joseph, and D.I. Hoult, *Selective spin inversion in nuclear-magnetic resonance and coherent optics through an exact solution of the Bloch Riccati equation*, Phys.Rev.A **31**, 2753-2755 (1985)
155. L. Mitschang, B. Ittermann, F. Schubert, and H. Rinneberg, *Design of a constant adiabaticity pulse for selective population inversion*, J.Magn.Res. **168**, 103-109 (2004)
156. K.E. Cano, M.A. Smith, and A.J. Shaka, *Adjustable, broadband, selective excitation with uniform phase*, J.Magn.Res. **155**, 131-139 (2002)
157. H.R. Gray, R.M. Whitley, and C.R. Stroud, *Coherent trapping of atomic populations*, Opt.Lett. **3**, 218-220 (1978)
158. K. Bergmann, H. Theuer, and B.W. Shore, *Coherent population transfer among quantum states of atoms and molecules* , Rev.Mod.Phys. **70**, 1003-1025 (1998)
159. H. Lin, T. Wang, and T.W. Mossberg, *Demonstration of 8-Gbit/in*^{2} *areal storage density based on swept-carrier frequency-selective optical memory*, Opt.Lett. **20**, 1658-1660 (1995)

160. M. Zhu, W.R. Babbitt, and C.M. Jefferson, *Continuous coherent transient optical processing in a solid*, Opt.Lett. **20**, 2514-2516 (1995)
161. X.A. Shen and R. Kachru, *Time-domain optical memory for image storage and high-speed image-processing*, Appl.Opt. **32**, 5810-5815 (1993)
162. S. Kröll and U. Elman, *Photon-echo-based logical processing*, Opt.Lett. **18**, 1834-1836 (1993)
163. I. Zeylikovich, G. Bai, A. Gorokhovsky, and R.R. Alfano, *Terabit speed retrieval of femtosecond accumulated photon- echoes*, Opt.Lett. **20**, 749-751 (1995)
164. S. Kröll and P. Tidlund, *Recording density limit of photon-echo optical storage with high-speed writing and reading*, Appl.Opt. **32**, 7233-7242 (1993)
165. W.R. Babbitt and T.W. Mossberg, *Quasi-2-dimensional time-domain color memories - process limitations and potentials*, J.Opt.Soc.Am.B **11**, 1948-1953 (1994)
166. F.R. Graf, B.H. Plagemann, E.S. Maniloff, S.B. Altner, A. Renn, and U.P. Wild, *Data compression in frequency-selective materials using frequency-swept excitation pulses*, Opt.Lett. **21**, 284-286 (1996)
167. X.J. Wang, M. Afzelius, N. Ohlsson, U. Gustafsson, and S. Kröll, *Coherent transient data-rate conversion and data transformation*, Opt.Lett. **25**, 945-947 (2000)
168. T. Wang, H. Lin, and T.W. Mossberg, *Optical bit-rate conversion and bit-stream time-reversal by the use of swept-carrier frequency-selective optical-data storage techniques*, Opt.Lett. **20**, 2033-2035 (1995)
169. K.D. Merkel and W.R. Babbitt, *Optical coherent transient header/data isolation technique*, Opt.Lett. **21**, 71-73 (1996)
170. J.M. Zhang, D.J. Gauthier, J. Huang, and T.W. Mossberg, *Use of phase-noisy laser fields in the storage of optical pulse shapes in inhomogeneously broadened absorbers*, Opt.Lett. **16**, 103-105 (1991)
171. X.A. Shen and R. Kachru, *Use of biphase-coded pulses for wide-band data-storage in time-domain optical memories* , Appl.Opt. **32**, 3149-3151 (1993)
172. X.A. Shen, R. Hartman, and R. Kachru, *Impulse-equivalent time-domain optical memory*, Opt.Lett. **21**, 833-835 (1996)
173. Y.S. Bai and R. Kachru, *Coherent time-domain data-storage with a spread-spectrum generated by random biphase shifting*, Opt.Lett. **18**, 1189-1191 (1993)
174. X.A. Shen and R. Kachru, *Coherent saturation removal in time-domain optical memory by storage of frequency-chirped data pulses*, Opt.Lett. **18**, 1967-1969 (1993)
175. S.O. Elyutin, S.M. Zakharov, and E.A. Manykin, *Theoretical pulse shapes for the photon (light) echo*, Sov.Phys.JETP **49**, 421-426 (1979)
176. V.A. Zuikov, V.V. Samartsev, and R.G. Usmanov, *Correlation of the shape of light-echo signals with the shape of the excitation pulses*, JETP Lett. **32**, 270-274 (1980)
177. A.G. Anderson, R.L. Garwin, E.L. Hahn, J.W. Horton, G.L. Tucker, and R.M. Walker, *Spin echo serial storage memory*, J.Appl.Phys. **26**, 1324-1338 (1955)
178. N.W. Carlson, L.J. Rothberg, A.G. Yodh, W.R. Babbitt, and T.W. Mossberg, *Storage and time-reversal of light-pulses using photon-echoes*, Opt.Lett. **8**, 483-485 (1983)
179. W.R. Babbitt and T.W. Mossberg, *Time-domain frequency-selective optical-data storage in a solid-state material*, Opt.Commun. **65**, 185-188 (1988)
180. M.K. Kim and R. Kachru, *Many-bit optical-data storage using stimulated echoes*, Appl.Opt. **28**, 2186-2188 (1989)
181. S. Kröll, L.E. Jusinski, and R. Kachru, *Frequency-Chirped Copropagating Multiple-Bit Stimulated-Echo Storage and Retrieval in Pr^{3+}-$YAlO_3$*, Opt.Lett. **16**, 517-519 (1991)
182. M. Mitsunaga and N. Uesugi, *248-bit optical-data storage in Eu^{3+}-$YAlO_3$ by accumulated photon-echoes*, Opt.Lett. **15**, 195-197 (1990)

183. H. Lin, T. Wang, G.A. Wilson, and T.W. Mossberg, *Experimental demonstration of swept-carrier time-domain optical memory*, Opt.Lett. **20**, 91-93 (1995)
184. S. Kröll, E.Y. Xu, M.K. Kim, M. Mitsunaga, and R. Kachru, *Intensity-Dependent Photon-Echo Relaxation in Rare-Earth-Doped Crystals*, Phys.Rev.B **41**, 11568-11571 (1990)
185. A.E. Johnson, E.S. Maniloff, and T.W. Mossberg, *Spatially distributed spectral storage*, Opt.Lett. **24**, 1526-1528 (1999)
186. N.W. Carlson, W.R. Babbitt, and T.W. Mossberg, *Storage and phase conjugation of light-pulses using stimulated photon-echoes*, Opt.Lett. **8**, 623-625 (1983)
187. M.K. Kim and R. Kachru, *Storage and phase conjugation of multiple images using backward-stimulated echoes in Pr-3+-LaF3*, Opt.Lett. **12**, 593-595 (1987)
188. A. Renn and U.P. Wild, *Spectral hole burning and hologram storage*, Appl.Opt. **26**, 4040-4042 (1987)
189. M. Mitsunaga, N. Uesugi, H. Sasaki, and K. Karaki, *Holographic motion-picture by* Eu^{3+}-Y_2SiO_5, Opt.Lett. **19**, 752-754 (1994)
190. X.A. Shen, E. Chiang, and R. Kachru, *Time-domain holographic image storage*, Opt.Lett. **19** , 1246-1248 (1994)
191. W.R. Babbitt and J.A. Bell, *Coherent transient continuous optical processor*, Appl.Opt. **33**, 1538-1548 (1994)
192. K.D. Merkel and W.R. Babbitt, *Optical coherent-transient true-time-delay regenerator*, Opt.Lett. **21**, 1102-1104 (1996)
193. M.Z. Tian, R. Reibel, and W.R. Babbitt, *Demonstration of optical coherent transient true-time delay at 4 Gbits/s* , Opt.Lett. **26**, 1143-1145 (2001)
194. K.D. Merkel, R.K. Mohan, Z. Cole, T. Chang, A. Olson, and W.R. Babbitt, *Multi-gigahertz radar range processing of baseband and RF carrier modulated signals in Tm:YAG*, J.Lumin. **107**, 62-74 (2004)
195. T. Wang, H. Lin, and T.W. Mossberg, *Experimental demonstration of temporal-waveform-controlled spatial routing of optical beams by spatial-spectral filtering*, Opt.Lett. **20**, 2541-2543 (1995)
196. T.L. Harris, Y. Sun, R.L. Cone, R.M. Macfarlane, and R.W. Equall, *Demonstration of real-time address header decoding for optical data routing at 1536 nm*, Opt.Lett. **23**, 636-638 (1998)
197. Y.S. Bai and T.W. Mossberg, *Photon-echo optical pulse-compression*, Appl.Phys.Lett. **45**, 1269-1271 (1984)
198. Y.S. Bai and T.W. Mossberg, *Experimental studies of photon-echo pulse-compression*, Opt.Lett. **11**, 30-32 (1986)
199. Hecht, E., *Optics*, Addison-Wesley (1987)
200. Wilson, J. and Hawkes, J.F.B., *Opto-Electronics: An Introduction*, Prentice-Hall, New York (1987)
201. L. Levin, *Mode-hop-free electro-optically tuned diode laser*, Opt.Lett. **27**, 237-239 (2002)
202. B. Boggs, C. Greiner, T. Wang, H. Lin, and T.W. Mossberg, *Simple high-coherence rapidly tunable external-cavity diode laser*, Opt.Lett. **23**, 1906-1908 (1998)
203. R.W.P. Drever, J.L. Hall, F.V. Kowalski, J. Hough, G.M. Ford, A.J. Munley, and H. Ward, *Laser phase and frequency stabilization using an optical resonator*, Appl.Phys.B-Photo. **31**, 97-105 (1983)
204. M.J. Sellars, R.S. Meltzer, P.T.H. Fisk, and N.B. Manson, *Time-resolved ultranarrow optical hole-burning of a crystalline solid -* $Y_2O_3Eu^{3+}$, J.Opt.Soc.Am.B **11**, 1468-1473 (1994)
205. V. Crozatier, F. de Seze, L. Haals, F. Bretenaker, I. Lorgeré, and J.L. Le Gouet, *Laser diode stabilisation for coherent driving of rare earth ions*, Opt.Commun. **241**, 203 (2004)

206. Mini Circuits, *Application Notes*, http://www.minicircuits.com/application.html
207. Tektronix, http://www.tek.com
208. A.V. Turukhin, V.S. Sudarshanam, M.S. Shahriar, J.A. Musser, B.S. Ham, and P.R. Hemmer, *Observation of ultraslow and stored light pulses in a solid*, Phys.Rev.Lett. **88**, 023602 (2002)
209. Sze, S.M., *Semiconductor devices*, John Wiley & Sons (1985)
210. Hamamatsu Photonics, *Photomultiplier Tubes*, product catalogue (2002)
211. J.P. Gordon, H.J. Zeiger, and C.H. Townes, *Maser - New type of microwave amplifier, frequency standard, and spectrometer*, Phys.Rev. **99**, 1264-1274 (1955)
212. P.G. O'Shea and H.P. Freund, *Laser technology - Free-electron lasers: Status and applications*, Science **292**, 1853-1858 (2001)
213. J.J. Rocca, V. Shlyaptsev, F.G. Tomasel, O.D. Cortazar, D. Hartshorn, and J.L.A. Chilla, *Demonstration of a discharge pumped table-top soft-X-ray laser*, Phys.Rev.Lett. **73**, 2192-2195 (1994)
214. C. Salomon, D. Hils, and J.L. Hall, *Laser stabilisation at the millihertz level*, J.Opt.Soc.Am.B **5**, 1576-1587 (1988)
215. D.J. Jones, S.A. Diddams, J.K. Ranka, A. Stentz, R.S. Windeler, J.L. Hall, and S.T. Cundiff, *Carrier-envelope phase control of femtosecond mode-locked lasers and direct optical frequency synthesis*, Science **288**, 635-639 (2000)
216. M. Hentschel, R. Kienberger, C. Spielmann, G.A. Reider, N. Milosevic, T. Brabec, P. Corkum, U. Heinzmann, M. Drescher, and F. Krausz, *Attosecond metrology*, Nature **414**, 509-513 (2001)
217. P.M. Paul, E.S. Toma, P. Breger, G. Mullot, F. Auge, P. Balcou, H.G. Muller, and P. Agostini, *Observation of a train of attosecond pulses from high harmonic generation*, Science **292**, 1689-1692 (2001)
218. P. Antoine, A. LHuillier, and M. Lewenstein, *Attosecond pulse trains using high-order harmonics*, Phys.Rev.Lett. **77**, 1234-1237 (1996)
219. T. Sauter, R. Blatt, W. Neuhauser, and P.E. Toschek, *Quantum jumps observed in the fluorescence of a single ion*, Opt.Commun. **60**, 287-292 (1986)
220. W.P. Ambrose and W.E. Moerner, *Fluorescence spectroscopy and spectral diffusion of single impurity molecules in a crystal*, Nature **349**, 225-227 (1991)
221. J.T. Hoffges, H.W. Baldauf, W. Lange, and H. Walther, *Heterodyne measurement of the resonance fluorescence of a single ion*, Journal Of Modern Optics **44**, 1999-2010 (1997)
222. S. Weiss, *Fluorescence spectroscopy of single biomolecules*, Science **283**, 1676-1683 (1999)
223. D. Gammon, E.S. Snow, B.V. Shanabrook, D.S. Katzer, and D. Park, *Homogeneous linewidths in the optical spectrum of a single gallium arsenide quantum dot*, Science **273**, 87-90 (1996)
224. A.P. Bartko, L.A. Peyser, R.M. Dickson, A. Mehta, T. Thundat, R. Bhargava, and M.D. Barnes, *Observation of dipolar emission patterns from isolated Eu^{3+}:Y_2O_3 doped nanocrystals: new evidence for single ion luminescence*, Chem.Phys.Lett. **358**, 459-465 (2002)
225. Y.V. Malyukin, A.A. Masalov, and P.N. Zhmurin, *Single-ion fluorescence spectroscopy of a Y_2SiO_5 :Pr_{3+} nanocluster*, Phys.Lett.A **316**, 147-152 (2003)
226. Oxford Instruments, http://www.oxford-instruments.com
227. Helsinki University of Technology - Low Temperature Laboratory, http://boojum.hut.fi/Low-Temp-Record.html
228. K.B. Davis, M.O. Mewes, M.R. Andrews, N.J. Vandruten, D.S. Durfee, D.M. Kurn, and W. Ketterle, *Bose-Einstein condensation in a gas of sodium atoms*, Phys.Rev.Lett. **75**, 3969-3973 (1995)

229. M.H. Anderson, J.R. Ensher, M.R. Matthews, C.E. Wieman, and E.A. Cornell, *Observation of Bose-Einstein condensation in a dilute atomic vapor*, Science **269**, 198-201 (1995)
230. R. Folman, P. Kruger, D. Cassettari, B. Hessmo, T. Maier, and J. Schmiedmayer, *Controlling cold atoms using nanofabricated surfaces: Atom chips*, Phys.Rev.Lett. **84**, 4749-4752 (2000)
231. K.J. Boller, A. Imamoglu, and S.E. Harris, *Observation of electromagnetically induced transparency*, Phys.Rev.Lett. **66**, 2593-2596 (1991)
232. S.E. Harris, *Electromagnetically induced transparency*, Physics Today **50**, 36-42 (1997)
233. M.O. Scully, S.Y. Zhu, and A. Gavrielides, *Degenerate quantum-beat laser - Lasing without inversion and inversion without lasing*, Phys.Rev.Lett. **62**, 2813-2816 (1989)
234. L.V. Hau, S.E. Harris, Z. Dutton, and C.H. Behroozi, *Light speed reduction to 17 metres per second in an ultracold atomic gas*, Nature **397**, 594-598 (1999)
235. P.A.M. Dirac, *The Quantum Theory of the Emission and Absorption of Radiation*, Proc.R.Soc.Lond.Ser.A **114**, 243-265 (1927)
236. Z.L. Yuan, B.E. Kardynal, R.M. Stevenson, A.J. Shields, C.J. Lobo, K. Cooper, N.S. Beattie, D.A. Ritchie, and M. Pepper, *Electrically driven single-photon source*, Science **295**, 102-105 (2002)
237. P. Michler, A. Kiraz, C. Becher, W.V. Schoenfeld, P.M. Petroff, L.D. Zhang, E. Hu, and A. Imamoglu, *A quantum dot single-photon turnstile device*, Science **290**, 2282 (2000)
238. B. Lounis and W.E. Moerner, *Single photons on demand from a single molecule at room temperature*, Nature **407**, 491-493 (2000)
239. D.F. Walls, *Squeezed states of light*, Nature **306**, 141-146 (1983)
240. A.R. Kessel and S.A. Moiseev, *Delayed Self-Interference of a Photon*, JETP Lett. **58**, 80-84 (1993)
241. S.A. Moiseev, *Time-Delayed Interference of a Photon and the One-Photon Echo in media with Phase Memory*, Optics And Spectroscopy (Optika i Spektroskopiya) **83**, 261-274 (1997)
242. R. Friedberg and S.R. Hartmann, *Photon/Zen echoes*, Laser Phys. **9**, 1083-1101 (1999)
243. R.K. Mohan, B. Luo, S. Kröll, and A. Mair, *Delayed single-photon self-interference*, Phys.Rev.A **58**, 4348-4358 (1998)
244. I. Marcikic, H. De Riedmatten, W. Tittel, V. Scarani, H. Zbinden, and N. Gisin, *Time-bin entangled qubits for quantum communication created by femtosecond pulses*, Phys.Rev.A **66**, 062308 (2002)
245. Saers, R. *Stabilising a Ring Dye Laser to Iodine Transitions*, Lund Reports on Atomic Physics, LRAP-282, Diploma paper, Lund, Sweden (2002)
246. Dirac, P.A.M., *Principles of Quantum Electronics*, Oxford University Press, London (1958)
247. S.A. Moiseev, *Time-delayed quantum interference and single-photon echo in coherent three-level systems*, Quantum Electronics **31**, 557-563 (2001)
248. W.H. Zurek, *Decoherence, einselection, and the quantum origins of the classical*, Rev.Mod.Phys. **75**, 715-775 (2003)
249. S.A. Moiseev, *Time-delayed quantum interference and single-photon echo in coherent three-level systems*, Quantum Electronics (Kvantovaya Elektronika) **31**, 557 (2001)
250. S.A. Moiseev, *Special features of detection of a One-Photon Echo and a Time-Delayed Photon Interference in a Three-Level Medium*, Optics And Spectroscopy (Optika i Spektroskopiya) **82**, 943-948 (1997)
251. J.D. Franson and K.A. Potocki, *Single-photon interference over large distances*, Phys.Rev.A **37**, 2511-2515 (1988)
252. J. Wrachtrup, C. von Borczyskowski, J. Bernard, R. Brown, and M. Orrit, *Hahn echo experiments on a single triplet electron spin*, Chem.Phys.Lett. **245**, 262-267 (1995)

253. J.I. Cirac, P. Zoller, H.J. Kimble, and H. Mabuchi, *Quantum state transfer and entanglement distribution among distant nodes in a quantum network*, Phys.Rev.Lett. **78**, 3221-3224 (1997)
254. A.E. Kozhekin, K. Mølmer, and E. Polzik, *Quantum memory for light*, Phys.Rev.A **62**, 033809 (2000)
255. S.A. Moiseev and S. Kröll, *Complete reconstruction of the quantum state of a single-photon wave packet absorbed by a Doppler-broadened transition*, Phys.Rev.Lett. **87**, 173601 (2001)
256. M. Fleischhauer and M.D. Lukin, *Quantum memory for photons: Dark-state polaritons*, Phys.Rev.A **65**, 022314 (2002)
257. D.F. Phillips, A. Fleischhauer, A. Mair, and R.L. Walsworth, *Storage of light in atomic vapor*, Phys.Rev.Lett. **86**, 783-786 (2001)
258. C. Liu, Z. Dutton, C.H. Behroozi, and L.V. Hau, *Observation of coherent optical information storage in an atomic medium using halted light pulses*, Nature **409**, 490-493 (2001)
259. B. Julsgaard, J. Sherson, J.I. Cirac, J. Fiurásek, and E.S. Polzik, *Experimental demonstration of quantum memory for light*, Nature **432**, 483 (2004)
260. N.W. Carlson, W.R. Babbitt, Y.S. Bai, and T.W. Mossberg, *Spectrally ordered Zeeman coherences and optical pulse-shape storage*, J.Opt.Soc.Am.B **2**, 908-914 (1985)
261. T. Wang, C. Greiner, and T.W. Mossberg, *Photon echo signals: beyond unit efficiency*, Opt.Commun. **153**, 309-313 (1998)
262. C.S. Cornish, W.R. Babbitt, and L. Tsang, *Demonstration of highly efficient photon echoes*, Opt.Lett. **25**, 1276-1278 (2000)
263. S.A. Moiseev and M.I. Noskov, *Technique of quantum memory on the basis of a photon echo in gases*, Optics And Spectroscopy (Optika i Spektroskopiya) **96**, 714-720 (2004)
264. S.A. Moiseev, V.F. Tarasov, and B.S. Ham, *Quantum memory photon echo-like techniques in solids*, Journal Of Optics B-Quantum And Semiclassical Optics **5**, S497-S502 (2003)
265. Tittel, W., personal communication
266. B.S. Ham, P.R. Hemmer, and M.S. Shahriar, *Efficient electromagnetically induced transparency in a rare- earth doped crystal*, Opt.Commun. **144**, 227-230 (1997)
267. B.S. Ham, M.S. Shahriar, and P.R. Hemmer, *Enhanced nondegenerate four-wave mixing owing to electromagnetically induced transparency in a spectral hole-burning crystal*, Opt.Lett. **22**, 1138-1140 (1997)
268. P.R. Hemmer, K.Z. Cheng, J. Kierstead, M.S. Shahriar, and M.K. Kim, *Time-domain optical data storage by use of Raman coherent population trapping*, Opt.Lett. **19**, 296-298 (1994)
269. B.S. Ham, M.S. Shahriar, M.K. Kim, and P.R. Hemmer, *Frequency-selective time-domain optical data storage by electromagnetically induced transparency in a rare-earth-doped solid*, Opt.Lett. **22**, 1849-1851 (1997)
270. B.S. Ham, M.S. Shahriar, and P.R. Hemmer, *Radio-frequency-induced optical gain in* Pr^{3+}*:*Y_2SiO_5, J.Opt.Soc.Am.B **15**, 1541-1544 (1998)
271. Atomic Physics, LTH, http://www-atom.fysik.lth.se
272. Centre Interdisciplinaire de Recherche Ions Lasers, http://www.ganil.fr/ciril/index_gb.htm
273. Laboratoire Aimé Cotton, http://www.lac.u-psud.fr/LAC/us_index.html
274. Laboratoire de Chimie Appliquée de l'Etat solide, http://www.enscp.jussieu.fr/labos/LCAES/
275. Danish National Research Foundation Center for Quantum Optics, http://www.phys.au.dk/quantop/
276. ANU - Laser Physics Centre, http://laserspark.anu.edu.au
277. Stolze, J. and Suter, D., *Quantum Computing: A short course from theory to experiment*, John Wiley & Sons (2004)

278. P. Benioff, *The Computer as a Physical System - A Microscopic Quantum-Mechanical Hamiltonian Model of Computers as Represented by Turing-Machines*, J.Stat.Phys. **22**, 563-591 (1980)
279. A. Peres, *Reversible logic and quantum computers*, Phys.Rev.A **32**, 3266-3276 (1985)
280. R.P. Feynman, *Simulating Physics with Computers*, Int.J.Theor.Phys. **21**, 467-488 (1982)
281. S. Lloyd, *Universal quantum simulators*, Science **273**, 1073-1078 (1996)
282. DiVincenzo, D. P., *Topics in quantum computers*, cond-mat/9612126 (1996)
283. Wesenberg, J. H., *Quantum Information Processing in Rare-Earth-Ion Doped Crystals,* dissertation, QUANTOP, Department of Physics and Astronomy, University of Aarhus, Denmark (2004)
284. D. Collins, *Modified Grover's algorithm for an expectation-value quantum computer*, Phys.Rev.A **65**, 052321(2002)
285. J.I. Cirac and P. Zoller, *Quantum Computations With Cold Trapped Ions*, Phys.Rev.Lett. **74**, 4091-4094 (1995)
286. C. Monroe, *Quantum information processing with atoms and photons*, Nature **416**, 238-246 (2002)
287. S. Gulde, M. Riebe, G.P.T. Lancaster, C. Becher, J. Eschner, H. Haffner, F. Schmidt-Kaler, I.L. Chuang, and R. Blatt, *Implementation of the Deutsch-Jozsa algorithm on an ion-trap quantum computer*, Nature **421**, 48-50 (2003)
288. I.H. Deutsch, G.K. Brennen, and P.S. Jessen, *Quantum computing with neutral atoms in an optical lattice*, Fortschritte Der Physik-Progress Of Physics **48**, 925-943 (2000)
289. H.J. Briegel, T. Calarco, D. Jaksch, J.I. Cirac, and P. Zoller, *Quantum computing with neutral atoms*, J.Mod.Opt. **47**, 415-451 (2000)
290. Q.A. Turchette, C.J. Hood, W. Lange, H. Mabuchi, and H.J. Kimble, *Measurement of conditional phase-shifts for quantum logic*, Phys.Rev.Lett. **75**, 4710-4713 (1995)
291. A. Rauschenbeutel, G. Nogues, S. Osnaghi, P. Bertet, M. Brune, J.M. Raimond, and S. Haroche, *Coherent operation of a tunable quantum phase gate in cavity QED*, Phys.Rev.Lett. **83**, 5166-5169 (1999)
292. C.A. Sackett, D. Kielpinski, B.E. King, C. Langer, V. Meyer, C.J. Myatt, M. Rowe, Q.A. Turchette, W.M. Itano, D.J. Wineland, and I.C. Monroe, *Experimental entanglement of four particles*, Nature **404**, 256-259 (2000)
293. A. Imamoglu, D.D. Awschalom, G. Burkard, D.P. DiVincenzo, D. Loss, M. Sherwin, and A. Small, *Quantum information processing using quantum dot spins and cavity QED*, Phys.Rev.Lett. **83**, 4204-4207 (1999)
294. E. Knill, R. Laflamme, and G.J. Milburn, *A scheme for efficient quantum computation with linear optics*, Nature **409**, 46-52 (2001)
295. M.D. Lukin and A. Imamoglu, *Nonlinear optics and quantum entanglement of ultraslow single photons*, Phys.Rev.Lett. **84**, 1419-1422 (2000)
296. D. Loss and D.P. DiVincenzo, *Quantum computation with quantum dots*, Phys.Rev.A **57**, 120-126 (1998)
297. B.E. Kane, *A silicon-based nuclear spin quantum computer*, Nature **393**, 133-137 (1998)
298. J.L. O'Brien, S.R. Schofield, M.Y. Simmons, R.G. Clark, A.S. Dzurak, N.J. Curson, B.E. Kane, N.S. McAlpine, M.E. Hawley, and G.W. Brown, *Towards the fabrication of phosphorus qubits for a silicon quantum computer*, Phys.Rev.B **64**, 161401 (2001)
299. N.A. Gershenfeld and I.L. Chuang, *Bulk spin-resonance quantum computation*, Science **275**, 350-356 (1997)
300. L.M.K. Vandersypen, M. Steffen, G. Breyta, C.S. Yannoni, M.H. Sherwood, and I.L. Chuang, *Experimental realization of Shor's quantum factoring algorithm using nuclear magnetic resonance*, Nature **414**, 883-887 (2001)

301. D.G. Cory, R. Laflamme, E. Knill, L. Viola, T.F. Havel, N. Boulant, G. Boutis, E. Fortunato, S. Lloyd, R. Martinez, C. Negrevergne, M. Pravia, Y. Sharf, G. Teklemariam, Y.S. Weinstein, and W.H. Zurek, *NMR based quantum information processing: Achievements and prospects*, Fortschritte Der Physik-Progress Of Physics **48**, 875-907 (2000)
302. K. Ichimura, *A simple frequency-domain quantum computer with ions in a crystal coupled to a cavity mode*, Opt.Commun. **199**, 453-453 (2001)
303. M.S. Shahriar, P.R. Hemmer, S. Lloyd, P.S. Bhatia, and A.E. Craig, *Solid-state quantum computing using spectral holes*, Phys.Rev.A **66**, 032301 (2002)
304. M.D. Lukin and P.R. Hemmer, *Quantum entanglement via optical control of atom-atom interactions*, Phys.Rev.Lett. **84**, 2818-2821 (2000)
305. D. Jaksch, J.I. Cirac, P. Zoller, S.L. Rolston, R. Cote, and M.D. Lukin, *Fast quantum gates for neutral atoms*, Phys.Rev.Lett. **85**, 2208-2211 (2000)
306. M.Z. Tian, Z.W. Barber, J.A. Fischer, and W.R. Babbitt, *Geometric manipulation of the quantum states of two-level atoms*, Phys.Rev.A **69**, 050301(2004)
307. J.J. Longdell and M.J. Sellars, *Selecting ensembles for rare earth quantum computation*, quant-ph/0310105 (2002)
308. S.B. Altner, U.P. Wild, and M. Mitsunaga, *Photon-echo demolition spectroscopy in* Eu^{3+}*:*Pr^{3+}*:*Nd^{3+}*:*Y_2SiO_5, Chem.Phys.Lett. **237**, 406 (1995)
309. V.V. Khodos, D.A. Ryndyk, and V.L. Vaks, *Fast-passage microwave molecular spectroscopy with frequency sweeping*, Eur.Phys.J.Appl.Phys. **25**, 203-208 (2004)
310. J. Wesenberg and K. Mølmer, *Robust quantum gates and a bus architecture for quantum computing with rare-earth-ion-doped crystals*, Phys.Rev.A **68** 012320 (2003)
311. P. Goldner and F. Pelle, *Site selection and up-conversion studies in Erbium and Ytterbium doped CsCdBr3*, J.Lumin. **55**, 197-207 (1993)
312. J. Neukum, N. Bodenschatz, and J. Heber, *Spectroscopy and up-conversion of* $CsCdBr_3Pr^{3+}$, Phys.Rev.B **50**, 3536-3546 (1994)
313. R.M. Shelby and R.M. Macfarlane, *Frequency-dependent optical dephasing in the stoichiometric material* EuP_5O_{14}, Phys.Rev.Lett. **45**, 1098-1101 (1980)
314. R.M. Macfarlane, R.M. Shelby, A.Z. Genack, and D.A. Weitz, *Nuclear-quadrupole optical hole burning in the stoichiometric material* EuP_5O_{14}, Opt.Lett. **5**, 462-464 (1980)